Université de Montréal

Étude de diffusion des macromolécules et des macroassemblages dans les biofilms bactériens et de leurs interactions avec les membranes modèles.

Par

Lucie Marcotte

Département de chimie
Faculté des arts et des sciences

Thèse présentée à la faculté des études supérieures
en vue de l'obtention du grade de
Philosophiae Doctor (Ph. D.)
en chimie

Décembre 2004

Université de Montréal

Faculté des études supérieures

Cette thèse intitulée :

Étude de diffusion des macromolécules et des macroassemblages dans les biofilms bactériens et de leurs interactions avec les membranes modèles.

Présentée par :

Lucie Marcotte

a été évaluée par le jury composé des personnes suivantes :

Xiaoxia Zhu

président-raporteur

Michel Lafleur

directeur de recherche

Jean Barbeau

codirecteur

Antonella Badia

membre du jury

Ashraf Ismail

examinateur externe

Raynald Laprade

représentant du doyen de la FES

Sommaire

Les biofilms bactériens peuvent être décrits comme une organisation de microcolonies bactériennes à l'intérieur d'une matrice formée principalement d'exopolysaccharides. Dans certains cas, les bactéries participant à ces structures complexes et hétérogènes se sont avérées être plus de 1000 fois plus résistantes aux bactéricides que les bactéries cultivées sous forme planctonique. Les biofilms se retrouvent souvent aux interfaces solide-liquide, comme dans le cas de la plaque dentaire. Dans nos travaux, nous avons cherché à mieux comprendre l'origine de la résistance des biofilms aux bactéricides dans le but d'aider le développement de traitements efficaces contre les biofilms. Ce sont les biofilms de *Streptococcus mutans*, une espèce bactérienne importante de la plaque dentaire, qui ont été utilisés dans ces travaux.

L'effet de la taille et de la charge sur le coefficient de diffusion de divers solutés dans les biofilms a été étudié par spectroscopie infrarouge à réflexion totale atténuée. L'effet de taille a été isolé par l'utilisation de polyéthylène glycol (PEG) de différentes masses molaires, alors que l'effet de la charge a été examiné grâce à des micelles de détergents anioniques, cationiques et neutres. Les coefficients de diffusion relatifs et les pourcentages de pénétration à l'intérieur du biofilm des macromolécules et auto-assemblages neutres se sont montrés très dépendants de la taille des solutés. Ces résultats ont suggéré l'existence d'endroits inaccessibles dans le biofilm aux solutés avec un rayon hydrodynamique > 10 Å. Nous avons confirmé cette hypothèse par microspectroscopie Raman en cartographiant la distribution spatiale de PEG 10k après diffusion dans le biofilm. Les mesures de diffusion du D_2O ont montré que l'ensemble du biofilm lui était accessible alors que la pénétration du PEG 10k était modulée par la densité de biomasse du biofilm.

Les micelles anioniques et cationiques ont pour leur part montré une plus grande pénétration du biofilm par rapport à ce qui était attendu pour leur dimension.

De plus, la diffusion du détergent cationique, le chlorure de cétylpyridinium répertorié comme un composé d'ammonium quaternaire (QAC), a montré une association irréversible avec le biofilm. Les QACs sont utilisés comme antiseptiques et cette association avec le biofilm a suscité notre intérêt de mieux comprendre leur mode d'action.

Les QACs sont réputés pour agir sur la membrane bactérienne. C'est pourquoi nous avons étudié l'affinité des QACs ainsi que leur effet sur la perméabilité des membranes lipidiques pour diverses compositions des membranes lipidiques ainsi qu'une variété de QACs. Les constantes d'affinité ont été mesurées par calorimétrie à titration isotherme. L'effet des détergents sur la perméabilité des membranes a été suivi par la fuite d'une sonde fluorescente encapsulée dans des vésicules lipidiques. De manière générale, une association favorable des QACs avec les membranes lipidiques a été trouvée et celle-ci résultait principalement d'un effet hydrophobe plutôt qu'électrostatique. Aussi, les détergents dont la chaîne aliphatique comportait 16 atomes de carbone se sont montrés plus efficaces à causer des défauts dans les membranes.

En conclusion, à la lumière de nos résultats, l'élaboration de traitements dans le but d'éradiquer les biofilms doit prendre en compte que la taille des solutés nuit à l'accessibilité à l'intérieur du biofilm et que certaines sections de celui-ci peuvent s'avérer carrément inaccessibles. Par contre, la présence de molécules chargées, comme les ammoniums quaternaires, semble augmenter le potentiel de pénétration. Les QACs ont montré une forte affinité pour les membranes lipidiques ainsi que pour les biofilms.

Mots clés : Diffusion, Biofilms, QAC, FTIR-ATR, Microspectroscopie Raman, ITC, Relargage, Constante de partage

Abstract

Bacterial biofilms can be described as an organization of bacterial microcolonies inside a matrix made principally of polysaccharides. In some cases, bacteria that form these complexes and heterogeneous structures were found to be more than 1000 times more resistant to bactericides compared to the same bacteria grown in a planctonic form. Biofilms are usually found at solid-liquid interfaces, like in the case of dental plaque. The aim of our work was to better understand the origin of the bactericidal resistance of biofilms in order to help the development of new efficient treatments against biofilms. We used the *Streptococcus mutans* biofilm in this study, a bacterial species implicated in dental plaque.

The effect of the size and of the charge on the diffusion coefficient of various solutes inside biofilms was studied by using attenuated total reflectance infrared spectroscopy. The size effect was isolated using polyethylene glycol (PEG) of various molecular weights, and the charge effect was investigated using anionic, cationic and neutral surfactant micelles. The relative diffusion coefficients and penetration percentages in biofilms found for the investigated macromolecules and the neutral auto-assemblagies depend on the solute size. These results suggest the existence of regions of the biofilms inacessible to solutes with a hydrodynamic radius larger than 10 Å. The Raman microspectroscopy technique has confirmed this hypothesis by mapping the spatial distribution of PEG with a molecular mass of 10k after its diffusion inside the biofilm. Measurements with D_2O showed that the biofilm was completely accessible to small molecules and that the biomass density of the biofilm modulated the PEG penetration.

Anionic and cationic micelles have shown a higher penetration in the biofilm compared to PEG with a similar size. Furthermore, the diffusion of cetylpyridinium chloride, a cationic surfactant that is a quaternary ammonium compound (QAC) showed irreversible association with the biofilm. QACs are used

as antiseptic and this strong association with the biofilm led us to examine in more details their action mode.

QACs are known to act at the bacterial membrane level. On this basis, we studied the QACs affinity for lipid membranes and their effect on the membrane permeability as a function of the membrane lipid composition and of the molecular details of QACs. Affinity constants were determined by isothermal titration calorimetry. The surfactant effect on membrane permeability was studied by following the release of a fluorescent probe entrapped inside lipid vesicles. For all the studied QACs, a favorable association between surfactants and the lipid membrane was found and this association was mainly the result of a hydrophobic effect, relative to an electrostatic contribution. Also, surfactants with an aliphatic chain length of 16-carbon atoms were more efficient at inducing defects in lipid membranes.

In conclusion, from our results, the elaboration of treatments to eradicate biofilms has to take into consideration that the size of the solute may impede the biofilm accessibility and that some regions of biofilms can be inaccessible to the solutes. On the other hand, charged molecules, like the QACs, seem to enhance the penetration potential. QACs have demonstrated strong affinity for lipid membranes and for biofilms.

Key words : Diffusion, Biofilms, QAC, FTIR-ATR, Raman microspectroscopy, ITC, Release, Partition constant

Table des matières

Liste des tableaux

Liste des figures

Liste des sigles et abbreviations

ATR	Attenuated total reflection
BDDAC	Benzyldimethyldodecylammonium chloride
BDHAC	Benzyldimethylhexadecylammonium chloride
Card	Cardiolipine
Chol	Chlosterol
CMC	Critical micelle concentration
CPC	Cetylpyridinium chloride
CTAC	Cetyltrimethylammonium chloride
D	Diffusion coefficient
D_o	Diffusion coefficient in water
DPC	Dodecylpyridinium chloride
DTAC	Dodecyltrimethylammonium chloride
FTIR	Fourier transformed infrared spectroscopy
ITC	Isothermal titration calorimetry
LUV	Large unilamellar vesicle
PEG	Polyethylene glycol
POPC	1-palmitoyl-2-oleoyl-sn-glycerol-3-phosphocholine
POPG	1-palmitoyl-2-oleoyl-sn-glycerol-3-phosphoglycerol
QAC	Quaternery ammonium compound
SDS	Sodium dodecylsulfate

À mon trésor,

Remerciements

Je tiens tout d'abord à remercier Michel Lafleur pour m'avoir accueilli dans son groupe de recherche et pour m'avoir donné la chance de poursuivre mes études au niveau doctoral sur un sujet qui m'a tan passionné. Je le remercie aussi pour sa patience face à mes erreurs multiples, pour sa disponibilité précieuse, sa rigueur scientifique et ses conseils judicieux. J'aimerais aussi remercier Jean Barbeau, sans qui l'aspect microbiologique de cette thèse n'aurait jamais été aussi bien compris, et aussi pour nos discussions qui ont plus d'une fois sues me sortir de l'embarras.

Merci aussi à mes co-auteurs, Héloïse Thérien-Aubin, Christophe Sandt, Katarina Edwards et Göran Karlsson, grâce à qui certaines parties du travail m'auraient été plus difficiles à réaliser.

Un merci tout spécial à mes collègues, passés et présents, de l'aile C-600 et du laboratoire de microbiologie. Mon séjour avec vous a été des plus agréables et me manque déjà. Un merci tout spécial à Marjolaine pour les couleurs qu'elle a données à mon quotidien, à Iren pour nos soirées inoubliables, à Rémisss pour avoir enrichi ma culture et à Marie-Christine pour sa vision différente de la vie.

Finalement, j'aimerais remercier mes parents pour l'amour et la confiance aveugle qu'ils ont toujours eu à mon égard. À Zaza, Jaja, Julie, Mélanie, Patrice pour être là dans les moments bons et moins bons. Mais surtout, je veux remercier Stéphane pour son amour et son soutien. Durant cette thèse, nous avons connu la plus belle journée de notre vie, mais aussi la pire; sans toi rien n'aurait été possible. Merci pour ta générosité, merci de me faire rire, merci d'être là. Je te l'ai dis mille fois au moins, et tu l'entendras encore longtemps : « je t'aime ».

Chapitre 1

Introduction

1.1 Problématique des biofilms

Les bactéries ont été depuis longtemps étudiées avec des conditions de croissances optimisées où chaque cellule a accès à suffisamment de nutriments pour se diviser. Or, dans la nature, les bactéries ont adopté différentes stratégies de croissance pour survivre à leur environnement souvent pauvre en nutriments ou encore hostile à leur croissance. Il y a un peu plus d'une quinzaine d'années, la communauté des microbiologistes s'entendait pour définir un nouveau mode de croissance des bactéries appelé biofilm.[1] Les biofilms se retrouvent la plupart du temps à l'interface solide-liquide. Dans un premier temps, les bactéries adhèrent de façon réversible à la surface avec des liens électrostatiques, des forces de van der Walls et des ponts hydrogènes, par la suite l'attachement irréversible est assuré par des liens hydrophobes et par la synthèse de glycoprotéines et de polysaccharides.[2] Finalement, le développement du biofilm se fait en fonction des conditions physiques de son environnement. De manière générale, on peut décrire les biofilms comme une organisation de microcolonies insérées dans une matrice de polysaccharides. Cette matrice est principalement constituée d'un hydrogel dont le contenu en eau peut atteindre jusqu'à 97 %.[3] On y retrouve, en plus des polysaccharides, des déchets métaboliques et des nutriments. De plus, tous les biofilms montrent une hétérogénéité à plusieurs niveaux.[2] Tout d'abord, ils sont hétérogènes dans leur structure. Un exemple de structure celle sous forme de champignon; cette conformation a été montrée pour les biofilms de *Pseudomonas aeruginosa*.[1] Comme on peut le voir à la Figure 1.1, les amas de biomasse, en forme de champignon, sont séparés par ce qui est communément appelé des « water

channels », c'est-à-dire, des canaux d'eau.[1] On soupçonne que ces tunnels servent à l'irrigation du biofilm.[1]

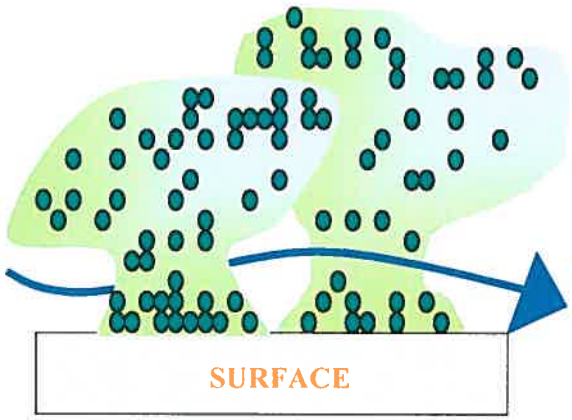

Figure 1.1 : Schématisation d'un biofilm bactérien à l'interface solide-liquide.

Une expérience avec des billes de latex de 0.282 µm a d'ailleurs montré la présence d'un débit dans les canaux.[4] Malgré la présence de ces canaux d'eau, il a été montré qu'il subsistait des gradients importants dans l'apport de nutriments entre les microcolonies qui se trouvaient à la surface du biofilm et celles qui se trouvaient au cœur de celui-ci.[1,2,5,6] Il est de plus en plus accepté que cette hétérogénéité en nutriment mène à une variation dans le taux de croissance des bactéries selon l'endroit où elles se retrouvent dans le biofilm.[2] La variation dans l'apport en nutriment au cœur du biofilm peut être aussi conséquente d'une hétérogénéité de la diffusion dans le biofilm. Comme nous le discuterons plus loin, il a été montré qu'un même composé ne montrait pas la même vitesse de migration selon l'endroit où il se trouvait dans le biofilm.[7] Bien que la structure en forme de champignon aie été souvent rapportée, les conformations des biofilms sont très dépendantes de leurs conditions de croissances (apport en nutriment, surface de croissance, remous dans le milieu liquide, etc.), mais aussi de la souche microbienne.[2]

Une des premières méthodes utilisées pour observer la structure des biofilms a été la microscopie optique.[8] Par contre, le contraste et l'épaisseur des échantillons ne permettaient pas l'obtention d'images qui soient très révélatrices. Alors, à la microscopie optique, on a combiné des méthodes de colorations afin de mettre en évidence certains constituants du biofilm, comme les exopolysaccharides.[8-10] Par contre, ces méthodes de coloration ont surtout aidé à détecter la présence des biofilms plus qu'à faire l'étude de leur structure. La microscopie électronique, pour sa part, a permis d'identifier les microcolonies et la présence d'une matrice extracellulaire autour de celles-ci.[11-14] Cette méthode a apporté beaucoup d'informations sur les biofilms, mais elle implique une manipulation importante de l'échantillon (séchage et des coupes au microtome) apportant certainement des artefacts aux résultats obtenus. C'est pourquoi la microscopie laser confocale (CLSM) est devenue sans doute la technique la plus utilisée pour l'étude de l'organisation tridimensionnelle des biofilms.[1,2,15-17] Dans cette technique, un laser

donne une impulsion d'énergie aux fluorophores présents dans l'échantillon à un endroit bien précis et ces derniers émettent une fluorescence qui est détectée par des tubes photomultiplicateurs.[15] L'avantage de cette méthode est que si l'échantillon possède des fluorophores de manière intrinsèque, il n'est pas nécessaire de traiter l'échantillon. Or, il faut procéder à une coloration pour identifier les composantes des biofilms qui ne présentent pas de fluorescence. La principale limite des colorants est qu'il subsiste toujours un doute quant au fait que le colorant ait adhéré à tout ce qu'on cherchait à mettre en évidence, laissant paraître de faux négatifs.

La présence des biofilms est reliée à plusieurs problèmes, comme : les maladies récurrentes (telle la fibrose kystique), les rejets d'implants, la corrosion de métaux, la contamination de canalisation d'eau, etc.[2] Cependant, les humains ont réussit à exploiter les propriétés des biofilms pour les utiliser comme bioréacteurs pour filtrer des eaux usées ou pour produire des biopolymères.[2,18] De plus, l'étude des biofilms permet, sur le plan fondamental, de mieux comprendre cette microniche où plusieurs espèces de bactéries cohabitent dans un même environnement[2] et même communiquent entre elles.[19]

Par contre, l'habileté des bactéries sous forme de biofilm à résister aux bactéricides et aux antibiotiques demeure un fait préoccupant. Effectivement, plusieurs études ont montré qu'une espèce cultivée sous forme de biofilm se montrait jusqu'à des milliers de fois plus résistante que si elle était cultivée sous forme planctonique.[1,2,20-22] Plusieurs hypothèses ont été avancées pour expliquer cette résistance. De plus en plus, on s'entend pour dire qu'il n'existerait pas qu'une seule raison, mais plutôt une combinaison de plusieurs facteurs.[2] Un de ces facteurs serait une présélection lors de la toute première étape de la croissance du biofilm. Seules les bactéries avec un phénotype particulier pourraient adhérer à la surface des solides et posséderaient le gène de résistance à certains antibiotiques.[2] Une autre hypothèse prône que la résistance aux antibiotiques, apportée par la

croissance en biofilm, vient de l'hétérogénéité du taux de croissance des bactéries.[14,21,23] Beaucoup d'antibiotiques agissent sur les cellules qui se divisent rapidement. Or, dans un biofilm, le faible apport en nutriment crée un ralentissement de la croissance bactérienne ce qui rendrait les antibiotiques moins efficaces. D'autres recherches ont montré que les bactéricides étaient désactivés lors de leurs transports vers les bactéries dans le biofilm.[24,25] Effectivement, la matrice d'exopolysaccharides est remplie d'ions, de protéines et autres molécules qui sont susceptibles de réagir avec le médicament et de lui enlever ses propriétés bactéricides. Finalement, plusieurs croient que la présence des exopolysaccharides ralentit ou même empêche les bactéricides de pénétrer le biofilm jusqu'aux bactéries.[7,26-34]

La résistance aux bactéricides rencontrée chez les biofilms et une meilleure compréhension de ce qui influence leur efficacité a été le fil conducteur dans mes travaux de thèse. Premièrement, il est primordial que les bactéricides atteignent les bactéries situées au cœur du biofilm. Ces pourquoi nous avons cherché à mieux comprendre la diffusion de solutés dans les biofilms à travers deux facteurs, soit : la taille des particules diffusantes et leur charge. Aussi, nous avons examiné la distribution de la biomasse dans les biofilms et l'effet de cette biomasse sur la diffusion de macromolécules ainsi que l'accessibilité des biofilms par divers analytes.

L'autre aspect important dans l'étude de la résistance des biofilms est leur susceptibilité aux bactéricides. Une meilleure compréhension de leur mode d'action contre les bactéries pourrait mener au développement de bactéricides plus efficaces. Nous nous sommes donc intéressés plus particulièrement à l'association des ammoniums quaternaires avec les membranes bactériennes. Comme il sera expliqué plus loin, cette classe de détergents est connue comme des bactéricides réputés pour agir au niveau des membranes cytoplasmique des bactéries. Il en existe une très grande variété. Nous avons étudié l'association de certain d'entre

eux d'un point de vue thermodynamique en fonction de leur type de tête polaire, de la longueur de leur chaîne aliphatique et du mélange de lipides dans la membrane. Puis, nous nous sommes intéressés à leur influence sur la perméabilité des membranes lipidiques.

Pour effectuer nos travaux, nous avons utilisé un biofilm de *Streptococcus mutans*. *S. mutans* est une des bactéries la plus abondante de la plaque dentaire et est connue pour être responsable de la carie dentaire.[35-37] *S. mutans* possède plusieurs glycotransférases capables de transformer les sucres complexes en polysaccharides intracellulaires ou extracellulaires. Les polysaccharides extracellulaires sont principalement des fructans et des glucans.[36,37] Cette caractéristique du *S. mutans* à produire beaucoup d'exopolysaccharides en présence de sucrose en a fait un bon candidat pour notre recherche. De plus, les conditions de croissance menant à la formation d'un biofilm capable d'adhérer à des surfaces lisses et solides étaient déjà rapportées dans la littérature.[38]

1.2 La diffusion dans les biofilms

La diffusion est due au mouvement brownien qui cause un déplacement continuel des molécules. On parle de « coefficient d'auto-diffusion » lorsque la diffusion d'un composé A est mesurée à l'intérieur de A pure. Par contre, le terme de « coefficient d'auto-diffusion » est aussi utilisé dans la situation où le déplacement de A en solution dans B est suivit en absence de gradient de concentration.

La diffusion fickienne, pour sa part, est décrite comme le transport de la matière d'un endroit vers un autre via le mouvement brownien, mais dans ce cas-ci, en fonction d'un gradient de concentration. Le flux (ou la vitesse de migration) à travers une surface donnée (F) dépend de la densité du gradient de concentration selon la loi de Fick en une dimension :

$$F = -D\frac{\partial C}{\partial x} \qquad \text{Éq. 1.1}$$

Où C est la concentration de la substance qui diffuse, x la coordonné de la distance et D le coefficient de diffusion dont les unités sont données en distance^2/temps, ex : m^2s^{-1}. Le signe négatif indique que le flux s'oppose au gradient.

Des mesures de diffusion à l'intérieur des biofilms ont été faites via plusieurs techniques. Une des premières utilisées consiste à faire croître un biofilm sur une membrane poreuse et à suivre la diffusion d'un soluté à travers la membrane qui est placée entre deux récipients.[14,26] L'information obtenue est alors sur le transport d'une molécule à travers l'ensemble du biofilm, y compris de ses « water channels ». Une autre manière de mesurer la diffusion dans les biofilms est de déterminer la concentration d'un soluté à l'intérieur même du biofilm en fonction du temps, lorsque celui-ci est mis en contact avec un analyte. Une méthode pour effectuer cette mesure de diffusion consiste à suivre le profil de concentration d'un soluté en fonction de la profondeur dans le biofilm à l'aide de microélectrodes.[1,6,24,39] Les solutés les plus souvent dosés à l'aide de microélectrodes sont l'oxygène et les chlorures. Cette méthode est limitée à ce qui peut se doser par des réactions d'oxydoréduction. Une autre méthode est la microscopie confocale à fluorescence (CLSM) qui permet de prendre des images par strate dans le biofilm et de reconstituer une image en trois dimensions, et donc, de localiser des sondes fluorescentes à l'intérieur de celui-ci.[15,16] La spectroscopie infrarouge par réflexion totale atténuée (IR-ATR) s'est aussi avérée appropriée pour suivre la diffusion de soluté dans les biofilms.[16,40-43] Dans cette technique, le signal de la molécule diffusante est obtenu sur l'ensemble du biofilm et à partir de sa base (soit l'interface cristal-biofilm). La IR-ATR étant la technique retenue pour notre étude, une description plus détaillée en sera faite plus bas. Une variante à la CLSM, beaucoup utilisée pour étudier la diffusion à l'intérieur des biofilms, est le retour de fluorescence après photoblanchiement plus connu sous l'appellation « fluorescence recovery after photobleaching » (FRAP). Dans cette technique, une impulsion lumineuse éteint la fluorescence à un endroit précis du biofilm. Le

signal de fluorescence réapparaissant est alors associé à la diffusion des molécules non éteintes par l'impulsion à l'intérieur du volume blanchit et du déplacement des molécules éteintes vers l'extérieur du volume blanchit. On obtient par la méthode FRAP un coefficient d'auto-diffusion à un endroit très précis dans le biofilm. Ces méthodes ont mené à la détermination de coefficients de diffusion (et d'auto-diffusion) dans divers biofilms. Ces valeurs sont compilées dans le tableau 1.1.

Tableau 1.1 : Coefficients de diffusions (D) de diverses macromolécules rapportés pour différents biofilms et leur ratio par rapport à leur coefficient de diffusion dans l'eau (D^o).

Soluté (M.M.)	Type de biofilm	Méthode	D x 10^{11} (m^2 s^{-1})	D/D^o
Dextran (10k)[a]	Modèle de plaque sans sucrose	FRAP	4.38	0.25
Dextran (40k)[a]			9.94	0.61
Dextran (500k)[a]			2.93	0.65
Dextran (10k)[a]	Modèle de plaque avec sucrose	FRAP	15.7	0.89
Dextran (40k)[a]			10.5	1.3
Dextran (500k)[a]			2.19	0.48
Particules anioniques (4.5 à 55 nm)[b]	*Lactococcus lactis*	CLSM	0.2 - 0.02	0.044 - 0.059
	Stenotrophonas maltophilia		0.54 - 0.025	0.12 - 0.073
Fluorescein (332)[c]	Biofilm mixte	FRAP	58 (± 1.0)	ND
TRITC-IgG (150k)[c]			0.20 (± 0.03)	ND
Phycoerythrin (240k)[c]			0.23 (±0.03)	ND
Chlorhexidine digluconate[d]	*Candida albicans*	FTIR-ATR	11.9 (±8.5)	ND
		Raman	10.9 (±4.4)	ND
Fluorescein (332)[e]	*Pseudomonas putida*	FRAP	50	0.91
Dextran (10k) [e]			0.62 (±0.01)	0.28
Dextran (70k)[e]			0.26 (±0.02)	0.15
BSA (68k)[e]			3.73 (±0.02)	0.54
DNA ($3.2x10^6$)[e]			0.0015 (±0.0003)	0.19
Petites molécules (<44)[f]	Voir Tableau 1.2	Variable	ND	0.46
Grosses molécules (>44)[f]				0.39
Solutés ioniques[f]				0.15
Dextran (3k)[g]	Modèle de plaque	CLSM	0.659	0.03
Dextran (10k)[g]			0.069	0.006
Dextran (40k)[g]			0.059	0.017
Dextran (70k)[g]			0.036	0.012
Dextran (4k)[h]	*Pseudomonas fluorescens*	FRAP	0.31	0.024
Dextran (40k)[h]			0.17	0.021
Dextran (70k)[h]			0.11	0.030
Dextran (500k)[h]			0.11	0.035
Dextran (2 000k)[h]			0.07	0.125

a[32],b[33],c[34],d[44],e[7],f[29],g[28],h[27]

Tableau 1.2 : Coefficients de diffusion relatifs pour divers soluté. Tableau adapté de ref. 29

Soluté	Type de biofilm	Méthode[a]	D/D^0
O_2	Biofilm mixte	REI	0.048
	Cullot *A. niger*	REI	0.58
	Biofilm mixte	REI	0.60
	Tapis cyanobacterien	DEI	0.71
	---	DEI	0.23 - 0.69
Xe	Plaque dentaire	NEI	0.46
HCO_3	Plaque dentaire	REI	0.05
Acetate	Plaque dentaire	REI	0.09
	Plaque dentaire	---	0.29
	Plaque dentaire	DEI	0.31
Lactate	Plaque dentaire	REI	0.09
	Plaque dentaire	DEI	0.31
	Plaque dentaire	DEI	0.08
Butyrate	Plaque dentaire	REI	0.12
Sucrose	Plaque dentaire	REI	0.11
	Plaque dentaire	DEI	0.43
	Plaque dentaire	DEI	0.045
SO_4^-	Tapis cyanobacterien	DEI	0.13
H_2S	Tapis cyanobacterien	DEI	0.16
NaF^-	Plaque dentaire	NEI	0.23
Glucose	Biofilm mixte	NEI	0.5
Br^-	Biofilm mixte	NEI	0.5 - 0.8
Phenol	Biofilm mixte	DEI	0.13 - 0.39
^3H_2O	Plaque dentaire	---	0.30
Fluorescein	Biofilm mixte	NI	0.023
	Biofilm mixte	NEI	0.97
	P. putida	NEI	0.91

[a] R=soluté réactif, N=soluté non-réactif, D=biofilm désactivé, E=résistance externe de transfert de masse, I=biofilm intact

Les coefficients de diffusion (D) rapportés à l'intérieur des biofilms sont, de manière générale, plus petits que le coefficient de diffusion du même soluté mesuré dans l'eau (D_o). Les molécules de tailles plus importantes montrent une diffusion plus lente dans le biofilm par rapport aux molécules de plus petite taille. Cependant cette tendance est associée au transfert de masse et est aussi observée dans l'eau. Le coefficient de diffusion relatif (D/D_o) se présente donc comme une manière plus appropriée pour comparer la diffusion de solutés différents dans les biofilms. Une autre constatation est à noter lorsqu'on compare les valeurs de D dans la littérature : ceux-ci varient en fonction du biofilm étudié. Pour une même molécule, par exemple le dextran avec une masse molaire de 10 000, le coefficient de diffusion varie de 0.069 à 15.7 x 1011 m^2s^{-1} (Tableau 1.1). Ceci laisse donc

croire que les composantes et la conformation tridimensionnelle du biofilm sont des facteurs qui influencent la diffusion. Une bonne compréhension de la structure des biofilms et des interactions entre les solutés diffusants à l'intérieur de ceux-ci avec les composantes du biofilm est donc primordiale pour le développement de nouvelles stratégies bactéricides.

Comme nous l'avons mentionné plus haut, nous avons choisi la spectroscopie infrarouge à transformée de Fourier par réflexion totale atténuée (FTIR-ATR) pour étudier la diffusion de macromolécules et de macroassemblages - formées des détergents dodécylsulfate de sodium (SDS), chlorure de cétylpyridinium (CPC) et Triton X-100 (Figure 1.2) – dans les biofilms de *S. mutans*. Cette technique est très bien indiquée pour l'étude de la diffusion puisqu'elle permet l'acquisition spectrale de manière *in situ* et en fonction du temps. De plus, la cellule ATR permet la croissance directe du biofilm à la surface du crystal (voir Chapitre 2) et donc de suivre l'évolution de l'échantillon dans le temps sans intervention externe. Contrairement à la spectroscopie par transmission, le faisceau IR ne traverse pas l'échantillon mais permet d'enregistrer le spectre infrarouge de ce qui se trouve à la surface d'un cristal et sur quelques micromètres d'épais.

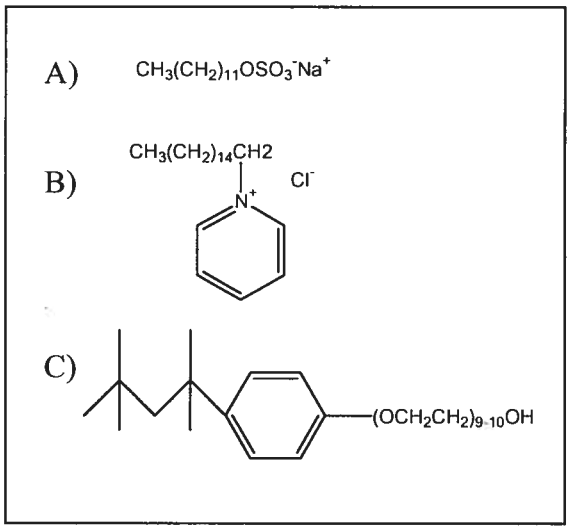

Figure 1.2 : Détergents sélectionnés pour l'étude de diffusion dans le biofilm de *Streptococcus mutans* : A) dodécylsulfates de sodium (SDS), B) chlorure de cétylpéridium (CPC) et C) Triton X-100.

En mode ATR, le faisceau infrarouge voyage dans le cristal via des réflexions dues à une différence d'indice de réfraction entre le cristal et le milieu à sa surface (Figure 1.3). À chaque réflexion, une partie du faisceau infrarouge, appelé onde évanescente, interagit avec les molécules qui se trouvent à la surface du cristal. Le signal enregistré dépendra de la quantité de matière qui a été détectée par l'onde évanescente, donc, de sa profondeur de pénétration dans l'échantillon. La profondeur de pénétration (d_p) de l'onde évanescente dans le milieu dépend de l'angle incident de la réflexion (θ), de la longueur d'onde (λ) du faisceau et des indices de réfraction des milieux ($n_{21}=n_2/n_1$). Cette relation est décrit selon l'équation suivante :[45]

$$d_p = \frac{\lambda_1}{2\pi(\sin^2\theta - n_{21}^2)^{1/2}} \qquad \text{Éq. 1.2}$$

Dans le cadre de notre étude, le biofilm a été cultivé directement à la surface du cristal puis nous avons fait diffuser les macromolécules et macroassemblages dans celui-ci. Le cristal que nous avons utilisé était composé de séléniure de zinc (n=2.403) et l'angle était de 45°. Ces conditions nous ont permis de sonder les 2 à 4 µm à la base des biofilms cultivés à la surface de notre cristal (pour plus de détails voir le Chapitre 2).

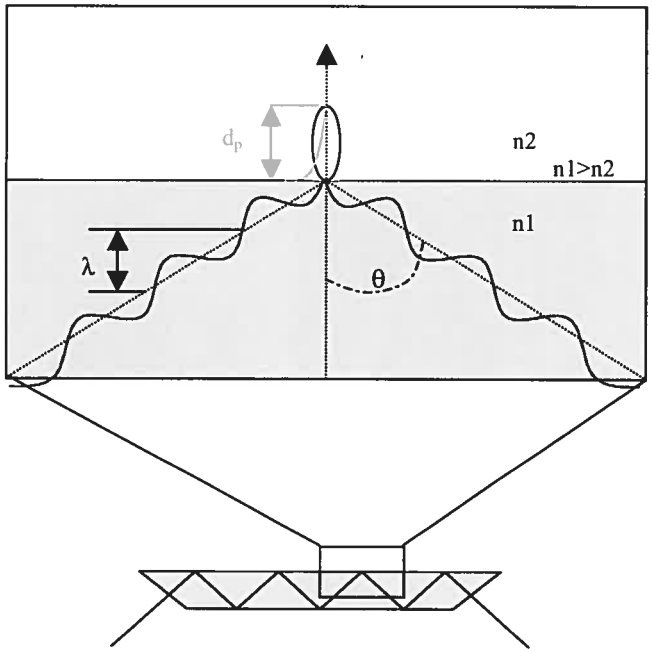

Figure 1.3 : Représentation d'une onde évanescente, d'une épaisseur dp, qui se produit lorsque le faisceau infrarouge, d'une longueur d'onde λ, effectue une réflexion totale à l'interface cristal-air. n_1 et n_2 représente les indices de réfraction du cristal et de l'air respectivement. L'angle du faisceau incident est donné par θ.

La détermination des coefficients de diffusion dans les biofilms est complexe dû à l'hétérogénéité de leur structure. La mise en place d'un modèle de diffusion qui représenterait parfaitement la réalité est très laborieuse étant donnée la structure tridimensionnelle complexe des biofilms et de la variabilité de leur composition, de la forme et de la densité des agrégats de biomasses qui est très variable. Pour traiter nos données, nous avons utilisé un modèle simplifié. Dans ce modèle, on suppose un biofilm uniforme d'une épaisseur l à l'intérieur duquel la diffusion est homogène (c'est-à-dire caractérisée par un seul coefficient de diffusion.)

La spectroscopie ATR nous a permis de suivre la variation de concentration du soluté étudié en fonction du temps. Ceci fait donc référence à la deuxième loi de Fick:

$$\frac{\partial C}{\partial t} = D\frac{\partial^2 C}{\partial x^2} \qquad \text{Éq.1.3}$$

Donc, la concentration est fonction du temps (t) et de la position (x), i.e. C= X(x)T(t). Il est possible d'obtenir la solution analytique de cette équation. Un moyen d'y parvenir est de procéder par la méthode de séparation de variables.[46] Pour ce faire, il faut réécrire la 2e loi de Fick en remplaçant C dans l'équation 1.3 ce qui donne les formes suivantes :

$$X\frac{dT}{dt} = DT\frac{d^2X}{dx^2} \qquad \text{Éq. 1.4}$$

$$\frac{1}{T}\frac{dT}{dt} = \frac{D}{X}\frac{d^2X}{dx^2} \qquad \text{Éq. 1.5}$$

Si on pose $C=\lambda^2 D$,[46] on obtient:

$$\frac{1}{T}\frac{dT}{dt} = -\lambda^2 D \qquad \text{Éq. 1.6}$$

et

$$\frac{1}{X}\frac{d^2X}{dx^2} = -\lambda^2 \qquad \text{Éq. 1.7}$$

Une solution de la partie temporelle de l'équation est:

$$T = e^{-\lambda^2 Dt} \qquad \text{Éq. 1.8}$$

Pour la partie spatiale, une solution est :

$$X = A\sin\lambda x + B\cos\lambda x \qquad \text{Éq. 1.9}$$

Où A et B sont des constantes. La forme générale, non linéaire, aura donc la forme suivante :[46]

$$C = \sum_{1}^{\infty} (A_m \sin\lambda_m x + B_m \cos\lambda_m x)\exp(-\lambda_m^2 Dt) \qquad \text{Éq.1.10}$$

Les constantes A_m, B_m et λ_m sont alors déterminées par des conditions frontières définies par le problème étudié.

Dans le modèle qui nous concerne, la concentration de soluté à la surface du biofilm est constante (C_1). L'épaisseur du biofilm est donnée par l où la position x=0 correspond à l'interface cristal-biofilm. La solution analytique de la variation de la concentration dans le biofilm (C) en fonction du temps (t) et de la position (x) est alors décrite comme suit :[46]

$$\frac{C}{C_\infty} = 1 - \frac{4}{\pi}\sum_{n=1}^{\infty}\frac{(-1)^n}{2n+1}\exp\{-D(2n+1)^2\pi^2 t/4l^2\}\cos\frac{(2n+1)\pi x}{2l} \qquad \text{Éq. 1.11}$$

Ici, C_∞ est la concentration que l'on trouve en tout point dans le biofilm à un temps infini. Dans nos expériences par ATR, la concentration du soluté est suivie par l'intégration d'une de ses bandes caractéristiques dans les spectres infrarouges. Comme le signal vient de la base du biofilm (la profondeur de l'onde évanescente (2-4 μm) est minime par rapport à l'épaisseur du biofilm (> 100 μm)), on considère que x=0 et l'équation 1.11 devient :

$$\frac{C}{C_\infty} = 1 - \frac{4}{\pi}\sum_{n=1}^{\infty}\frac{(-1)^n}{2n+1}\exp\{-D(2n+1)^2\pi^2 t/4l^2\} \qquad \text{Éq. 1.12}$$

En simulant les résultats expérimentaux avec cette équation, il est possible d'obtenir le coefficient de diffusion moyen dans le biofilm à partir du terme exponentiel si on connaît l. Un autre paramètre, la pénétrabilité, peut-être extraite de cette équation. En prenant l'intensité de la bande caractéristique du soluté que l'on fait diffuser dans le biofilm à un temps infini (C_∞ tiré de l'équation 1.4), il est possible de définir la pénétrabilité du soluté en la comparant à l'intensité de cette même bande en absence de biofilm. Il existe peu d'ouvrage qui font état de la pénétrabilité des solutés dans l'ensemble du biofilm. Dans ce travail, nous nous sommes penchés sur cet aspect. Il est bien établi, à partir des études faites dans les hydrogels, que les molécules de grandes tailles pénètrent difficilement un gel dont les mailles sont plus petites que leur rayon hydrodynamique.[47-50] Comme la matrice de base d'un biofilm est un hydrogel, on peut s'attendre à ce que certains endroits ne soient pas accessibles aux grosses molécules, ceci étant dicté par le rapport entre la porosité du gel et la taille du soluté. L'hétérogénéité de la structure des biofilms peut mener à des résultats complexes à interpréter. Par exemple, une très grosse macromolécule pourrait traverser un biofilm via les canaux d'eau et, si l'expérience est faite sur l'ensemble du biofilm, aucun effet de ralentissement ne serait enregistré lors de l'expérience. Par contre, la macromolécule n'aurait en fait atteint qu'un volume limité du biofilm. Donc pour toutes les molécules étudiées par la FTIR-ATR, nous avons trouvé leur coefficient de diffusion ainsi que leur pourcentage de pénétration.

Avec la microscopie Raman, nous avons caractérisé la conformation d'un biofilm de *S. mutans* et suivi la pénétrabilité du poly(éthylène glycol) de masse molaire 10 000 dans le biofilm afin d'identifier les régions accessibles et inaccessibles à la macromolécule dans le biofilm. Un des grands avantages de la spectroscopie Raman est la possibilité de faire des mesures sur les échantillons de manière *in situ* sans besoin de les avoir marqués préalablement. Cette technique permet d'enregistrer le spectre Raman à un endroit bien défini dans l'échantillon. Le spectre Raman contient de l'information sur les mouvements de vibrations des

groupes fonctionnels présents dans l'échantillon. La spectroscopie Raman couplée avec un microscope permet d'enregistrer un spectre sur une surface en xy de quelques micromètres de diamètre, correspondant au diamètre du faisceau. Lorsque le microscope est muni d'une platine mobile, on peut enregistrer périodiquement les spectres en déplaçant l'échantillon jusqu'au balayage complet de la surface désirée. L'analyse des spectres permet de faire de la microscopie chimique. Dans notre cas, nous sommes intéressés à obtenir la répartition de la biomasse dans le biofilm sur une certaine superficie de l'échantillon. À l'aide des spectres Raman enregistrés, on peut simultanément, faire le profil de la répartition de la biomasse, et aussi, détecter la présence d'une macromolécule dans le biofilm qu'on aurait fait diffuser au préalable. De cette manière, il est possible de voir à quel endroit se retrouve la molécule diffusante : dans les canaux d'eau et/ou dans les microcolonies.

1.3 Interactions des composées ammoniums quaternaires avec les biofilms

Comme nous l'avons mentionné plus haut, lorsque les bactéricides pénètrent dans le biofilm, il est possible que ceux-ci interagissent avec les divers composants du biofilm et soient ralentis, voir même stoppé, dans leur course vers les bactéries.[31,34,51,52] L'interaction des bactéricides avec les biofilms a été rapportée pour des molécules chargées positivement tel que la chlorhexidine.[44] De plus, une étude de pénétration de liposomes dans les biofilms a montré une accumulation des liposomes cationiques à l'interface liquide-biofilm.[31,51] Aussi, une étude sur la diffusion de particules neutres (des molécules de dextran de masse allant de 40K à 150K) et des particules chargées (des billes de latex greffées de carboxylates pour les anioniques et d'amines pour les cationiques) dans un biofilm a révélé que les nanoparticules cationiques ne pénétraient pas le biofilm supposant une association

avec celui-ci.[33] Les auteurs suggèrent que le biofilm agit comme barrière à la diffusion des particules chargées positivement dans le biofilm.[33] Dans ces deux situations, on propose que les particules chargées positivement s'associent avec les charges négatives qui se retrouvent dans le biofilm.[31,33,51] Les exopolysaccharides sont souvent constitués de charges négatives dues à la présence de fonctions phosphate et acide carboxylique.[3] Les molécules cationiques pourraient aussi s'associer avec les bactéries directement étant donné qu'elles possèdent un potentiel zêta négatif.[53] Les lipides anioniques et les protéines chargées négativement qui composent la membrane cytoplasmique peuvent permettre une interaction électrostatique avec les bactéricides cationiques.

Les composés d'ammonium quaternaire (QACs) sont une classe de bactéricides utilisés à titre d'antiseptique, d'agents antiplaque, ou encore, d'agent de conservation pharmaceutique.[20] Ceux-ci sont en fait des détergents dont la tête hydrophile est formée d'un ammonium quaternaire. Les QACs peuvent être très diversifiés, tant par leur type de tête polaire que par la variabilité de leur longueur de chaînes aliphatiques. Les deux types de tête polaire les plus souvent rapportés dans la littérature sont les benzylalkoniums et les alkylpyridiniums (Figure 1.4).[20,54-59] Par contre, on trouve aussi les alkyltrimethylamonium.[56,60] Il est a noter que selon l'IUPAC un ammonium quaternaire est défini comme un amine substitué par des hydrocarbyls. Or, dans la tête polaire alkylpyridinium, l'atome d'azote est inséré dans un cycle aromatique (et donc contient un lien double). Ce dernier devrait être alors classé comme un composé aminium toujours selon l'IUPAC. Par contre, ce dernier est touours classé avec les QACs dans le contexte des bactéricides. Bien que la longueur de la chaîne aliphatique des QACs puisse varier de manière considérable, il semble que les longueurs de chaînes qui privilégient l'effet bactéricide soient restreintes à 8 à 18 carbones.[56]

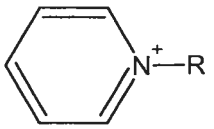

alkylpyridinium

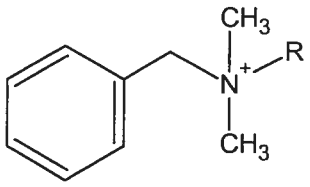

alkylbenzyldiméthylammonium

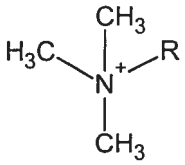

alkyltriméthylammonium

$R = (CH_2)_{7\text{-}17}CH_3$

Figure 1.4 : Représentation de quelques composés d'ammonium quaternaire (QACs) utilisés à titre de bactéricide.

Comme le phénomène de biorésistance des micro-organismes est en train de s'étendre aux bactéricides,[20] pourtant réputés pour agir de manière non sélective, une meilleure compréhension des facteurs qui influencent leur efficacité devient primordiale. Le mécanisme antibactérien des QACs semble être variable. Les QACs ont été rapportés pour leur interaction avec la membrane bactérienne.[20,56] Parmi les effets sur la membrane qui sont rapportés, on trouve : la perte de métabolites (les plus rapportés sont le K^+ et le PO_4^{2-}), la lyse des cellules, la disparition des enzymes membranaires, etc.[56] Plus spécifiquement, pour les bactéries riches en lipopolysaccharides dans leur membrane (Gram négatif), les QACs causeraient le déplacement des cations associés à la membrane externe modifiant alors leur équilibre, alors que pour les Gram positifs (dont la membrane est plus épaisse, uniforme et dense), les QACs affecteraient la perméabilité de leur membrane cytoplasmique.[20] Le chlorure de cétylpyridinium est un QAC utilisé dans les rinces bouche (Cépacol et Scope) afin de combattre la plaque dentaire.[43] Son effet bactéricide a d'ailleurs été démontré sur *Streptococcus mutans*.[57,58] Par contre, les détails de son mécanisme d'action ne sont pas donnés. Il a aussi été montré efficace en tant que bactéricide contre les biofilms *in vitro* de *Streptococcus sobrinus* lorsque incorporé dans un vernis dégradable.[59] Cet effet serait dû à une meilleure accumulation du CPC dans les biofilms.[59] Prenons un autre exemple; les benzyldimethylalkoniums qui sont utilisés comme agent bioactif dans les hydrogels transparents employés pour le contrôle de la croissance des biofilms à la surface de divers outils submersibles.[54] Leur pouvoir bactéricide a été montré sur les deux espèces suivantes : *Pseudomonas aeruginosa* et *Staphylococcus aureus*.[55]

La longueur de chaîne des QACs influence leur effet bactéricide. Par exemple, le benzyldimethylalkonium se montre efficace sur les *P. aeruginosa* à partir de 10 carbones et plus lorsque l'espèce est cultivée sous forme planctonique avec un maximum d'efficacité pour les chaînes plus longues (16 et 18 carbones). Mais si *P. aeruginosa* est cultivé sous forme biofilm, l'effet bactéricide se limite entre 10 et 16 carbones avec un maximum d'efficacité à 12 carbones.[55] De manière similaire,

le pouvoir bactéricide sur *S. aureus* n'apparaît que si la chaîne possède au moins 12 carbones.[55] Une autre étude met en évidence l'effet de la longueur de chaîne pour les triméthylalkoniums en tant qu'antimicrobien sur des levures de *Candida albicans*.[60] Lorsque la chaîne aliphatique possède 16 carbones, le détergent est plus efficace par rapport à celui dont la chaîne aliphatique n'a que 12 carbones.[60] Ces études semblent démonter qu'il existe une longueur de chaîne minimale, voir optimale, au pouvoir bactéricide des QACs.

Nous avons étudié l'effet des QACs sur la perméabilité et leur association avec des membranes lipidiques. Plus particulièrement, nous avons étudié l'effet de la composition lipidique des membranes modèles lors de l'association du chlorure de cétylpyridinium avec ces dernières. Les membranes bactériennes étant composées de phospholipides chargés négativement,[61] nous avons vérifié si l'efficacité des QACs en tan que bactéricide ne viendrait pas d'une affinité accrue avec les lipides anioniques de la bicouche. Nous avons aussi vérifié comment le chlorure de cétylpyridinium affectait la perméabilité des membranes modèles composées de différents phospholipides. Aussi, afin de sonder le potentiel bactéricide des QACs, nous avons vérifié l'influence du type de tête polaire et de la longueur de chaîne aliphatique des QACs sur la perméabilité et leur affinité avec les membranes lipidiques.

L'étude des détergents et de leur interaction avec les membranes lipidiques a été faite via diverses techniques. Entre autre, l'effet des détergents sur la morphologie des bicouches lipidiques a été étudié par turbidimétrie via la diffusion de la lumière,[62-64] par diffusion des neutrons (SANS) ou des rayons X (SAXS)[65]. La cryo microscopie électronique a même permis de voir directement la morphologie des systèmes détergent-lipide.[66-68] Aussi, la spectroscopie RMN s'est avérée comme une technique très puissante pour suivre la morphologie en fonction des mélanges lipides-détergents.[65,69,70] Plusieurs diagrammes de phase, réalisés avec les techniques énumérées ci-haut, ont été tracés pour des systèmes d'eau-détergent-

lipide.[62,70] La microcalorimétrie à titration isotherme (ITC) est une technique de plus en plus utilisée pour l'étude de l'affinité des détergents avec les membranes lipidiques.[71-74] De cette technique, il est possible d'obtenir la constante d'affinité des détergents pour les membranes lipidiques et d'obtenir les constantes thermodynamiques qui gèrent cette association.

Nous avons utilisé la méthode ITC pour définir l'affinité des QACs avec les membranes. Cette dernière est une technique suffisamment sensible pour détecter l'enthalpie de solubilisation des micelles.[75] Le microcalorimètre enregistre l'énergie produite ou absorbée lors de l'ajout d'une substance à un échantillon. S'il y a libération d'énergie, alors la puissance imposée à la cellule échantillon sera diminuée pour la ramener à la même température que la cellule de référence, il y a alors lecture d'un pic négatif. Inversement, s'il y a consommation d'énergie, il y aura alors augmentation de la puissance fournie à la cellule échantillon, et donc, un pic positif. En faisant l'intégration de ces pics, l'enthalpie de la transformation est obtenue (h_i).

Cette technique peut être utilisée pour la détermination de la concentration micellaire critique (CMC) d'un détergent.[75] Dans ce type d'expériences, une solution de détergent à une concentration supérieure à sa CMC est placée dans la seringue et des injections sont faites dans la cellule à échantillon qui ne contient que de l'eau ou le tampon dans lequel on cherche à déterminer la CMC du détergent. Lors des premières injections, les micelles sont diluées dans la cellule à une concentration inférieure à la CMC. Le signal enregistré correspond alors à l'enthalpie de dissociation des micelles à laquelle s'additionne celle associée à la dilution des micelles (Figure 1.5 A). Lorsque la concentration de détergents dans la cellule approche de la CMC, la quantité de micelles qui se dissocient diminue rapidement et l'enthalpie associée à chaque injection diminue aussi (Figure 1.5 A). Ceci se traduira par une diminution de l'intensité des pics. Une fois la CMC atteinte, le signal enregistré correspond essentiellement à la dilution des micelles.

Celui-ci se caractérise par des pics similaires pour chacune des injections (Figure 1.5 A). Il est alors possible de faire l'intégration des pics et de les normaliser par rapport à la quantité de détergent injecté. On peut ensuite tracer la courbe de l'enthalpie (h_i) pour chaque injection en fonction de la concentration de détergent dans la cellule (Figure 1.5 B). La CMC est considérée comme étant la concentration au minimum de la dérivée première de cette courbe (Figure 1.5 C). Une gaussienne est simulée pour identifier ce point plus exactement.

La technique ITC a déjà été utilisée pour l'étude de l'affinité des détergents pour des membranes lipidiques.[71-74] Dans ce type d'expérience, les lipides, sous forme de vésicules, sont injectés à une solution de détergent sous forme monomère. L'enthalpie enregistrée (h_i) après chaque injection *i* est interprétée comme l'énergie de transfert des détergents dans la membrane lipidique. On peut décrire ce phénomène un équilibre de partage entre les détergents libres (D_w) dans la phase aqueuse et ceux associés à la membrane (D_m), la phase lipidique :[71,72]

$$D_w \rightleftharpoons D_m \qquad \text{Éq. 1.13}$$

La constante de partage (K_w) décrivant l'équilibre est donnée par :[72]

$$K_w = \frac{C_{Dm}}{C_L}\frac{C_w}{C_{Dm}} = C_w K \qquad \text{Éq. 1.14}$$

Où C_w est la concentration de l'eau (55 M), C_{Dw} et C_{Dm}, les concentrations à l'équilibre du détergent dans la phase aqueuse et dans la phase lipidique respectivement. C_L correspondant à la concentration totale en lipide. Comme on connaît la concentration totale en détergent dans la cellule (C_D) et que $C_D = C_{Dw} + C_{Dm}$, il est possible de définir la concentration de détergent dans la membrane comme suit :

$$C_{Dm} = \frac{KC_L C_D}{KC_L + 1} \qquad \text{Éq. 1.15}$$

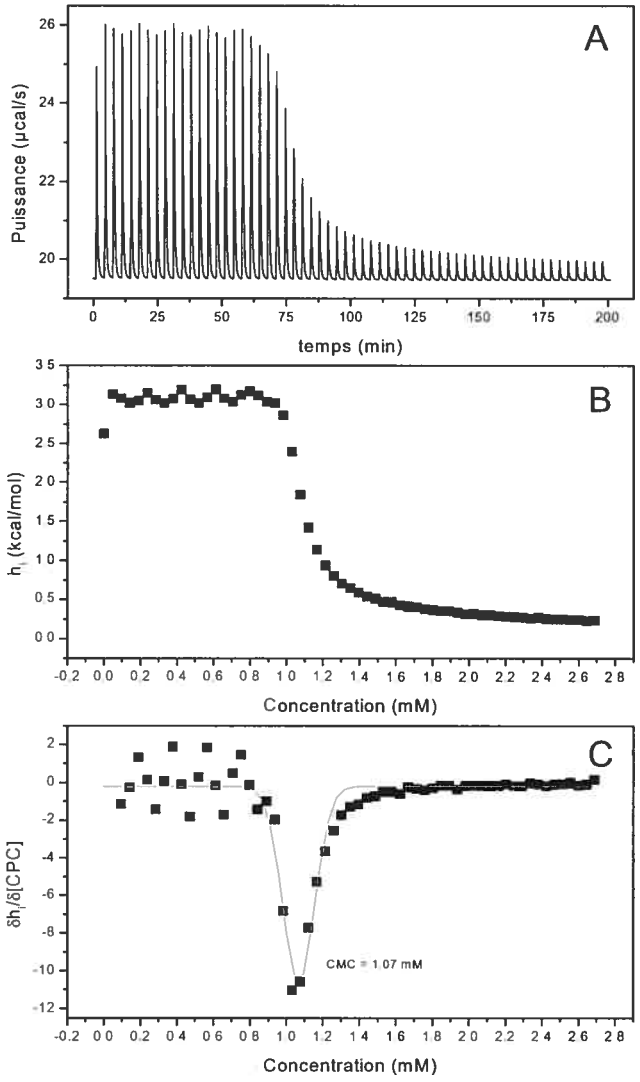

Figure 1.5 : Expérience ITC de la dilution du chlorure de cétylpyridinium (CPC) sous forme micellaire dans l'eau. A) Variation de puissance enregistrée à chaque injection au cours du titrage. B) Enthalpie donnée par l'intégration des pics divisée par le nombre de mol de CPC injecté en fonction de la concentration de CPC dans la cellule. C) Différentielle de la courbe B. Une courbe gaussienne a été simulée et la concentration micellaire critique du CPC dans l'eau est déterminé au minimum de cette courbe.

Alors que la concentration en lipide dans la cellule dépend des injections et est donnée par :

$$C_L = \frac{C_L^{\circ} i V_{inj}}{V^{\circ} + i V_{inj}} \qquad \text{Éq. 1.16}$$

Ici, C_L° réfère à la concentration en lipide dans la seringue alors que i et V_{inj}, au nombre d'injections et au volume injecté à chaque injection. V° correspond au volume initial de solution de détergent dans la cellule.

Dans ce modèle, on suppose que la variation de l'enthalpie molaire, associée au transfert d'une molécule de détergent de la phase aqueuse à la membrane, est constante durant le titrage. L'addition des enthalpies à chaque injection (H_i) est proportionnelle au nombre de moles de détergent (n_i) qui sont transférées dans la membrane selon l'équation suivante :

$$H_i = \Delta H n_i = \Delta H C_{Dm} \left(V^{\circ} + i V_{inj} \right) \qquad \text{Éq. 1.17}$$

Où ΔH est l'enthalpie molaire de partage du détergent entre les deux phases. Il est alors possible d'exprimer l'enthalpie totale (H_i) en fonction des concentrations expérimentales (et qui sont connues) de la manière suivante :

$$H_i = \Delta H C_L^{\circ} C_B V^{\circ} \frac{Ki}{KC_L^{\circ} i + \frac{V^{\circ}}{V_{inj}} + i} \qquad \text{Éq. 1.18}$$

Ce calcul n'inclut pas l'enthalpie de dilution des vésicules. Cette énergie de dilution est généralement très faible par rapport à l'énergie de partage du détergent avec la membrane. En simulant les données expérimentales avec l'équation 1.18, il est alors possible de trouver la constante de partage, K, et l'enthalpie molaire du partage (ΔH) pour divers systèmes détergent-membrane lipidique.

Comme mentionné auparavant, nous nous sommes aussi intéressés aux variations de la perméabilité de la membrane lipidique causées par les détergents QACs. Pour ce faire, nous avons suivi la fuite d'une sonde fluorescente encapsulée à l'intérieur de vésicules lipidiques. Cette approche est basée sur la propriété d'auto-extinction de la fluorescence de la sonde. Dans ce travail, la sonde fluorescente utilisée a été la calcéine. Comme cette molécule est chargée, la membrane lipidique agit en membrane quasi imperméable à la sonde, et de plus, à haute concentration la calcéine voit sa fluorescence auto-éteinte. Par exemple, en préparant les vésicules avec une concentration de calcéine au-delà de 80 mM, la fluorescence est auto-éteinte à 90%.[76]

Les perturbations des membranes, tel des défauts ou carrément des trous, causeront la fuite de la sonde encapsulée. Cette fuite sera caractérisée par une augmentation de la fluorescence car, il y aura dilution de la sonde dans le milieu environnement. Une expérience type est montrée à la Figure 1.6. Initialement (de 0 à 30 secondes), le fluorophore est encapsulé à haute concentration et, à cause de l'auto-extinction, la fluorescence enregistrée est minime (I_b). Ensuite, à 30 secondes, une quantité donnée de détergents est ajoutée aux vésicules. S'il y a un effet sur la perméabilité de la membrane, on enregistre une augmentation de la fluorescence (I_a). Une fois le système stabilisé, on ajoute une forte dose de Triton X-100, celui-ci est reconnu pour causer l'éclatement des vésicules.[76] Cette étape permet d'enregistrer le signal maximum de l'échantillon (I_t). Nous avons trouvé le pourcentage de libération de la calcéine avec l'équation suivante :

$$R\% = \left(\frac{I_a - I_b}{I_t - I_b}\right) x100 \qquad \text{Éq. 1.19}$$

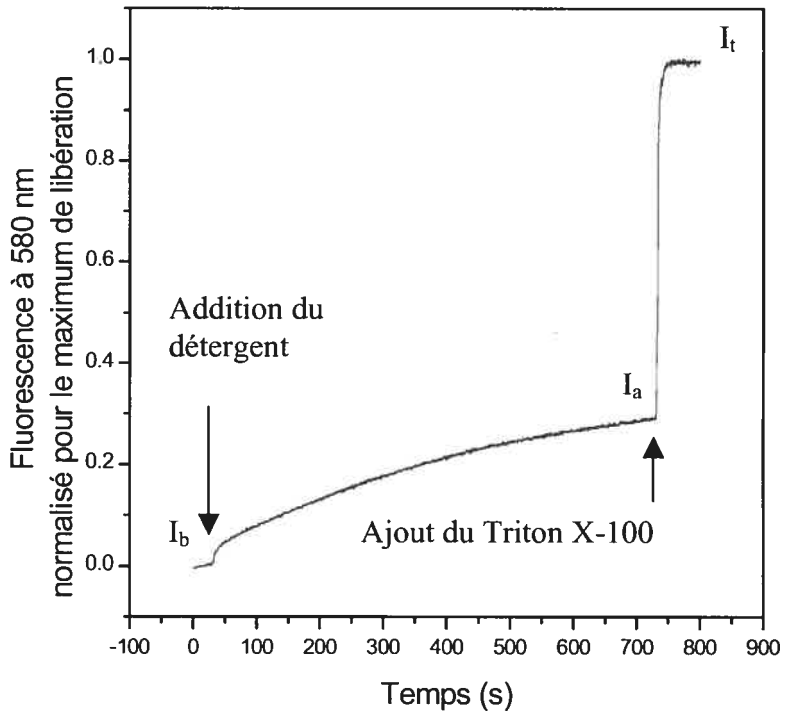

Figure 1.6 : La courbe de fluorescence montre où ont été enregistré les I_b, I_a et I_t qui permettent d'obtenir le pourcentage de libération.

1.4 Présentation des chapitres

Dans mes travaux de thèse, l'étude de la diffusion dans les biofilms ainsi que l'effet d'une classe de bactéricides sur les membranes modèles de bactéries ont été menées dans le souci d'apporter de l'information supplémentaire pour aider à la lutte ou au contrôle des biofilms bactériens.

Au chapitre 2, nous avons suivi la diffusion de polyéthylène glycol de différentes masses afin de vérifier l'effet de taille sur la diffusion. Aussi, le suivi de la diffusion de micelles de chlorure de cétylpyridinium, de dodécylsulfate de sodium et de Triton X-100 dans les biofilms de *Streptococcus mutans*, nous a permis d'explorer l'effet de la charge sur la diffusion de ces particules. La diffusion de macromolécules de différentes tailles et de macroassemblages a été étudiée via la spectroscopie infrarouge par ATR. Dans ce chapitre, nous faisons la démonstration de l'effet de taille sur la diffusion à l'intérieur du biofilm de *Streptococcus mutans* et de l'influence de la charge sur la diffusion de macroassemblages chargés. L'aspect de la pénétrabilité du biofilm par les solutés sera aussi discuté.

Dans le chapitre 3, la microspectroscopie Raman s'est avérée une technique très puissante pour définir la répartition de la biomasse dans les biofilms de *S. mutans*. De plus, nous avons montré qu'il est possible d'identifier la répartition de molécules diffusantes à l'intérieur du biofilm de *S. mutans* en fonction de la répartition de la biomasse.

Notre étude sur l'effet du chlorure de cétylpyridinium sur les membranes bactériennes est présentée au chapitre 4. Dans ces travaux, nous avons vérifié s'il y avait une influence sur la présence de charges négatives dans la membrane lipidique sur l'association du détergent ave celle-ci. De plus, l'effet du chlorure de cétylpyridinium sur la perméabilité des membranes modèles a aussi été étudié en fonction de la composition en lipides.

Dans le chapitre 5, nous avons plutôt étudié l'effet de la longueur de chaîne aliphatique et du type de tête polaire sur l'association du détergent dit composé d'ammonium quaternaire (QAC) avec les membranes lipidiques. Nous avons aussi vérifié l'effet de ces détergents sur la perméabilité des membranes.

Finalement, une conclusion générale de ces travaux est présentée au chapitre 6.

1.5 Références

1. J. W. Costerton, Z. Lewandowski, D. de Beer, D. Caldwell, D. Korber and G. James, J. Bacteriol. **176**, 8, 2137 (1994)
2. L. V. Evans. *Biofilms: Recent Advances in Thier Study and Control.* (Harwood Academic Plublishers, Amsterdam, 2000)
3. I. W. Sutherland, Microbiology **147**, 3 (2001)
4. A. Brooun, S. Lui and K. Lewis, Antimicrob. Agents Chemother. **44**, 3, 640 (2000)
5. J. Wimpenny, W. Manz and U. Szewzyk, FEMS Microbiol. Rev. **24**, 661 (2000)
6. X. Zhang and P. L. Bishop, J. Environ. Eng. **127**, 9, 850 (2001)
7. J. D. Bryers and F. Drummond, Biotechnol. Bioeng. **60**, 4, 462 (1998)
8. R. Baselga, I. Albizu, M. De la Cruz, E. Del Cacho, M. Barberan and B. Amorena, Infect. Immun. **61**, 11, 4857 (1993)
9. G. D. Christensen, L. M. Baddour and W. A. Simpson, Infect. Immun. **55**, 12, 2870 (1987)
10. G. D. Christensen, W. A. Simpson, J. J. Younger, L. M. Baddour, F. F. Barrett, D. M. Melton and E. H. Beachey, J. Clin. Microbiol. **22**, 6, 996 (1985)
11. S. Herles, S. Olsen, J. Afflitto and A. Gaffar, J. Dent. Res. **73**, 11, 1748 (1994)
12. B. Amorena, E. Gracia, M. Monzo, J. Leiva, C. Oteiza, M. Perez, J. ALabart and J. Hernandez-yago, J. Antimicrob. Chemother. **44**, 43 (1999)

13. J. Barbeau, L. ten Bokum, C. Gauthier and A. P. Prévost, Journal of Hospital Infection **40**, 303 (1998)
14. M. W. Jr. Dunne, E. O. Jr. Mason and S. L. Kaplan, Antimicrob. Agents Chemother. **37**, 12, 2522 (1993)
15. R. J. Palmer and C. Sternberg, Curr. Opin. Biotechnol. **10**, 263 (1999)
16. D. E. Nivens, R. J. Palmer and D. C. White, J. Ind. Microbiol. **15**, 263 (1995)
17. S. R. Wood, J. Kirkham, P. D. Marsh, R. C. Shore, B. Nattress and C. Robinson, J. Dent. Res. **79**, 1, 21 (2000)
18. Percot, A. 1995; Université de Rouen.
19. D. G. Cvitkovitch, Y.-H. Li and R. P. Ellen, J. Clin. Invest. **112**, 11, 1626 (2003)
20. A. D. Russell, Lancet Infectious Diseases **3**, 794 (2003)
21. D. J. Evans, D. G. Allison, M. R. Brown and P. Gilbert , J. Antimicrob. Chemother. **27**, 177 (1991)
22. N. W. Wright, M. J. Evans, M. P. E. Slack and H. L. Walmsley, J. Gen. Microbiol. **135**, 1291 (1989)
23. J. D. Vrany, P. S. Stewart and P. A. Suci, Antimicrob. Agents Chemother. **41**, 6, 1352 (1997)
24. P. S. Stewart, J. Rayner, F. Roe and W. M. Rees, J. Appl. Microbiol. **91**, 525 (2001)
25. N. W. Wright, S. M. Dorrington, M. P. E. Slack and H. L. Walmsley, Antimicrob. Agents Chemother. **32**, 4, 518 (1988)
26. B. D. Hoyle, J. Alcantara and J. W. Costerton, Antimicrob. Agents Chemother. **36**, 9, 2054 (1992)
27. J. R. Lawrence, G. M. Wolfaardt and D. R. Korber, Appl. Environ. Microbiol. **60**, 4, 1166 (1994)
28. T. Thurnheer, R. Gmür, S. Shapiro and B. Guggenheim, Appl. Environ. Microbiol. **69**, 3, 1702 (2003)
29. P. S. Stewart, Biotechnol. Bioeng. **59**, 3, 261 (1998)

30. H. Takahashi, Sinoda K. and Hatta I., Biochim. Biophys. Acta **1289**, 209 (1996)
31. K. Ahmed, P. Gribbon and M. J. Jones, J. Liposome Res. **12**, 4, 285 (2002)
32. J. J. Birmingham, N. P. Hugues and R. Treloar, Philos. Trans. R. Soc. London, B **350**, 325 (1995)
33. E. Guiot, P. Georges, A. Brun, M. P. Fontaine-Aupart, M. N. Bellon-Fontaine and R. Briandet, Photochem. Photobiol. **75**, 6, 570 (2002)
34. D. de Beer, P. Stoodley and Z. Lewandowski, Biotechnol. Bioeng. **53**, 151 (1997)
35. H. N. Newman and M. Wilson. *Dental Plaque Revisited Oral Biofilms in Healt and Desease* (Bioline, London, 1999)
36. R. J. Nisengard and M. G. Newman. *Oral Microbiology and Immunology* (W. B. Saunders Company, Philadelphia, 1994)
37. J. Barbeau. *Microbiologie et pathogénèse des infections bucco-faciales.* (Université de Montréal, Montréal, 1993)
38. J. Leduc, C. Gauthier and J. Barbeau, Journal Dentaire du Québec **36**, 289 (1999)
39. X. Chen and P. S. Stewart, Environ. Sci. Technol. **30**, 6, 2078 (1996)
40. G. O'Toole, H. B. Kaplan and R. Kolter, Annu. Rev. Microbiol. **54**, 49 (2000)
41. P. A. Suci, M. W. Mittelman, F. P. Yu and G. G. Geesey, Antimicrob. Agents Chemother. **38**, 9, 2125 (1994)
42. P. A. Suci, J. D. Vrany and M. W. Mittelman, Biomaterials **19**, 327 (1998)
43. A. S. Landa, H. C. van der Mei and H. J. Busscher, Adv. Dent. Res. **11**, 4, 528 (1997)
44. P. A. Suci, G. G. Geesey and B. J. Tyler, J. Microbiol. Methods **46**, 193 (2001)
45. N. J. Harrick. *Internal Reflection Spectroscopy* (Harrick Scientific Corporation, Ossining, 1979)
46. Crank, J. *The Mathematics of Diffusion;* 2nd ed. Clarendon press: Oxford, 1975.

47. J.-M. Petit, X. X. Zhu and P. M. Macdonald, Macromolecules **29**, 1, 70 (1996)
48. J.-M. Petit, B. Roux, X. X. Zhu and P. M. Macdonald, Macromolecules **29**, 6031 (1996)
49. S. Kwak and M. Lafleur, Macromolecules **36**, 3189 (2003)
50. S. Kwak and M. Lafleur, Appl. Spectrosc. **57**, 768 (2003)
51. H.-J. Kim, E. J. M. Gias and M. N. Jones, Colloids Surf. A **149**, 561 (1999)
52. P. Stoodley, D. de Beer and Z. Lewandowski, Appl. Environ. Microbiol. **60**, 8, 2711 (1994)
53. T. Saito, T. Takasuka, T. Kato, K. Ishihara and K. Okuda, Arch. Oral Biol. **42**, 8, 539 (1997)
54. M. J. Smith, T. H. Flowers, M. J. Cowling and H. J. Duncan, Water Res. **36**, 1423 (2002)
55. C. Campanac, L. Pineau, A. Payard, G. Baziard-Mouysset and C. Roques, Antimicrob. Agents Chemother. **46**, 5, 1469 (2002)
56. Russell, A. D.; Chopra, I. *Understanding Antibacterial Action and Resistance* Ellis Horwood: Chichester, 1990.
57. Y. Shimazaki, M. Mitoma, T. Oho, Y. Nakano, Y. Yamashita, K. Okano, Y. Nakano, M. Fukuyama, N. Fujihara, Y. Nada and T. Koga, Clinical and Diagnostic Laboratory Immunology **8**, 6, 1136 (2001)
58. J. Ali, R. Khar, A. Ahuja and R. Kalra, Int. J. Pharm. **238**, 1-2, 93 (2002)
59. D. Steinberg, M. Moldovan and D. Mulokandov, J. Antimicrob. Chemother. **48**, 2, 241 (2001)
60. B. Ahlström, M. Chelminska-bertilsson, R. A. Thompson and L. Edebo, Antimicrob. Agents Chemother. **41**, 3, 544 (1997)
61. E. I. Szabo, B. H. Amdur and S. S. Socransky, Caries Res. **12**, 21 (1978)
62. T. Inoue, T. Yamahata and R. Shimozawa, J. Colloid Interface Sci. **149**, 2, 345 (1992)
63. A. Partearroyo, A. Alonso, F. M. Goni, M. Tribout and S. Paredes, J. Colloid Interface Sci. **178**, 156 (1996)
64. M. Corti and V. Degiorgio, Opt. Commun. **14**, 3, 358 (1975)

65. M. Almgren, Biochim. Biophys. Acta **1508**, 146 (2000)
66. K. Edwards and M. Almgren, J. Colloid Interface Sci. **147**, 1, 1 (1991)
67. M. Silvander, G. Karlsson and K. Edwards, J. Colloid Interface Sci. **179**, 104 (1996)
68. K. Edwards, J. Gustafsson and G. Karlsson, J. Colloid Interface Sci. **161**, 299 (1993)
69. R. N. A. H. Lewis and R. N. McElhaney, Biophys. J. **79**, 1455 (2000)
70. R. Koynova and B. Tenchov, Curr. Opin. Colloid Surf. Sci. **6**, 277 (2001)
71. H. Heerklotz and J. Seelig, Biochim. Biophys. Acta **1508**, 69 (2000)
72. P. Hoyrup, J. Davidsen and K. Jorgensen, J. Phys. Chem. **105**, 2649 (2001)
73. M. R. Ewnk and J. Seelig, J. Phys. Chem. **101**, 5224 (1997)
74. A. Tan, A. Ziegler, B. Steinbauer and J. Seelig, Biophys. J. **83**, 1547 (2002)
75. P. R. Majhi and S. P. Moulik, Langmuir **14**, 3986 (1998)
76. A. Percot. *Développement de systêmes polymère-(poly)peptide en vue de l'immobilisation de vésicules lipidiques.* (Thèse de l'Univesité de Montréal, Montréal, 2000)

Chapitre 2

Solute Size Effects on the Diffusion in Biofilms of *Streptococcus mutans*.

Lucie Marcotte, Héloïse Thérien-Aubin, Christophe Sandt, Jean Barbeau and Michel Lafleur, *Biofouling* **20**, 189-201 (2004)

Key words: Biofilm, Diffusion, Polyethylene glycol, Detergent, FTIR, ATR

Abbreviated title: Size Effect on Diffusion in Biofilm

2.1 Abstract

The diffusion of poly(ethylene glycol) (PEG) (MW varying between 200 and 10 000), and of three different types of micelles were examined in *Streptococcus mutans* biofilms using infrared spectroscopy. PEGs were used because they show limited interactions with biological materials and their weight can be selected in order to cover a wide range of size. The study shows that a considerable fraction at the base of the biofilm is not accessible to the diffusing solute molecules and this inaccessible fraction is very dependent on the size of diffusing molecules. In parallel, it is found that the diffusion coefficients of these solutes in the biofilms are smaller than those in water and this reduction is less pronounced for large macromolecules, an effect proposed to be related to their limited penetration. Triton X-100, a neutral detergent, forms micelles that behave like PEG, suggesting that the behavior observed for neutral macromolecules can be extrapolated to neutral macroassemblies. However, the diffusion as well as the penetration of sodium dodecylsulfate micelles (a negatively charged surfactant), and cetylpyridinium chloride micelles (positively charged) in the biofilms appear to be significantly influenced by electrostatic interactions with biofilms components. The present findings provide useful insights associated to the molecular parameters required to penetrate efficiently bacterial biofilms. The study suggests a rationale for the limited bactericidal power of some antibiotics (the large ones). The restricted accessibility of macromolecules and macroassemblies to biofilms must be examined carefully to offer guidelines in the development of novel antibacterial treatments.

2.2 Introduction

Bacterial biofilms are complex suprastructures where microcolonies of bacteria are organized within exopolysaccharide matrices.[1-4] The matrices are mainly made of polysaccharides, but also contain proteins, DNA, and other metabolites.[1,3,5,6] This organization appears to provide some protection to the bacteria from environmental factors. For example, several papers in the literature report that higher doses of bactericide are needed to eradicate bacteria existing in biofilms compared to their planktonic form.[1,2,7-9] Rationales proposed to explain this phenomenon include changes in the bacterial physiological state,[7,10] inactivation of the antibacterial agents by some biofilm components,[11,12] and hindered diffusion of the agents in biofilms.[1,13,14] The present work examines the putative contribution of the latter and more specifically, how the size of a solute influences its transport properties in biofilms.

It is well established that molecular diffusion in polysaccharide hydrogels is generally limited (e.g. 15-18). In general, it is proposed that the polymer network acts as obstacles that hinder the diffusion of solutes (e.g. 15). Large solutes are generally more sensitive to the presence of polysaccharide hydrogels and the reduction of their diffusion coefficients is more pronounced.[18-21] Biofilms, indeed, show additional levels of complexity, because of the obstacles constituted by the bacteria themselves, the existence of water channels, and the fact that the matrix is heterogeneous from the composition.[3,22-28] Diffusion in biofilms has been studied using several approaches, including the dosage of antibiotics accumulation in biofilms[27], the passage of bactericides through biofilms grown on membranes,[29,30] confocal laser scanning microscopy,[13,31-34] vibrational spectroscopy,[35-37] and microelectrode probing.[38,39] From these studies, it is concluded that the diffusion in biofilms can be influenced by several factors, including the size of the analyte, its hydrophilicity, and the affinity of the diffusing solutes for specific gel

components.[35-37,40-43] The effect of the molecular weight of the diffusing solutes has been suggested to be determinant in the diffusion process.

The relative diffusion coefficient is expressed by D/D_0, where D and D_0 are the diffusion coefficients of a solute in a biofilm and in water, respectively. This parameter is suitable to highlight the effect of the solute size on its diffusion within biofilms as it is normalized for the different diffusion coefficients observed in water for the different solutes. There is a relative wide range of relative diffusion coefficients reported in the literature, probably as a result of the diversity of biofilms, of probes, of conditions that were explored, and, to a certain extent, of the techniques used for the measurements. In an effort to extract some trends from these data, it was calculated that the mean relative diffusion coefficient of small solutes (defined as having a molecular weight of 44 or less) in biofilms was 0.43 ± 0.22, whereas it was 0.29 ± 0.24 for the large molecules (i.e. MW > 44, the largest considered solutes being sucrose).[14] These averages, however, are associated to a large variability. For example, the relative diffusion coefficient of sucrose (MW= 342) in dental plaque was reported to be 0.043, and 0.18, in two independent studies.[44,45] A similar observation is made for diffusion of fluorescein (MW= 332), where the relative diffusion coefficient varies from 0.023 to 0.97.[14] The density of the biofilms, specific or non-specific association of the probe with biofilm components, and the consumption of the probes (such as sugars and O_2) by the cells can be associated with these differences. Interestingly, significant differences were reported for the diffusion of sucrose in dead and living dental plaque.[45] For macromolecules (MW > 3 kDa), the diffusion coefficients appear to be even more affected by the presence of biofilms. Measurements of the diffusion of dextrans in biofilms showed that the diffusion of these macromolecules (MW= 4 kDa to 2 000 kDa) was reduced considerably compared to those in aqueous solutions[13,32,46] and the calculated relative diffusion coefficients varied from 0.006 to 0.03 for multi-species biofilms,[46] and from 0.021 to 0.125 for *Pseudomonas fluorescens* biofilms.[32]

Streptococcus mutans, a main constituent of dental plaque, is well known for its ability to form dense biofilms *in vivo* and *in vitro* that tightly adhere to the substrata. The most effective way to eliminate dental plaque is by mechanical removal. Over the last few years, antibacterial mouthwashes and toothpastes have been elaborated to help controlling the production of dental plaque between the mechanical interventions.[43,47,48] One class of the antibacterial agents included in some oral products is surfactants. For example, sodium dodecylsulfate (SDS) is used in oral mouthwashes like Plax® whereas cetylpyridinium chloride (CPC) is used in Cepacol® and Scope®. In aqueous media, these surfactants aggregate and form micelles. The formation of micelles probably affects the diffusion properties of surfactants in biofilms because of their nanoscopic size.

In this work, the influence of the solute size on transport properties in biofilms was examined using infrared (IR) spectroscopy with attenuated total reflectance (ATR) sampling, an approach successfully applied for similar studies.[35,36,40] Two systems were investigated. First, the diffusion of a poly(ethylene glycol) (PEG) series with different MWs (107, 200, 1000 and 10 000) and, as a consequence, different size was characterized. In this study, these molecules were selected to cover a considerable range of hydrodynamic radii, from 2 to about 25 Å. PEGs are soluble in water, known to adopt a spherical shape in aqueous medium,[49] and to interact very weakly with biomolecules. As an indication of the limited interactions of PEGs with bacterial biofilms, it has been shown that the presence of PEG grafted at the surface of phospholipid vesicles inhibits the vesicle adsorption on biofilms.[50] These characteristics make the PEG series highly suitable for isolating size effects. Second, the diffusion of three surfactant micelles, CPC, SDS and Triton X-100 in *S. mutans* biofilms was examined. The comparison of the diffusion in biofilms of macromolecules (PEGs) and macroassemblies (micelles) is discussed. In addition, because SDS is negatively charged whereas CPC carries a positively charge, the putative influence of the electrostatic interactions between the micelles and the

biofilms was also examined. Triton X-100 was selected as a neutral micelles control. Triton X-100 also displays some antibacterial activity because of its ability to disrupt lipid membranes.[51] Microbiological characterization of the biofilms exposed to the micelles was also performed. Putative relationships between diffusion properties and antibacterial activity are discussed.

2.3 Materials and Methods

Streptococcus mutans NTCC 10 449 was used in this study. It was taken from an aliquot at -70°C, plated on sheep blood agar at 37° C for 48 hours, and then conserved at 4° C. For liquid cultures, the Trypticase Yeast Extract medium (TYE) was used: 17 g/L Trypticase Peptone (BBL$^{(R)}$ Becton Dickinson and Company, Cockeysville, USA), 3 g/L Yeast extract (BBL), 5 g/L NaCl (Fisher Scientific, Fair Lawn, USA) and 2.5 g/L Na_2HPO_4 (A&C American Chemical Ltd., Montreal, Canada). For all the experiments, ultra-pure water was used and all media were sterilized by autoclaving at 121° C for 20 minutes.

Biofilms were grown *in situ* in an attenuated total reflection (ATR) flow cell, and their formation on the crystal was probed by the observation of bands in the IR spectrum attributed to the main biofilm components, namely proteins, DNA and sugars. The experimental attenuated total reflection infrared (ATR-IR) set-up was similar to those developed by other groups (e.g. 35,36,42,43) except that the flow cell was thermostated at 36 ± 1° C during the whole experiments. This temperature helped to grow biofilms over reasonable periods of time. The flow cell (Harrick Scientific Corp., Ossining, USA) was equipped with a trapezoidal ZnSe crystal (50 x 10 x 2 mm^3, with an aperture angle of 45°). The volume of the flow cell was about 2.4 mL. All the tubing was made of Tygon whereas the connectors were in Teflon. Initially, the sterilization of the cell and the tubing was ensured by flowing ethanol (70%) through the system for 1 h. Subsequently, the system was rinsed with sterile ultra-pure water. The cell was then seeded with *S. mutans*. The

inoculums were prepared by inoculating TYE buffer containing 0.5 % (w/v) of sucrose with *S. mutans* and incubating the culture at 37° C with a slight agitation for 20 hours. In these conditions, the optical density of the culture was between 0.5 and 0.6 at 660 nm, corresponding to about 3.3 x 10^8 colony forming units (CFU). This corresponded to the beginning of the stationary phase in the growth curve (data not shown), and ensured that the ATR flow cell was seeded with physiologically similar bacteria. Two hundred and fifty milliliters of the inoculum was flown through the ATR cell at a flow rate of ~0.5 mL/min using a peristaltic pump (MasterFlex, Cole-Parmer, Montréal, Canada). Special care was taken to pump only the supernatant of the suspension because uptake of bacteria aggregate sediment during the inoculation led to non-uniform biofilms at a macroscopic scale. Subsequently, fresh TYE with 0.5% sucrose was passed through the system (0.5 mL min^{-1}) for 15 h to allow the biofilm formation. During the inoculation and the growth periods, IR spectra were recorded every hour by co adding 3 600 scans for each spectrum.

Experiments to examine the diffusion of D_2O, di(ethylene glycol), PEG 200, PEG 1000, PEG 10 000, SDS, Triton X-100, and CPC were performed after the 15-h growth phase. All these diffusing solutes were obtained from Sigma (Oakville, Canada). The diffusing solutes were added in the TYE 0.5% (w/v) sucrose medium flowing over the biofilms. The concentration of diethylene glycol was 5% (w/v), whereas that of PEG 200, PEG 1000, and PEG 10000 was 3% (w/v). In the case of SDS and Triton X-100, the dispersion was 10 % (w/v). For CPC, a concentration of 2% (w/v) in a sucrose-free TYE medium was used, since CPC was found to be poorly soluble in presence of sugar. The concentrations of the three surfactants were well above their critical micelle concentration (CMC), to ensure that most of the detergent molecules existed in the micellar form, and were selected to provide a reasonable signal to noise ratio in the IR spectra. Because they depend on the physico-chemical properties of the medium, the CMC of the detergents were determined in the TYE medium, using isotherm titration calorimetry.[52] A VP-ITC

microcalorimeter from MicroCal Incorporated (Northampton, MA) was used for these experiments. The resulting CMC values in the TYE medium were: CMC (SDS) = 0.60 ± 0.03 mM; CMC (CPC) = 23.4 ± 1.1 μM; CMC (Triton X-100) = 0.224 ± 0.010 mM. It should be noted that these values are similar to or smaller than the reported values in pure water (CMC (SDS) = 7.78 mM; CMC (CPC) = 1.12 mM; CMC (Triton X-100) = 0.23 mM).[52] In the experiment conditions, the concentrations used in the ATR cell corresponded to 830, 2500, and 690 times their CMC in the TYE medium for SDS, CPC, and Triton X-100, respectively. The transition between the fresh substrate and the diffusing media was accelerated by increasing the flow rate to 10 mL min^{-1} for 40 s for the PEG 10 000, 30 s for the other PEGs and diethylene glycol, and 20 s for Triton X-100 and CPC. After this period, the flow was reduced back to 0.5 mL min^{-1}. These periods took into account the different viscosity of the solute-containing solutions and were sufficient to perform the complete exchange of the fluid over a clean crystal in the ATR cell. Controls, where the fresh substrate flow was accelerated in the same fashion, showed no modification to the biofilms from a spectral point of view. In addition, the visual aspect of the biofilms after this step remained a smooth and uniform, covering the whole crystal.

The diffusion of the solutes in the biofilms and, as a consequence, their progression towards the ATR crystal and the region scanned by the evanescent wave, were followed by the evolution of IR bands of the diffusing solutes. The data acquisition frequency during the diffusion period was increased to one spectrum every 30 s (30 co-added scans). Typically, the diffusion period was 1 h for the PEGs, 20 min for SDS and Triton X-100, and 7 h for CPC. Subsequently, fresh medium was circulated in the cell for 4 h and the data acquisition was performed at a rate of one spectrum (3600 scans) per h. Each system was investigated in three independent experiments.

The spectra were acquired on a FTS-25 BioRad IR spectrometer, equipped with a water-cooled globar source and a MCT detector. For all the spectra, the background was recorded with the cell purged with N_2 gas for at least 5 min. The spectra were corrected for the dependence of the penetration depth of the evanescent wave on the wavelength, based on the non-absorbing medium hypothesis. The contribution of water was removed from the spectra by subtracting the spectrum of water. The subtraction coefficient was determined using an iterative method based on the elimination of the association band of water between 2650 to 1750 cm^{-1}.[53] An offset was performed at 1850 cm^{-1}, a position where no absorbance was observed. For every diffusing solute, subtracting the spectrum of the biofilm recorded immediately before the diffusion phase to the spectra acquired during the solute diffusion highlighted bands characteristic of the diffusing compound. For each spectrum, the subtraction factor was established to reproduce the main spectral elements of the diffusing solutes and subsequently, the spectra were baseline corrected and offset to 0 at 1850 cm^{-1}. One characteristic band was selected for each solute (indicated by an arrow in Figure 2.3), and its area was measured as function of the time. For the diethylene glycol and the different PEGs, the C-O stretching vibration was selected and was integrated between 1020 and 1180 cm^{-1}. For SDS, the sulfate stretching vibrational mode at 1250 cm^{-1} [54,55] was chosen. It is intense and in a region relatively free of interference. The band was integrated between 1270-1198 cm^{-1}. The characteristic band of Triton X-100 was that at 1246 cm^{-1}, assigned to a vibration involving an ether group linked to an aromatic ring.[55] It was integrated between 1270-1210 cm^{-1}. Finally, the C-H stretching modes between 3000-2830 cm^{-1} were selected for CPC because they were the most intense in the spectrum. There was indeed a spectral interference from the biofilm components but the similarity of the difference spectra and the CPC spectrum between 1500-1000 cm^{-1} suggested that the spectral subtractions were reasonable. As a reference, the diffusion of water was also examined. In this case, the milieu included 10 % D_2O. Therefore, the diffusion of HOD, the most

likely form, was followed by the area of the O-D stretching band integrated between 2050 and 2775 cm^{-1}.

Biofilms display complex structures and the solute diffusion is likely heterogeneous. Attempts to describe the diffusion is such complex milieus were proposed, taking into account, for example, the presence of bacteria[56] or introducing parameters related to the porosity and the tortuosity of the matrix.[31] In the study reported here, the increase of the solute band intensity as a function of time showed, in all cases, smooth, and monotonous profiles. They could be reproduced, assuming that biofilms are homogeneous slabs of a uniform thickness, and that the diffusion is described by a single diffusion coefficient, as hypothesized previously (e.g. 32,44,56). In this case, the increase in solute band intensity (I(t)) as a function of time can be described by :[57]

$$I(t) = I_{\infty}\left(1-\sum_{i=0}^{\infty}\frac{4(-1)^{i}}{\pi\,(2i+1)}\exp[-(2i+1)^{2}Bt]\right) \qquad \text{Eq. 2.1}$$

This function reports the variation of the solute concentration at the crystal-biofilm interface. In the equation, I_{∞} is area of the solute band at $t = \infty$. Because of the series, I(t=0) is 0. In order to fit the profiles, the series were limited to the first 9 terms, leaving only B and I_{∞} free to vary. B values represent a rate of penetration of the solutes in the biofilms. In the case of the small solutes (namely diethylene glycol, and D_2O), the intensity at t = 0 was already larger than 45% of the I_{∞} value. This means that during the change from buffer to the solute-containing buffer, the solute diffusion was fast enough to penetrate significantly in the biofilm and reach its base. In these cases, to take into account the diffusion occurring during the dead time of the experiments, I(t) on the left side of Equation 2.1 was replaced by $I(t)-I_0$, I_0 being a fitted parameter. From the fitted B values, it is possible to obtain the mean diffusion coefficient, D :[57]

$$B=\frac{D\pi^{2}}{4l^{2}} \qquad \text{Eq. 2.2}$$

where l is the thickness of the biofilm. Since the diffusion is characterized by a single diffusion constant, D is referred to as the overall diffusion coefficient.

Bacteria viability in the biofilm over the ATR crystal was characterized by counting the number of CFU. This count was done after the growth phase. The surface of the ATR crystal was carefully swabbed and the recuperated biomass was dispersed in 2.5 mL of PBS buffer pH=6.2 (8.76 g/L NaCl, 6.05 g/L K_2HPO_4 (A&C) and 0.7 g/L KH_2PO_4 (A&C)). The swab was left in the buffer, and the sample was sonicated for 4 min to disrupt the aggregates. The sample was diluted from 10^{-1} to 10^{-7} and 100 µL of the solution was plated on TYE 0.5% (w/v) sucrose agar and incubated at 37° C for 48 hours. The number of colonies were counted and normalized to CFU/cm^2, considering that the surface of the crystal was 4 cm^2.

Measurements of the hydrated biofilm thickness were performed directly on the ATR crystal, using a light microscope (Leica). First, the ATR cell was opened and the excess water was drained. A small section of the biofilm was then removed from the crystal surface with a swab. The focus was made at the surface of the crystal and the z position of the platform was then set to zero. The biofilm was brought in the field and the thickness was approximated as corresponding to the vertical displacement required to focus at the top of the biofilm.[58] The mean thickness was calculated from the average of two sets of 10 measurements recorded at different places, chosen randomly on two different biofilms, by two individuals.

2.4 Results

Biofilm growth

The ATR sampling technique followed the development of biofilms *in situ*. Bands characteristic of the main biofilm components are observed in the IR spectra (Figure 2.1). The C-H stretching band, between 2700 and 3000 cm^{-1}, is

representative of the biomass because most of the biofilm components, including sugars, lipids, proteins, contribute in this region. The Amide II band, characteristic of the amide bonds in the proteins, is observed around 1540 cm^{-1}.[59,60] The use of this band as a probe was preferred over the Amide I band, located at about 1650 cm^{-1} because the latter overlaps with the H_2O deformation mode at 1650 cm^{-1} and its area is considerably affected by the correction for the water contribution. The main contribution around 1240 cm^{-1} can be attributed to phosphate vibrations[59,61-63] of phospholipids and DNA, as well as a deformation mode of a hydroxyl group attached to an aromatic ring,[64] as found in some bioadhesive proteins.[65] This band also probed the growth of the biofilms. Finally, the region of the C-O vibrations between 1182 and 982 cm^{-1} is mainly assigned to sugar contributions because of their large content in alcohol groups.[55,64] This later contribution is therefore representative of the polysaccharide content.[66-68] It is observed that the sugar bands (region between 1182 - 982 cm^{-1}) are relatively intense. This is likely a consequence of the sucrose-rich milieu, and the growth conditions optimized for the biofilm formation.

The integrated intensities of the IR bands are related to the concentration of the associated chemicals in the volume probed by the evanescent wave. The penetration of the evanescent wave is estimated to be between 2 – 3 μm above the crystal, as determined for a non absorbing media.[69] This depth is decreased for the radiations whose wavelengths correspond to strong absorption of the samples (eg. OH stretching band at 3400 cm^{-1}). The increases in the integrated intensities of the main biofilm components as a function of time are presented in Figure 2.2. During the first five hours, the inoculation period, there is no significant evolution of the IR spectra. Subsequently, while fresh medium was flowing through the cell, the intensities of the 3 bands used to probe the growth of the biofilms increased.

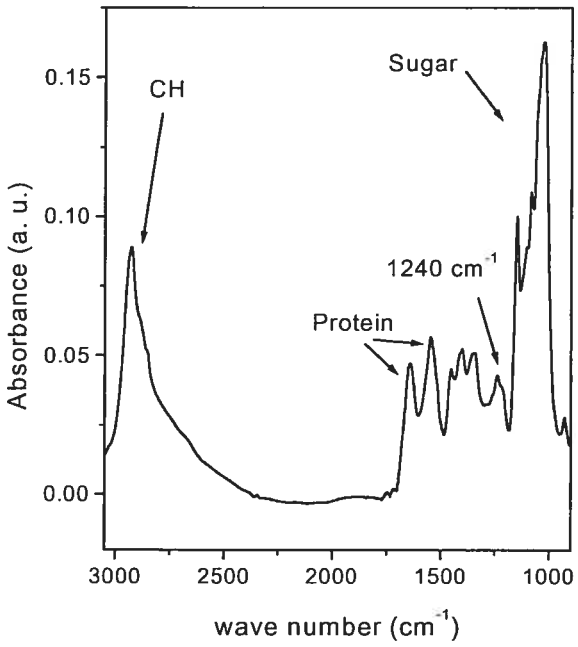

Figure 2.1 : IR spectrum of a *Streptococcus mutans* biofilm grown *in situ* in the ATR cell.

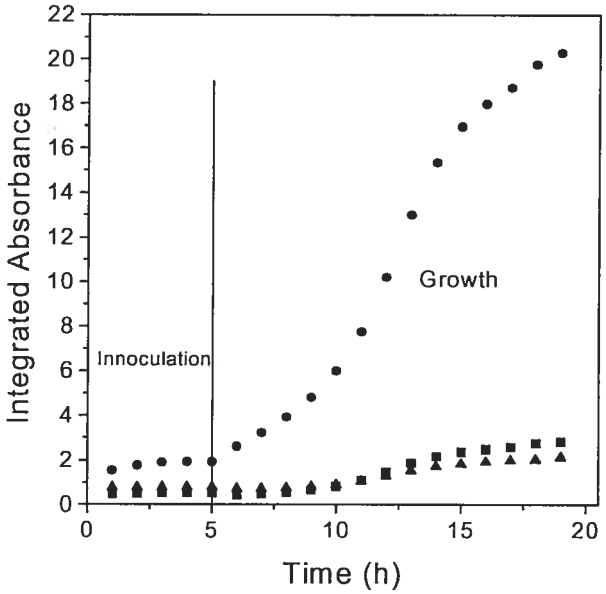

Figure 2.2 : Biofilm growth curves. The band areas were integrated: between 1478 and 1539 cm^{-1} for the Amide II band (▲), between 1270 and 1198 cm^{-1} for the 1240 cm^{-1} contributions (■), and between 1182 and 982 cm^{-1} for the sugar bands (●).

The increase was first relatively abrupt then progressively leveled off. The absolute values of the integrated intensities are indeed considerably different because of the different molar absorption coefficients associated to the different biofilms components. When normalized to their maximum intensity, the three curves showed very similar profiles, indicating their simultaneous production during the growth of the biofilm at the surface of the ATR crystal.

After about 15 h, the increase rate of the three band areas slowed down and leveled off. This is likely related to a reduction of the growth in the region probed by the evanescent wave. The formation of the biofilms was nicely reproducible, at least, as estimated by the integrated areas of the three bands that were used. The areas and their relative variations from different experiments (n=12) were 20 ± 2, 1.7 ± 0.4, and 2.3 ± 0.5 for the sugar, Amide II, and 1240 cm^{-1} bands respectively. We observed that the zone probed by the evanescent wave in the presence of biofilms was constituted by 98.3 (± 1.7) % water (n=12), based on the comparison of the intensity of the H_2O deformation band in the presence and the absence of biofilm on the crystal. This proportion is consistent with the water content reported previously for other biofilms.[2] The number of bacteria on the crystal at the end of the incubation time was estimated to 1.9 (± 0.8) x 10^8 CFU cm^{-2} (n=3). This value is consistent with a previous report.[42] The morphology of the resulting biofilms was examined under optical microscope. They appeared as films covering completely the crystal surface and including columnar structures, similar to those reported for *Pseudomonas aeruginosa.*[1] The biofilms were heterogeneous in thickness varying from 50 to 190 µm. Random measurements of the thickness at various places led to an average of 120 ± 32 µm.

Diffusion of solutes

After the growth phase, a solute was included in the system to examine its diffusion properties in the biofilm. In order to probe its penetration in biofilms, its IR signal was highlighted by spectral difference (the spectra of the biofilms during the

diffusion period minus the spectrum of the biofilm recorded just before the diffusion period). The resulting difference spectra were similar to those obtained for the diffusing solutes free in solution (Figure 2.3), indicating the validity of the approach.

The increase of the signal of PEG 10 000, SDS, Triton X-100 and CPC as a function of time are represented in Figure 2.4. The time was set to 0 at the end of the period with increased flow to change the media in the ATR flow cell. The penetration profiles of the PEG 10 000 shows that there is a rapid increase of the signal during the first 10 min, which subsequently, progressively levelled off. The resulting profiles were fitted using the Equation 2.1. The fitted parameters are reproduced in Table 2.1. In all the cases, the fits simulated reasonably well the penetration profiles. It must be noted that the diffusion period was much longer in the case of CPC.

Table 2.1: Fitting parameters for the diffusion model (Eq. 1). Errors are calculated for triplicates.

Diffusing solutes	I_0	I_∞	B (x 10^3 s^{-1})
D_2O	22 ± 10	48.30 ± 0.09	25.7 ± 2.0
Di(ethylene glycol)	0.66 ± 0.17	1.25 ± 0.06	19.9 ± 2.1
PEG 200	-	0.88 ± 0.36	7.0 ± 0.8
PEG 1000	-	0.68 ± 0.22	5.1 ± 1.5
PEG 10 000	-	0.56 ± 0.24	4.6 ± 1.4
SDS	-	2.7 ± 0.7	2.3 ± 1.1
Triton X-100	-	0.16 ± 0.05	3.9 ± 0.6
CPC[b]	-	2.2 ± 0.6	0.32 ± 0.16

[b] n=4

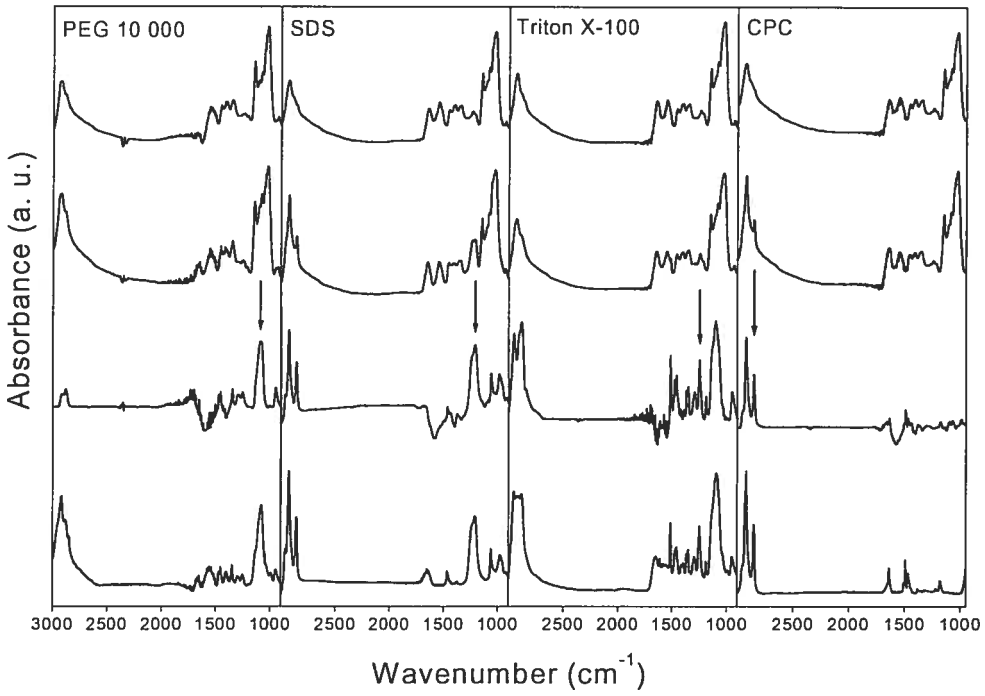

Figure 2.3 : Typical examples of the spectral treatment performed to probe the diffusion. The first and second rows show the biofilm spectra before and at the end of the diffusion period, respectively. The third row shows the spectral difference between the second- and the first-row spectra. The difference spectra are similar to the spectra of the diffusing products (bottom row). All the spectra were corrected for the water contribution as described in the Materials and Methods section. The arrows indicate the selected bands used to probe the diffusion of the different solutes.

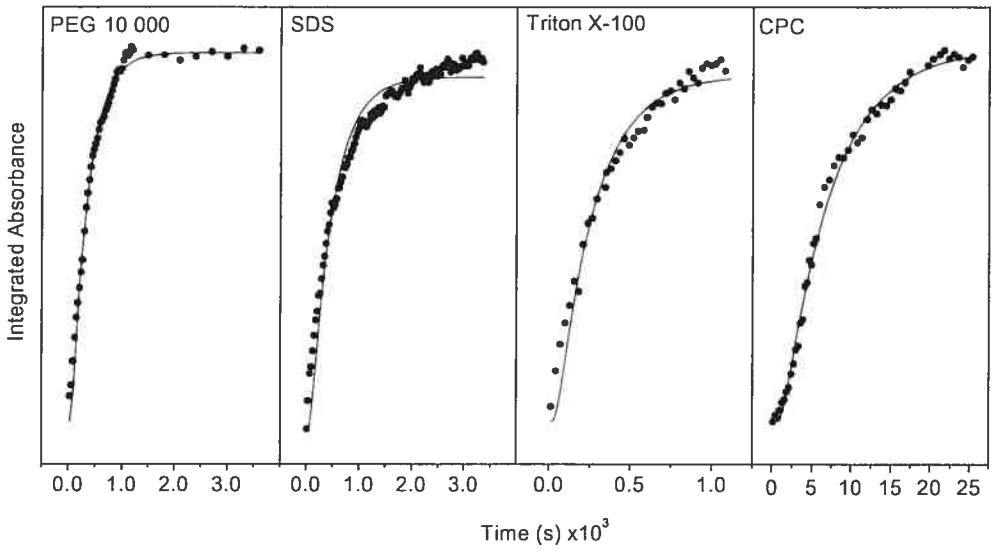

Figure 2.4 : Typical diffusion profiles of the investigated macromolecules and macroassemblies.

The penetration profiles provide two parameters related to the diffusion properties (Table 2.2). First, Equation 2.2 allows the estimation of the diffusion coefficient D, using the parameter B (Table 2.1), and the mean thickness of the biofilms. As pointed out, the diffusion coefficients provide an overall description of the diffusion because the model considers that the diffusion is described by a single D value. In addition, the model considers a uniform biofilm thickness (l) and the accuracy of D values are indeed directly related to l. The average thickness of the biofilms as measured by microscopy was used. This l value can be challenged. However, reasonable and workable assumptions had to be made to describe quantitatively the diffusion in these complex systems and it is believed that the extracted diffusion coefficients convey useful information. As shown below, these values are consistent with some of those previously reported for similar systems. In addition, it should be pointed out that the trends reported from the variations of D are also observed from the variations of B values, which are directly obtained from the simulation of the diffusion profiles. The second parameter extracted from the diffusing profiles is I_∞, which represents the concentration of the diffusing solutes at the base of the biofilm at $t = \infty$. I_∞ was used to calculate the penetration efficiency of the diffusing solutes. The penetration efficiency was obtained by comparing the area of the characteristic solute band at infinite time (I_∞) with the area of the band in the spectrum of the diffusion milieu recorded with the ATR cell in the absence of biofilm. This parameter actually compares the solute concentration at the base of the biofilm with the concentration in the diffusion medium. It should be noted that the influence of the partial volume occupied by the biofilm components is negligible. As shown above, the probed region was 98% water. Table 2.2 also includes the hydrodynamic radius (R_h) of the diffusing solutes. They were defined according to established methods and literature data (see footnotes of the Table). It should be pointed out that these radii are representative of the PEG size in water. The shape and size of the molecule may be somehow different in the biofilm environment.

Table 2.2: Hydrodynamic radii and diffusion parameters of the investigated solutes. Errors are calculated from triplicates.

Diffusing solutes	R_h Å	Penetration (%)	D^g (10^{-11} m^2/s)	D^o_w (10^{-10} m^2/s)	D/D^o_w
D_2O	1.7[a]	98 ± 3	15.0 ± 0.8	35[e]	0.040 ± 0.002
Diethylene glycol	2.9[a]	66 ±10	11.6 ± 1.2	13[e]	0.0892 ± 0.009
PEG 200	3.5[a]	50 ± 10	4.1 ± 0.5	10[e]	0.041 ± 0.005
PEG 1000	7.5[b]	27 ± 9	3.0 ± 0.9	4.3[f]	0.07 ± 0.02
PEG 10 000	27.9[b]	25 ± 10	2.7 ± 0.8	1.17[f]	0.23 ± 0.07
SDS	17[c]	79 ± 20	1.3 ± 0.6	1.9[f]	0.07 ± 0.03
Triton X-100	53[c]	13 ± 5	2.3 ± 0.3	0.62[f]	0.37 ± 0.05
CPC[d]	29[c]	86 ± 27	0.19 ± 0.09	1.1[f]	0.017 ± 0.008

[a] Calculated from van der Waals volumes.[72]
[b] Calculated from R_h=0.145 $M_w^{0.571}$.[19]
[c] [73-75]
[d] n=4.
[e] Obtained from the Stokes-Einstein relation corrected for small molecules.[72]
[f] Obtained from the Stokes-Einstein relation.
[g] Uncertainties represent the variability of B.

Two features can be observed from the data obtained from PEG and water (Table 2.2 and Figure 2.5). First, the size has a drastic effect on the percentage of penetration. The penetration of the biofilm by water is practically complete (98%) whereas it drops to 25% for the largest PEG investigated. The restriction of the penetration was observed even for small solutes, as the penetration of diethylene glycol (MW = 106) is limited to 66%. Secondly, the molecular size has also a strong influence on the parameter B (Table 2.1) and, therefore, on the derived diffusion coefficient (Table 2.2). The diffusion coefficients of PEGs in water are, indeed, dependent on their molecular weights.[19] The variation of the relative diffusion coefficients, D/D_0, of the various PEGs as a function of their molecular weight is reported in Figure 2.5 to highlight the solute size effect. Figure 2.5 shows that the diffusion of all the solutes is considerably hindered in the biofilms. This effect, however, seemed to be less pronounced for the larger solutes. The diffusion experiments were also performed for Triton X-100, CPC, and SDS micelles. Their

size, and the results extracted from their diffusion profiles are also presented in Table 2.2, and Figure 2.5.

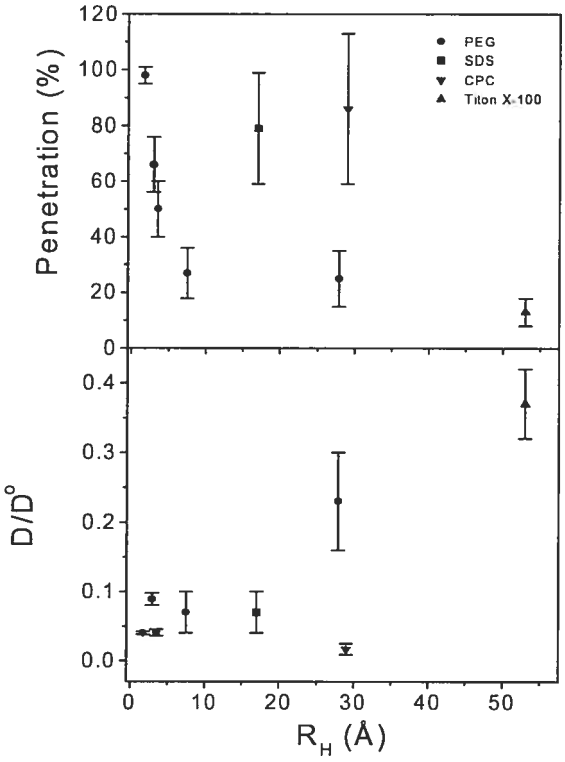

Figure 2.5 : Variations of the diffusion properties of the solutes as a function of their hydrodynamic radius. A) Penetrability efficiency, B) Relative diffusion coefficients.

After the diffusion period, the biofilms submitted to the action of surfactants were washed for 4 h with fresh medium. A spectrum of the biofilm after this wash period was recorded to determine the reversibility of the penetration of the detergent and their potential impacts on the biofilms (Figure 2.6). This step was also performed with PEGs but the polymer was completely washed from the biofilms that remained practically intact (data not shown). In the case of SDS, the detergent was partially washed from the biofilm as indicated by the decrease of the detergent IR band in the spectrum. Based on the remaining absorbance, we estimated that about 87 % of the SDS was washed away from the biofilm. Interestingly, a significant decrease in the intensity of the Amide II band at 1550 cm^{-1} is noticed after the passage of the SDS, illustrated by a negative component in the difference spectrum. This result shows that the detergent had probably extracted proteins from the bacterial biomass. Similar observations have been reported and it was suggested that this phenomenon was associated to the extraction of proteins at the surface of the bacterial membranes.[42] In the case of Triton X-100, the detergent was practically completely eliminated from the biofilms, as indicated by an almost flat difference spectrum. In the case of CPC, there was only a small reduction of the detergent signal during the 4-h wash with fresh substrate. This reduction was estimated to 15%. This result indicates that CPC associates strongly with some biofilm components and shows a limited reversibility. In addition, the fact that the biofilm contributions cancelled out in the difference spectra indicates that the detergents could not remove the biofilm from the crystal surface, illustrating the tenacious binding of such films.

The viability of the biofilms, characterized by the CFU cm^{-2}, was determined after being submitted to the action of the detergents. The absence of bactericidal power of PEG was confirmed because the CFU/cm^2 was not influenced by the PEG diffusion in the biofilm. The antibacterial efficacy of SDS and CPC was clearly observed, as submitting the biofilms to these detergents drastically affected the CFU value. No viable bacteria were found in the swab after diffusion of SDS and

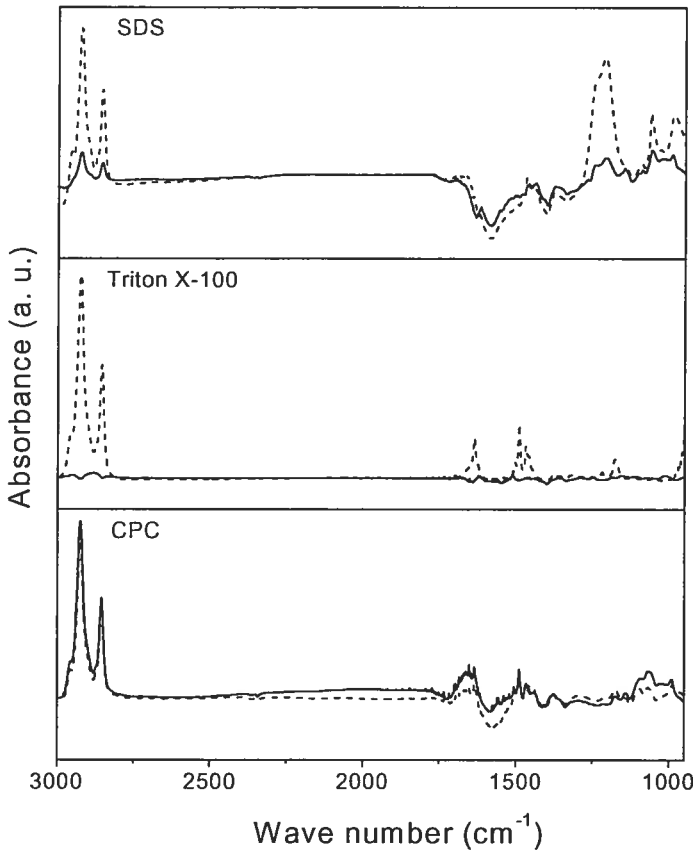

Figure 2.6 : Difference spectra highlighting the effects of the surfactants on the biofilm structures. (Solid line) Spectra of the biofilms submitted to the action of the surfactants and washed for 3 hours with fresh medium, from which the spectra of the biofilms prior to the surfactant diffusion was subtracted. (Dashed line) Spectra of the biofilms at the end of the surfactant-diffusion period, from which the spectra of the biofilms prior to the surfactant diffusion was subtracted. All spectra are represented on the same absorbance scale and were corrected for the water contributions.

CPC, and washing. Conversely, Triton X-100 showed little effects from a bactericidal point of view.

2.5 Discussion

The influence of the size of the diffusing solutes on the diffusion through *Streptococcus mutans* biofilms is illustrated by the behavior of the PEG series. To the authors' knowledge, these are the first infrared measurements of PEG diffusion in biofilms. As pointed out above, this set of molecules is suitable to highlight the size effects, as PEG are relatively inert and their size can be varied over a wide range while preserving the proportions of the functional groups forming the molecules. In addition, the data presented here cover a range of size for which the data in the literature are rather sparse. The results indicate that two aspects of the diffusion are influenced by the size of the macromolecules. First, some regions at the base of the biofilms are not accessible to solutes and the proportion of the biofilm inaccessible to the solutes increases with the solute size (Figure 2.5). Even though water can penetrate practically everywhere in the biofilms, < 30% of the biofilm appears to be accessible to PEG with a MW equal to or larger than 1 000. Biofilms are highly heterogeneous, and their structures include bacterial microcolonies, exopolysaccharide matrices, and water channels.[1,26] It is likely that macromolecules diffuse in regions with a low content of biomass, such as the water channels, whereas the dense regions show a limited accessibility to larger molecules. Therefore, large macromolecules, and macroassemblies can only invade partly biofilms, and the accessible regions may represent < 30% of the whole biofilm. Measurements with PEGs presented in this work provide a calibration curve describing this effect for molecular solutes that do not interact with biofilms. The FTIR technique does not give spatial information, but these results are consistent with measurements from other techniques on analogous systems. A recent study on the diffusion of PEG 10 000 inside *Streptococcus*

mutans biofilms by Raman microspectroscopy showed a correlation between the PEG distribution and the biomass density, the regions where PEG penetration was limited showing a high biomass density.[70] Similarly, confocal laser microscopy studies on polyspecies biofilms concluded to a heterogeneous spatial distribution of labeled dextrans.[13,32] The inhibition of the diffusion of fluorescent latex beads with a radius of 55 nm was also reported for the denser parts of *Stenotrophonas maltophilia* biofilms, as assessed by fluorescence correlation spectroscopy.[34] Moreover, it has been shown that large liposomes (100 nm of diameter) cannot penetrate in *Staphyloccocus aureus* biofilms.[50] The liposomes only adsorbed on the top 20 μm of the biofilms. Therefore, it appears that steric interactions are the main origin of the limited penetration of large solutes.

Second, the characteristic rate of the penetration, and, consequently, the diffusion coefficient also decreases as a function of size (Tables 2.1 and 2.2). The diffusion coefficients reported here for the small molecules (water, diethylene glycol) are comparable with those reported for sucrose in dental plaque,[45] and fluorescein in mixed-species biofilms.[32] The values are, however, significantly smaller than the mean reported for small solutes.[14] As mentioned above, two points have to be kept in mind. First, several factors influence the diffusion of solutes in biofilms, leading to a wide range of values for systems that are basically similar. Differences can be associated with the nature of the biofilms (e.g. compositions and density) and with the diffusing solutes (e.g. charge and hydrophobicity). From this point of view, the advantage presented of PEGs is clear. Secondly, the absolute values of D depend on the estimated biofilm thickness. This thickness, even though reasonable, may introduce systematic errors in the D values. Only additional measurements will assess the validity of the calculated D values. Only additional measurements will assess the validity of the calculated D values. In the case of the large molecules that we have investigated (>1000 MW), the calculated diffusion coefficients are in the same order of magnitude as those previously obtained with dextrans of similar size.[32,46] For example, the diffusion coefficient of dextran (M.W. = 4 000, ca. R_h of

15.4 Å) in mixed biofilms was estimated to 3.2 x 10^{-12} m^2 s^{-1}.[32] But again, there is a considerable range of reported values for different biofilms. For example, the diffusion coefficient of dextran MW 10 000 is reported to be 0.69 x 10^{-12} m^2 s^{-1} in supragingival plaque,[46] and 43.8 x 10^{-12} m^2 s^{-1} in a model of oral biofilms.[56] There are considerable variations in local chemical composition of biofilms and, consequently, the diffusion within biofilms is expected to be heterogeneous. In fact, Fluorescence Recovery After Photobleaching (FRAP) measurements have shown that diffusion coefficient of dextran (MW 10 000) varies within the very same biofilm, from 0.62 to 20 x 10^{-12} m^2 s^{-1}.[13,56] In general, the values reported here for PEGs are consistent with those previously reported for macromolecules.

This study indicates that the relative diffusion parameter (D/D_o) for the PEG series tends to increase as a function of PEG size/molar weight. A similar behavior was in fact observed when the diffusion of sucrose, and dextrans in oral biofilms was compared.[56] In addition, even though not explicitly reported in the article, a similar trend can be inferred from the diffusion coefficients of dextran in mixed-species biofilms.[32] It is proposed that the restricted accessibility to some regions of the biofilms is at the origin of the increased D/D_o values observed for larger PEGs. If large molecules have only access to regions with relatively open structures, their diffusion coefficients should approach those in water. On the other hand, the small molecules are able to penetrate almost everywhere in the biofilms and their diffusion in the areas rich in biomass may be slow; this would lead to a reduced D/D_o. This interpretation is supported by FRAP measurements that have shown that the diffusion is considerably reduced in the cell microcolonies relative to that measured in the water channels.[13] It should be noted however that a study examining the diffusion of dextrans in supragingival plaque[46] reported that the relative diffusion coefficients increase as a function of decreasing dextran molecular weight. This different behavior may be associated to the different nature of the biofilms or of the physico-chemical properties of the probes. The

examination of several other systems is required to identify the general trends and the parameters having key influence in this aspect of the diffusion behaviour.

The three investigated micellar systems show distinct behaviours. In the case of Triton X-100, the parameter B, associated to the diffusion coefficient, and the penetration efficiency are consistent with those obtained for PEG 10 000, a macromolecule slightly smaller than Triton X-100 micelles. In addition, Triton X-100 showed very little influence on the biofilms since it could be completely washed out, leaving behind viable biofilms. These results indicate very limited interactions with biofilm components. The results obtained from Triton X-100 suggest that the conclusions obtained from the PEG series can be extrapolated to macroassemblies, as long as the surfactant does not interact with biofilms components. They are also consistent with the link that we proposed between the limited accessibility to the dense regions of the biofilms, and the increased relative diffusion coefficient.

SDS forms relatively small micelles. However, the characteristic rate associated to its diffusion is significantly smaller than that of PEG with an equivalent size (Table 2.1). This phenomenon is also illustrated by a small relative diffusion coefficient. Conversely, SDS shows a penetration efficiency that is considerably higher than expected based on the results obtained with PEG (Figure 2.5). These results are indicative that SDS micelles interact with the biofilms and these interactions influence its diffusion properties. Despite the fact that SDS could be washed out from the biofilms by the flow of the fresh medium, it leaves behind damaged biofilms. A diminution of the Amide II band attributed to proteins was observed, likely a consequence of surface protein extraction caused by SDS, in agreement with a previous study.[42] This transformation may be at the origin of non-viable biofilms (the CFU cm^{-2} was 0 after the SDS diffusion). The penetration efficiency of SDS reaches 79 (± 20) %, which is considerably larger than the measured value for a PEG of equivalent size. Landa et al. (1997) have obtained similar results on

S. oralis showing that only 60% of the biofilm were accessible to SDS when a 10% (w/v) SDS suspension was used. However, they subsequently showed that SDS bioaccumulates at the base of *S. mutans* biofilms when a SDS concentration of 4% (w/v) was used.[42] All these results indicate an improved penetration compared to the PEG series. It is possible that SDS disrupts the architecture of the biofilms allowing a better invasion by the surfactant. However, it must be noted that the penetration is an overall measurement obtained over the whole region sampled by the evanescent wave. Therefore, it is also possible that SDS interacts strongly with some biofilm constituents and accumulates locally. The measured penetration efficiency is not strictly indicative of improved penetration within the biofilm but may also be explained by large and local bioaccumulations of the detergent. This later hypothesis seems more compatible with the reported dose effect.[42,43] Further experiments, including a complete concentration-dependence investigation is required to assess the validity of this hypothesis.

CPC clearly displays a slower diffusion compared to equivalent PEG, Triton X-100, and SDS. The characteristic rate is at least 10 times slower for CPC compare to the two other surfactants; almost 7 h are required to reach the plateau phase. The maximum penetration of CPC was estimated to be 86% (Table 2.2). In addition, the fresh medium did not wash out the CPC from the biofilms and only about 15% of the CPC could be eliminated from the biofilms. These findings suggest a strong interaction between the CPC micelles and biofilms, leading to a practically irreversible association. CPC is a positively charged molecule. The zeta potential of bacterial cell membranes of *S. mutans* is generally negatively charged.[34,71] In addition, biofilms generally include charges brought by ionizable groups on the polysaccharides such as carboxylate and sulfate.[2] Consequently, there may be electrostatic interactions anchoring the molecules (or micelles) of CPC to biofilms components. This conclusion is in fact in good agreement with a study using fluorescence correlation spectroscopy that investigated the diffusion of cationic latex beads in biofilms.[34] This report indicates the absence of diffusion of these

beads in *Lactococcus lactis* and *Stenotrophonas maltophilia* biofilms, a behavior that was associated to electrostatic interactions between the beads and some biofilm components. As discussed for SDS, the high penetration efficiency of CPC could be related to the local bioaccumulation rather than an improved penetrability over the whole biofilm. The bacterial count after the passage of CPC gave 0 CFU cm^{-2}, providing another indication of the strong interaction of the detergent with biofilm components.

2.6 Conclusion

The present study on the diffusion of macromolecules, and macroassemblies in *Streptococcus mutans* biofilms indicates that the diffusion coefficients, and the penetration efficiency are associated to the size of the solutes. These two aspects associated to the invasion of biofilms by large solutes appear to be related: the restricted penetration of macromolecules likely limits the diffusion to zones within the biofilms that are not dense from a organic matter point of view, leading to greater apparent relative diffusion coefficients. In addition, the results on micelles indicate that not only size but also charge matters. Both charged micellar assemblies (one negatively and the other, positively charged) show slow relative diffusion coefficients, but high penetration coefficient, relative to the behaviour of the neutral PEGs and Triton X-100. These parameters seem to be indicative of significant interactions between the detergent and some biofilm components. The enhanced penetration of the charged micelles could be associated to local bioaccumulations that would lead to an apparent augmentation in concentration over the entire probed zone. These inter-related aspects of the diffusion of macromolecules in heterogeneous biofilms have to be taken into account to provide a detailed understanding of the transport properties. It must be pointed out that the structure, and probably the transport properties, of the short-term *in vitro* biofilm model used in this study differ from those of biomedical or environmental biofilms

and the extrapolation of the findings inferred here to the more complex biofilms should be examined and validated.

2.7 Acknowledgement

The Canadian Dairy Farmers, Fonds de recherche en Santé du Québec (FRSQ), and the Natural and Engineering Research Council (Canada) are gratefully acknowledged for their financial support.

2.8 References

1. J. W. Costerton, P. S. Stewart and E. P. Greenberg, Science **284**, 1318 (1999)
2. I. W. Sutherland, Microbiology **147**, 3 (2001)
3. D. G. Allison, Biofouling **19**, 139 (2003)
4. H. Beyenal, Z. Lewandoski and G. Harkin, Biofouling **20**, 1 (2004)
5. L. V. Evans. *Biofilms: Recent Advances in Thier Study and Control.* (Harwood Academic Plublishers, Amsterdam, 2000)
6. V. Sihorkar and S. P. Vyas, Pharm. Res. **18**, 9, 1247 (2001)
7. D. J. Evans, D. G. Allison, M. R. Brown and P. Gilbert , J. Antimicrob. Chemother. **27**, 177 (1991)
8. G. O'Toole, H. B. Kaplan and R. Kolter, Annu. Rev. Microbiol. **54**, 49 (2000)
9. A. Brooun, S. Lui and K. Lewis, Antimicrob. Agents Chemother. **44**, 3, 640 (2000)
10. C. A. Gordon, N. A. Hodges and C. Marriott, J. Antimicrob. Chemother. **22**, 667 (1988)
11. P. S. Stewart, F. Roe, J. Rayner, J. G. Elkins, Z. Lewandowski, U. A. Ochsner and D. J. Hassett, Appl. Environ. Microbiol. **66**, 836 (2000)
12. J. N. Anderl, M. J. Franklin and P. S. Stewart, Antimicrob. Agents

Chemother. **44**, 1818 (2000)

13. J. D. Bryers and F. Drummond, Biotechnol. Bioeng. **60**, 4, 462 (1998)
14. P. S. Stewart, Biotechnol. Bioeng. **59**, 3, 261 (1998)
15. J.-M. Petit, B. Roux, X. X. Zhu and P. M. Macdonald, Macromolecules **29**, 6031 (1996)
16. L. Masaro, M. Ousalem, W. E. Baille, D. Lessard and X. X. Zhu, Macromolecules **32**, 4375 (1999)
17. S. Kwak, M. T. Phan Viet and M. Lafleur, J. Magn. Reson. **162**, 198 (2003)
18. S. Kwak and M. Lafleur, Macromolecules **36**, 3189 (2003)
19. L. Johansson, U. Skantze and J.-E. Löfroth, Macromolecules **24**, 6019 (1991)
20. A. Krol, J. Maresca, M. W. Dewhirst and F. Yuan, Cancer Res. **59**, 4136 (1999)
21. J. Tong and J. L. Anderson, Biophys. J. **70**, 1505 (1996)
22. Z. Lewandowski, P. Stoodley and S. Altobelli, Water Sci. Technol. **31**, 1, 153 (1995)
23. D. E. Caldwell, D. R. Korber and J. R. Lawrence, Adv. Microb. Ecol. **12**, 1 (1992)
24. J. R. Lawrence, D. R. Korber, B. D. Hoyle, J. W. Costerton and D. E. Caldwell, J. Bacteriol. **173**, 6558 (1991)
25. D. de Beer, J. C. van den Heuvel and S. P. Ottengraf, Appl. Environ. Microbiol. **59**, 573 (1993)
26. J. W. Costerton, Z. Lewandowski, D. de Beer, D. Caldwell, D. Korber and G. James, J. Bacteriol. **176**, 8, 2137 (1994)
27. W. W. Nichols, M. J. Evans, M. P. E. Slack and H. L. Walmsley, J. Gen. Microbiol. **135**, 1291 (1989)
28. X. Zhang and P. L. Bishop, J. Environ. Eng. **127**, 9, 850 (2001)
29. B. D. Hoyle, J. Alcantara and J. W. Costerton, Antimicrob. Agents Chemother. **36**, 9, 2054 (1992)
30. M. W. Jr. Dunne, E. O. Jr. Mason and S. L. Kaplan, Antimicrob. Agents Chemother. **37**, 12, 2522 (1993)

31. D. de Beer, P. Stoodley and Z. Lewandowski, Biotechnol. Bioeng. **53**, 151 (1997)
32. J. R. Lawrence, G. M. Wolfaardt and D. R. Korber, Appl. Environ. Microbiol. **60**, 4, 1166 (1994)
33. R. J. Palmer and C. Sternberg, Curr. Opin. Biotechnol. **10**, 263 (1999)
34. E. Guiot, P. Georges, A. Brun, M. P. Fontaine-Aupart, M. N. Bellon-Fontaine and R. Briandet, Photochem. Photobiol. **75**, 6, 570 (2002)
35. P. A. Suci, J. D. Vrany and M. W. Mittelman, Biomaterials **19**, 327 (1998)
36. P. A. Suci, M. W. Mittelman, F. P. Yu and G. G. Geesey, Antimicrob. Agents Chemother. **38**, 9, 2125 (1994)
37. J. D. Vrany, P. S. Stewart and P. A. Suci, Antimicrob. Agents Chemother. **41**, 6, 1352 (1997)
38. P. S. Stewart, J. Rayner, F. Roe and W. M. Rees, J. Appl. Microbiol. **91**, 525 (2001)
39. X. Chen and P. S. Stewart, Environ. Sci. Technol. **30**, 6, 2078 (1996)
40. D. E. Nivens, R. J. Palmer and D. C. White, J. Ind. Microbiol. **15**, 263 (1995)
41. P. A. Suci, G. G. Geesey and B. J. Tyler, J. Microbiol. Methods **46**, 193 (2001)
42. A. S. Landa, B. van de Belt-Gritter, H. C. van der Mei and H. J. Busscher, Eur. J. Oral Sci. **107**, 236 (1999)
43. A. S. Landa, H. C. van der Mei and H. J. Busscher, Adv. Dent. Res. **11**, 4, 528 (1997)
44. A. Tatevossian, Caries Res. **13**, 154 (1979)
45. A. Tatevossian, Arch. Oral Biol. **30**, 4, 365 (1985)
46. T. Thurnheer, R. Gmür, S. Shapiro and B. Guggenheim, Appl. Environ. Microbiol. **69**, 3, 1702 (2003)
47. S. Herles, S. Olsen, J. Afflitto and A. Gaffar, J. Dent. Res. **73**, 11, 1748 (1994)
48. P. Pan, M. L. Barnett, J. Coelho, C. Brogdon and M. B. Finnegan, J. Clin. Periodontol. **27**, 256 (2000)

49. J. E. Mark and P. J. Flory, J. Am. Chem. Soc. **87**, 1415 (1965)
50. K. Ahmed, P. Gribbon and M. J. Jones, J. Liposome Res. **12**, 4, 285 (2002)
51. Y. Liu and S. L. Regen, J. Am. Chem. Soc. **115**, 708 (1993)
52. P. R. Majhi and S. P. Moulik, Langmuir **14**, 3986 (1998)
53. F. Dousseau, M. Therrien and M. Pézolet, Appl. Spectrosc. **43**, 538 (1989)
54. A. D. Russell, J. Pharm. Pharmacol. **52**, 2, 227 (2000)
55. D. C. Harris and M. D. Bertulocci. *Symmetry and Spectroscopy, An Introduction to Vibrational and Electronic Spectroscopy* (Dover Publication, inc., New York, USA, 1978)
56. J. J. Birmingham, N. P. Hugues and R. Treloar, Philos. Trans. R. Soc. London, B **350**, 325 (1995)
57. Crank, J. *The Mathematics of Diffusion;* 2nd ed. Clarendon press: Oxford, 1975.
58. M. G. Trulear and W. G. Characklis, Journal WPCF **54**, 9, 1288 (1982)
59. F. S. Parker. *Applications of Infrared, Raman, and Resonance Raman Spectroscopy in Biochemistry* (Plenum Press, New York, USA, 1983)
60. S. Y. U. Venyaminov and N. N. Kalnin, Biopolymers **30**, 1259 (1990)
61. H. Akutsu, M. Ikematsu and Y. Kyogoku, Chem. Phys. Lipids **28**, 149 (1981)
62. R. E. Baier and P.-O. Glantz, Acta Odontol. Scand. **36**, 289 (1978)
63. P. T. T. Wong and H. H. Mantsch, Chem. Phys. Lipids **46**, 213 (1988)
64. R. M. Silverstein, G. C. Basslerand T. C. Morrill. *Spectrometric Identification of Organic Compounds, Fifth Edition* (John Willey & Son, inc. New York, 1991)
65. M. P. Olivieri, R. E. Baier and R. E. Loomis, Biomaterials **13**, 14, 1000 (1992)
66. A. Hashimoto and T. Kameoka , Appl. Spectrosc. **54**, 7, 1005 (2000)
67. D. Lefier, R. Grappin and S. Pochet, J. AOAC Int. **79**, 3, 711 (1996)
68. H. J. Luinge, E. Hop, E. T. G. Lutz, J. A. van Hemert and E. A. M. de Jong, Anal. Chim. Acta **284**, 419 (1993)
69. N. J. Harrick. *Internal Reflection Spectroscopy* (Harrick Scientific

Corporation, Ossining, 1979)

70. L. Marcotte, J. Barbeau and M. Lafleur, Appl. Spectrosc. **58**, 11, 1295-1301 (2004)
71. T. Saito, T. Takatsuka, T. Kato, K. Ishihara and K. Okuda, Arch. Oral Biol. **42**, 8, 539 (1997)
72. J. T. Edward, J. Chem. Educ. **47**, 4, 261 (1970)
73. G. Duplâtre, M. F. F. Marques and M. da Graça Miguel, J. Phys. Chem. **100**, 41, 16608 (1996)
74. K. Streletzky and G. D. J. Phillies, Langmuir **11**, 42 (1995)
75. A. B. Mandal and B. U. Nair, J. Phys. Chem. **95**, 9008 (1991)

Chapitre 3

Characterization of the Diffusion of Poly(ethylene glycol) in Streptococcus mutans Biofilms by Raman Microspectroscopy

Lucie Marcotte, Jean Barbeau and Michel Lafleur,

Applied Spectroscopy **58**, 11, 1295-1301 (2004)

Key words: Biofilm; Raman microspectroscopy; diffusion; mapping

Abbreviated title: Raman microspectroscopy on biofilm

3.1 Abstract

We used Raman microspectroscopy to investigate *in situ* the spatial distribution of the biomass in *Streptococcus mutans* biofilms. We used the CH stretching band to probe the organic matter, and the area of the OH stretching band as an internal standard intensity, the biofilms being highly hydrated. The size of the biofilm regions that were mapped was 300 x 300 μm. We also recorded, in the confocal mode, the z profiles describing the biomass distribution as a function of depth in the biofilms. In our growth conditions, the biofilm is described as a ~ 75-μm thick mat covering completely the surface and includes columnar clusters with a diameter of ~100 μm, surrounded by voids filled with water. Raman mapping was also used to examine the diffusion of HOD, and polyethylene glycol with a molar mass of 10 000 (PEG-10k) in the biofilms. This study establishes that HOD can diffuse practically everywhere in the biofilms but the penetration of PEG-10k is limited. There is a correlation between the restricted penetration of the macromolecule and the biomass content in the different regions of the biofilms. The method presented here provides a convenient approach to determine the diffusion of molecules, including antibacterials, in bacterial biofilms.

3.2 Introduction

Biofilms are complex structures that grow at a solid-liquid or solid-air interface.[1,2] They are described as microcolonies of bacteria embedded in an extracellular matrix maintaining the microcolonies together. The matrix, representing up to 85% of the dry weight of biofilms, is mostly composed of polysaccharides but contains also other metabolites such as proteins, nucleic acids, ions, etc.[3-5] Biofilms are highly hydrated (~97%)[3,6,7] and their heterogeneous structures are proposed to include water channels that bring nutrients to the cells and evacuate their metabolic products.[1,2,8]

A variety of techniques has been used to characterize biofilm structure (see refs. 9 and 10 for reviews). Optical microscopy was one of the first to be used. In order to improve the contrast, various dyes were used to detect biochemical and physiological characteristics of biofilms. This technique presents limitations for quantification and may be difficult to use with thick samples.[9,10] Electron microscopy has been useful to study the morphology of the microcolonies inside biofilms.[11] However the dehydration, fixation, staining and slicing of the samples should be performed with cautious to avoid potential artefacts.[10,11] Confocal laser microscopy (CLM) has emerged as one of the powerful techniques for the characterization of the biofilm structure.[5,8,10-15] It provides a three-dimensional description of the structure, with a microscopic resolution. A laser light source provides an intense collimated light that can penetrate biofilms. With the confocal mode, it is possible to examine thin planes of biofilms. If the sample has intrinsic fluorophores, the information obtained from these specific components. Otherwise, the biofilms need to be stained. Raman microspectroscopy has been used to examine the chemical structure of various biological materials but, to our knowledge, has never been applied to characterize the structure of biofilms. The technique has been successfully used to determine the diffusion coefficient of an antibiotic inside *Pseudomonas aeruginosa* biofilms.[16] The combination of the

Raman spectrometer with a microscope made possible the acquisition *in situ* of the analyte signal over a very small region of the biofilms. In this paper, we report a Raman microspectroscopic study of biofilms that illustrates the potential of the technique to characterize the spatial distribution of the biomass and solutes inside *Streptococcus mutans* biofilms.

Bacteria in biofilms become highly resistant to several biocides: it has been shown that the biofilm mode of growth (sessile) can be associated to an increase by up to a thousand fold of the antibacterial resistance compared to their planktonic counterparts.[2,3,17,18] Rationales proposed to explain this phenomenon include changes in the bacterial physiologic state,[18,19] inactivation of the antibacterial agents by some biofilm components,[20,21] and hindered diffusion of the agents in biofilms.[2,7,22] The restricted diffusion of solutes inside biofilms has been reported by several techniques.[7,23-27] In addition, it was shown that a considerable fraction of biofilms is not accessible to large solutes.[22,23,26,28] Recently, it has been shown, using a series of polyethylene glycol of various size, that the proportion of inaccessible region in the *S. mutans* biofilms was dependant on the size of the diffusing solute.[28] For example, only 25 % of the base of the biofilm was accessible to poly(ethylene glycol) with a molar mass of 10 000 (PEG-10K), which has a hydrodynamic diameter of about 28 nm. It is known that PEGs does not interact much with biofilms[29] and their limited penetration into the biofilms was proposed to be associated to steric interactions. In this study, we have used Raman microspectroscopy to determine whether there is a correlation between the inaccessible regions, and the distribution of the biomass inside the biofilms or if the limited penetration is observed over all the biofilms. In order to address this question, we have examined the distribution of PEG-10k in *S. mutans* biofilms. In addition, we have, in a simultaneous and independent manner, assessed the spatial distribution of HOD, using the O-D stretching band as a marker. This small molecule is expected to penetrate uniformly in biofilms and is used to validate the Raman microspectroscopy approach.

3.3 Materials and Methods

Biofilms of *Streptococcus mutans* NTCC 10 449 were grown directly from an aliquot preserved at -80° C. We used Trypticase Yeast Extract (TYE) broth (17 g/L Trypticase Peptone (BBL$^{(R)}$ Becton Dickinson and Company, Cockeysville, USA), 3 g/L Yeast extract (BBL), 5 g/L NaCl (Fisher Scientific, Fair Lawn, USA), and 2.5 g/L Na_2HPO_4 (A&C American Chemical Ltd., Montreal, Canada)) supplemented with 0.5 % sucrose. Ultra-pure water was used and the media were sterilized by autoclaving at 121° C for 20 minutes. The sugar was added to the TYE medium after autoclaving and this solution was then sterilized by a filtration on a polycarbonate filter with pores of 0.2 µm of diameter. Polyethylene glycol with a molar mass of 10 000 (PEG-10k), and D_2O were purchased from Aldrich-Sigma (Oakville, Canada).

Biofilm Growth

Biofilms were grown in a home build flow cell (Figure 3.1). The base of the cell was made of stainless steel while the top was a microscope glass cover (22 x 22 mm with a thickness of 100 µm) (Fisherbrand, Fisher Scientific) that was maintained in place by a top made of Teflon. Tygon tubing with Teflon connectors were used, and the medium flow was provided by a peristaltic pump (Masterflex). The cell and all the tubing were sterilized by circulating an ethanol solution (70%) for 2 hours and rinsed for 30 minutes with of sterilized water.

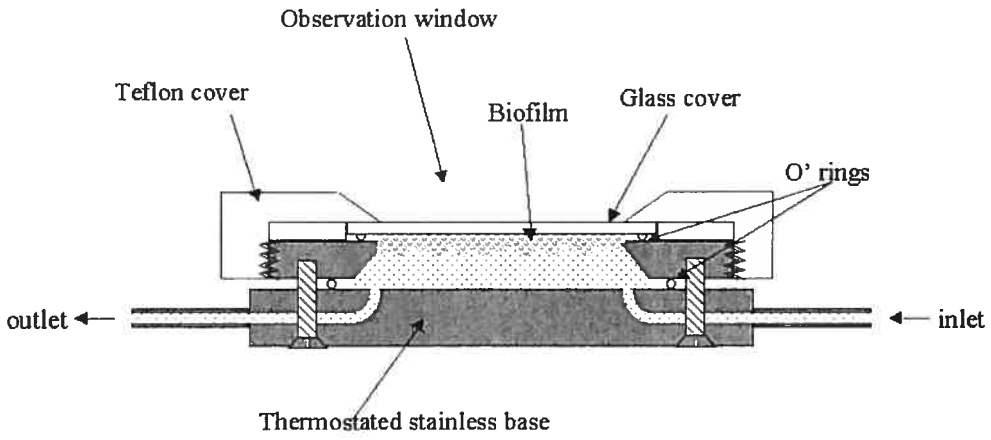

Figure 3.1 : Schematic representation of the flow cell used for the *in situ* Raman microspectroscopy sampling of the *Streptococcus mutans* biofilms.

Biofilms were obtained from an inoculum prepared with 200µL of strain, dispersed in 300 mL of TYE 0.5 % sucrose (w/v), and incubated at 37° C for 20 hours with agitation. The bacterial culture was circulated at ~ 0.5 mL/min for 5 hours in the flow cell turned upside down to let the bacteria seeding the glass cover. Precautions were taken to avoid the uptake of sediment made of bacteria aggregates from the bottom of the flask. The cell was thermoregulated at 37° C. After the cell inoculation, fresh media was circulated for 20 hours at the same flow rate. After this initial growth phase, the thermoregulation was stopped and PBS buffer pH 6.5 (8.76 g/L NaCl, 6.05 g/L K_2HPO_4 (A&C), and 0.7 g/L KH_2PO_4 (A&C)) was circulated in the cell for 30-45 minutes to eliminate air bubbles and loose aggregates.

Raman microspectroscopy

Raman microspectroscopy was performed using a Renishaw Raman Imaging Wire V1.3.15 3000 system (Renishaw, Gloucestershire, UK) equipped with a holographic grating (1800 grooves mm^{-1}), a Leica microscope with long-working-distance objectives with magnification of x50 and x20, a Peltier cooled charge-couple device (CCD) detector (600 x 400 pixels), and an argon ion (Ar^+) laser, providing the 514.5 nm line. The laser power at the sample was ~ 2.5 mW. The diameter of the beam at the sample, as measured on its reflection on a silicone surface, was ~ 2.5 and ~ 7 µm of diameter with the x50 and x20 objective respectively. This configuration led to a spectral resolution of ~2 cm^{-1} and the digital resolution was of one data point/1.3 cm^{-1}. All spectra were acquired at room temperature.

The spectral mapping for the determination of the biomass distribution in the plane of the biofilm (defined here as the *xy* plane) was performed with the x20 objective through the glass cover, i.e. examining the substratal region of the biofilm. The Raman spectra were recorded from 3800 to 2700 cm^{-1}, over three 30-second periods. They were subsequently corrected for the fluorescence background using a

least-square fitted cubic polynomial baseline. Typically, a surface of 300 µm x 300 µm was scanned with 15-µm steps. A spectral map, formed with 441 spectra, was acquired over ~ 18 h.

The biomass distribution as a function of depth in the biofilm, defined here as *z* profile, was determined working in the confocal mode, using the x50 objective. We estimated the resolution along the *z* axis for the optical set-up by recording the depth profiles of a sample formed by a 10 µm-Teflon film, and a 14 µm-Mylar film, squeezed between two glass covers (data not show). The Raman signal of the Teflon, and the Mylar corresponded to roughly 10% of its maximum intensity when the spectra were recorded 15 µm above the film surfaces, suggesting that the spatial resolution along the *z* axis was about 15-20 µm. For the biofilms, 30 scans, each one representing a 60-second acquisition, were typically co-added for the first 100 µm. Subsequently, to provide a reasonable signal/noise ratio, 90 60-second acquisitions were co-added for depths between 100 µm and 300 µm. The spectra were recorded with 25-µm steps along the *z* axis.

Raman microspectroscopy allowed us to characterize simultaneously the penetration of PEG-10k, and D_2O in the biofilms. First, a 60 x 60 µm area was investigated by recording the Raman spectra between 3800 and 2200 cm^{-1} (four 78-second acquisitions were co-added) with the x50 objective. The stage was moved with 5-µm step, leading to a total of 196 spectra per map (~22 h per map). Subsequently, a solution containing PEG-10k 3% (w/v) and D_2O 10 % (v/v) in a PBS buffer was circulated in the cell for 5 minutes, with a flow rate of 10 mL/min. These conditions ensured that the liquid milieu was completely replaced by the solute-containing solution. The flow was then stopped and another map over the very same area was recorded. The fluorescence contribution was removed using a least-square fitted cubic polynomial baseline.

3.4 Results and Discussion

Biomass Distribution

Figure 3.2 shows spectra of a biofilm recorded before (left side), and after (right side) the diffusion of PEG-10k and HOD in the biofilm. In the biofilm spectra, the band situated between 3725 and 3040 cm^{-1} is assigned to the OH stretching (ν_{OH}) and is essentially associated to water[30], the biofilm being highly hydrated (the water content is up to 97 %).[3] It is likely that hydroxyl groups from the polysaccharides also contribute to the Raman signal in this region but to a much lesser extent given their concentration. The CH stretching (ν_{CH}) band situated between 3030 and 2840 cm^{-1} [30] was used to probe the biomass. Almost every biofilm component (lipids, proteins, polysaccharides, etc.) contributes to the CH band. This region is thus well suited to determine the spatial distribution of the organic matter. The first observation that can be made from the biofilm spectra is that the biomass is not distributed uniformly in the *xy* plane of the biofilm, at the microscopic resolution, as assessed by the considerable variations of the intensity of the ν_{CH} band relative to that of the ν_{OH} band. This spatial heterogeneity is represented by the ν_{CH} area / ν_{OH} area ratio. The ν_{OH} area was integrated between 3725 and 3040 cm^{-1} (S_{OH}), and the CH area, between 3020 to 2820 cm^{-1} (S_{CH}). The OH stretching band of water was used as an internal intensity standard. For the spectra presented in Figure 3.2, the S_{CH}/S_{OH} ratio varies from 0.025 (top) to 0.175 (bottom).

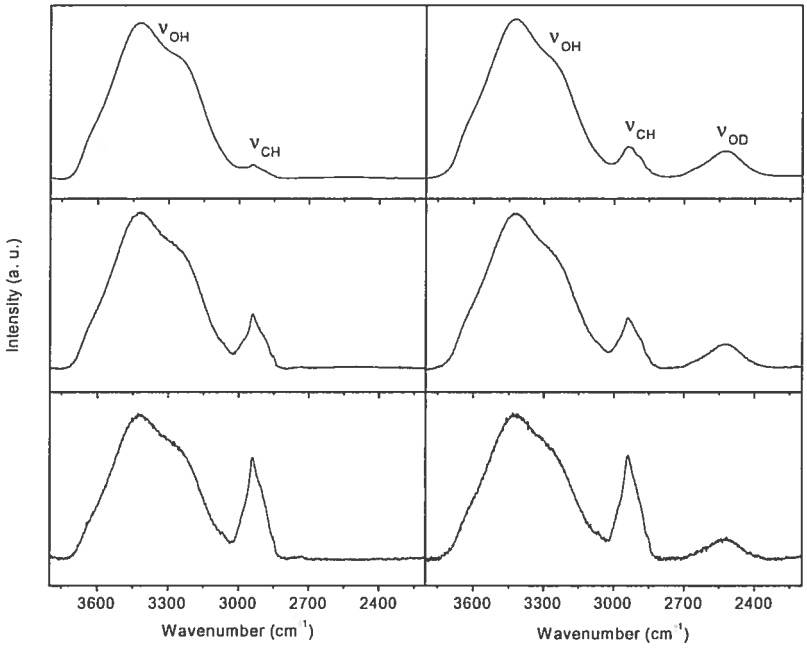

Figure 3.2 : Raman spectra of a given biofilm recorded at three different places. The left column presents the spectra recorded at the end of the growth period and prior to the equilibration with the solution containing PEG-10k, and HOD, whereas the right column represents the spectra recorded from the very same regions, after the diffusion of PEG-10k, and HOD.

Figure 3.3 shows the maps representing the biomass spatial distribution (as defined by S_{CH}/S_{OH}), of two 300 x 300 µm areas scanned for two different biofilms. For every biofilm map, it is possible to identify biomass clusters (brighter pixels) surrounded by regions with smaller quantity of biomass. In some cases, the spectra showing very weak CH bands defined structures (darker pixels) that could be associated to the water channels reported previously for other biofilms.[1,2,8] The reproducibility of the maps was assessed by mapping twice the same area with recording separated by a period of 24 hours. The spectra averaged over the whole investigated area were practically similar and the comparison between the spectra of a given pixel led to a mean variation of ± 14% of the S_{CH}/S_{OH} ratios. Raman chemical microimaging indicates that the structure of *Streptococcus mutans* biofilms is formed by biomass clusters with size in the range of 100 µm, surrounded by voids or channels filled with water. This type of structure is qualitatively similar to that of biofilms formed by other bacterial species.[4,8,14,31-33]

The mean S_{CH}/S_{OH} ratio averaged over a whole map characterizes the biomass proportion in the sampled area of the biofilm. For the biofilm examined in Figure 3.3 A, and B, the mean S_{CH}/S_{OH} ratios were 0.10, and 0.07 whereas it is 0.04 for the biofilm associated to Figure 3.3 C, and D. The average biomass is different for these biofilms, illustrating the natural variation of biological systems. However, the scanned areas appear to be large enough to provide a representative sampling of the biomass distribution for a given biofilm. The biofilm structures extracted from the Raman maps were described quantitatively using parameters proposed by Yang and al.[31] The areal porosity is defined by the ratio of the number of pixels corresponding to voids (the black ones) over the total number of pixels of the map. For this analysis, we defined as voids the pixels whose S_{CH}/S_{OH} ratio was between 0, and 17% of the highest value measured for this map. The calculated areal porosity is 0.03 and 0.15 for the two areas presented in Figure 3.3 A, and B,and 0.20 and 0.23 for the images C and D recorded from the other biofilm.

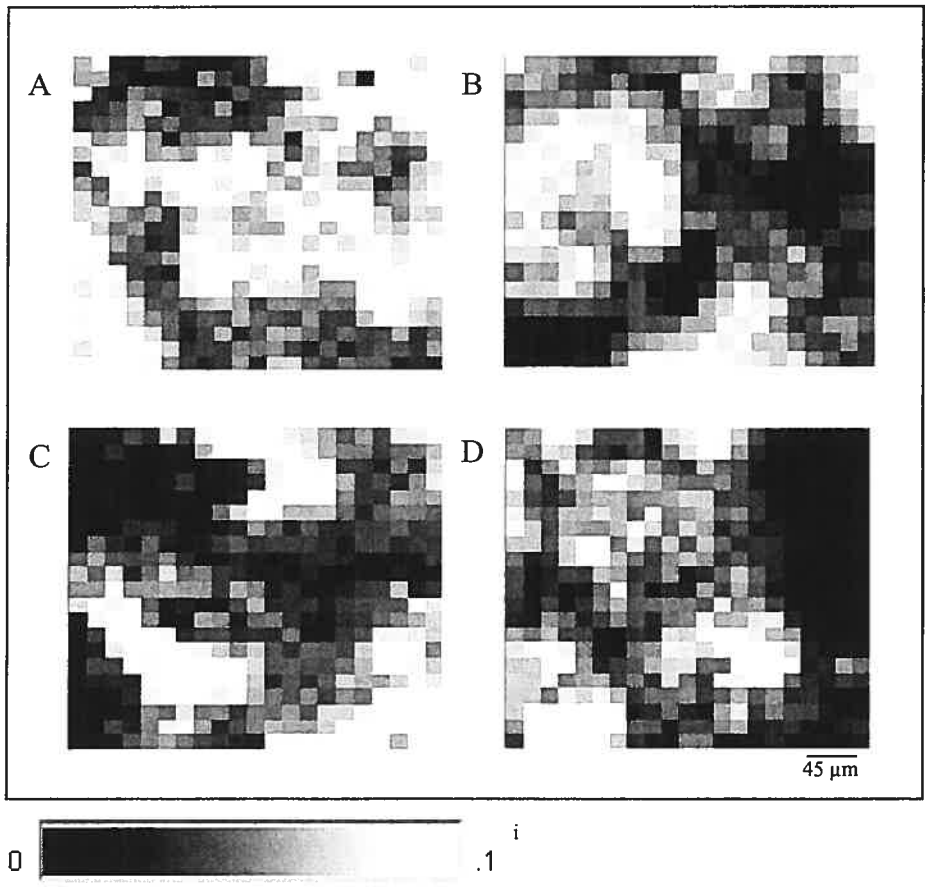

Figure 3.3 : Maps describing the spatial distribution of the biomass in biofilms, constructed from the S_{CH}/S_{OH} ratios. On this grey scale, the white pixels correspond to high ratios and black pixels, to ratios near zero. Each row corresponds to two maps recorded from two different areas of the same biofilm.

[i] L'échelle de gris va de 0 pour le noir à 0.1 pour le blanc

These values are consistent with the S_{CH}/S_{OH} ratios measured over the maps, the more porous biofilm corresponding to the lowest density of biomass (i.e. with the smaller S_{CH}/S_{OH} ratio). The mean areal porosity calculated from the 4 images is 0.15 ± 0.09. This value corresponds to mature biofilms, indicating extensive covering of the surface.[31]

In order to characterize the microscale heterogeneity of the biofilms, the textural entropy (TE) has been determined. The textural entropy is a measurement of "the pure randomness in the gray scale image."[31] Higher TE values can be associated to more heterogeneous biofilms. The calculation procedure is well described in the paper of Yang and al.[31] For simplification, the S_{CH}/S_{OH} ratios were grouped to provide six levels on a gray scale. For the first biofilm, the calculated TE was 2.50 and 2.78 (Figure 3.3 A and B respectively). For the second biofilm, TE was 2.80, and 2.60 (Figure 3.3 C and D respectively). These values are fairly similar and give an averaged TE value of 2.67 ± 0.14. It is difficult to conclude about the universal character of this value taking into account the limited number of available data but the values reported here are in the same range as those reported earlier for a multispecies biofilms.[31]

The *z* profiles of the biomass distribution as a function of depth in the biofilms are presented in Figure 3.4. The zero position corresponds to the biofilm-glass interface. Fourteen *z* profiles were recorded on 7 different biofilms. They were grouped in three types based on the S_{CH}/S_{OH} ratio associated to the locations where the profile measurements were performed. The first one, represented in Figure 3.4 A, shows the profile corresponding to biomass dense regions of the biofilms, with a mean S_{CH}/S_{OH} ratio of 0.121 ± 0.014 (n=7). The profile shows a progressive decrease of the biomass content from the interface to the top of the biofilm. A significant amount of biomass was detectable even 300 µm above the glass slide. The second profile, associated to intermediate S_{CH}/S_{OH} values (mean S_{CH}/S_{OH} = 0.041 ± 0.016; n=3), displays a relatively uniform biomass content for the first 150

µm, followed by a rapid decrease between 150 and 225 µm. Finally, the third profile, associated to regions with small biomass content (mean S_{CH}/S_{OH} ratio =0.009 ± 0.006; n=4) indicates the presence of a small content of biomass in the first 75 µm and no biomass could be detected any further. This type of profiles along the *z* axis has been reported for the total solid density of other biofilms.[6] Moreover, gradients of pH, and dissolved oxygen were also reported.[6,35] The profiles characterized in the present work provide some insights into the three-dimensional structure of the *Streptococcus mutans* biofilms obtained in our culture conditions. There is a layer of biomass of about 75 µm covering completely the surface. In the regions where the biomass content at the base level is high, the extension of the z profile suggests the existence of columnar clusters. These structural elements would be separated above the carpet by water "channels".

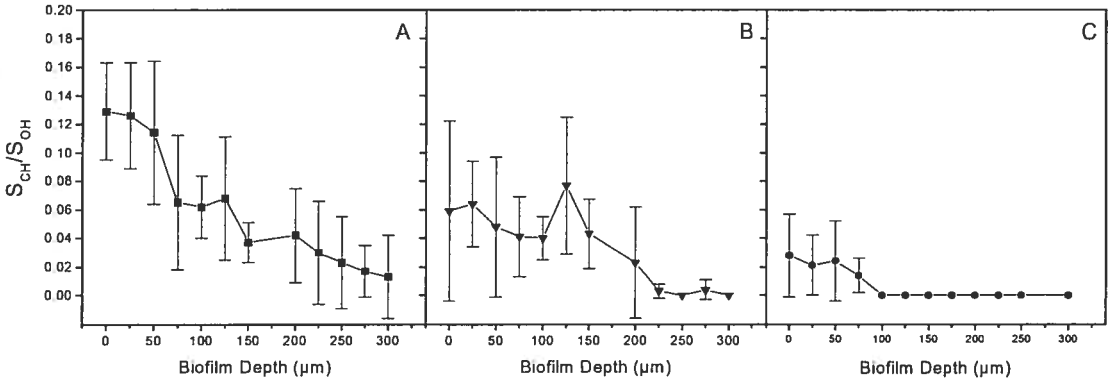

Figure 3.4 : *z* profiles associated to the biomass content as a function of the depth in the biofilms. The zero position corresponds to the biofilm-glass cover interface. The average profiles were obtained from regions where S_{CH}/S_{OH} ratio was A) 0.121 ± 0.014 (n= 7); B) 0.041 ± 0.016 (n=3); and C) 0.009 ± 0.006(n= 4).

Diffusion in the Biofilm

Raman microspectroscopy was successfully applied to characterize the distribution of solutes in biofilms. We determined the spatial distribution of HOD and PEG-10k in biofilms, using the Raman spectral maps of biofilms equilibrated in the presence of a buffer containing the two diffusing species. HOD was followed using the OD elongation band (ν_{OD}) at ~ 2520 cm^{-1} (Figure 3.2). The ratio of the OD band surface (S_{OD}), integrated from 2750 to 2340 cm^{-1}, over S_{OH} was used to represent the HOD penetration. The S_{OD}/S_{OH} ratios were compared to that obtained from the spectrum of the solute-containing solution to calculate the HOD penetration. The presence of PEG was probed using the CH stretching region. The shape of this region is significantly different depending on the PEG content of the scanned area of the biofilm (see the right sides of Figures 3.2, and 3.5). This is associated to different patterns of C-H bands for the spectrum of PEG-10k solution, and that of a biofilm; these regions of the experimental spectra are displayed in Figure 3.5 (labelled as 100, and 0% PEG, respectively). The penetration percentage of PEG-10k could be extracted from the spectra using the following approach, in order to determine whether there is a correlation between the distribution of HOD and PEG-10k in the biofilm and the biomass distribution. The spectra associated to the biofilm maps acquired before diffusion were divided into 6 groups, according to their ratio $S_{CH}^{biofilm}/S_{OH}$ (where $S_{CH}^{biofilm}$ represent the contribution of the biofilm in the CH stretching region; in the present case, $S_{CH}^{biofilm}$ corresponds to the entire area of the CH stretching region). The corresponding spectra of the maps recorded after diffusion were divided among these 6 groups and an average post-diffusion spectrum was calculated for each group. The HOD penetration percentage was determined from the S_{OD}/S_{OH} ratios. For PEG-10k, a series of spectra was generated by the addition in various

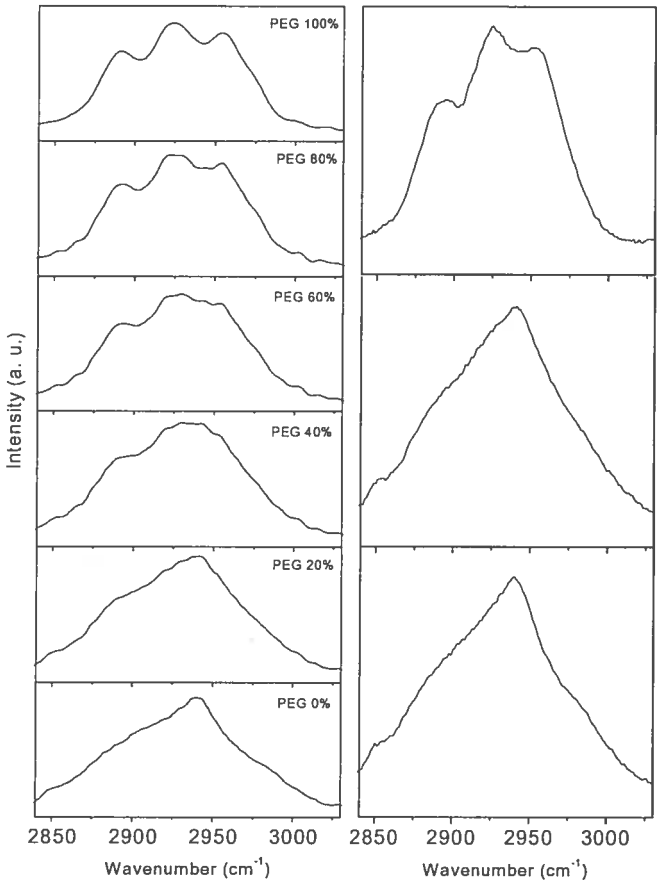

Figure 3.5 : Left side: CH stretching region of the simulated spectra obtained from the sum of the experimental biofilm spectrum (referred to in the figure as PEG 0%), and that of a PEG-10k solution (referred to as PEG 100%). The corresponding contribution of the PEG-10k spectrum to the Raman signal is indicated for each spectrum. Right side: CH stretching region of the spectra recorded in three different regions on the same biofilm after the diffusion of PEG-10k and HOD.

proportions of the spectrum of a PEG-10k solution, and that of the biofilm (the average spectrum over the whole biofilm, prior to the diffusion). The resulting spectra are shown on the left side of Figure 3.5 and illustrate the shape changes in the CH stretching region as a function of the PEG-10k content. The determination of the PEG contribution in the ν_{CH} band region of a biofilm spectrum after the diffusion period was determined by the comparison with this series of simulated spectra. First, an iterative procedure identified the subtraction factor for which the difference between the experimental spectrum and a given simulated spectrum was minimal, based on the smallest residual in the CH stretching region between 3020 to 2820 cm^{-1}. The χ^2 value associated to the residual, relative to a straight line between 3020, and 2820 cm^{-1} was calculated. This step was performed for the 4 simulated spectra, and the experimental spectra of the biofilm (PEG 0%), and of the PEG solution (PEG 100%). The PEG-10k contribution to the CH stretching region was estimated to correspond to the minimum of the curve of the χ^2 values as a function of the PEG-10k proportion of the simulated spectra. For example, the CH stretching region of 3 spectra recorded from a biofilm after the PEG-10k diffusion is presented in the right panel of Figure 3.5. The calculated contribution of PEG is from the top to the bottom: 68, 10 and 0 %. The visual comparison between these experimental spectra and the simulated ones on the left side substantiates these proportions. The area of the CH stretching region associated to the PEG-10k contribution (S_{CH}^{PEG}) was obtained by multiplying the total area of the CH stretching region by the calculated contribution of PEG obtained in the previous step. The penetration of PEG-10k in the biofilm was inferred from the S_{CH}^{PEG}/S_{OH} ratios, compared to the S_{CH}^{PEG}/S_{OH} ratio obtained from the PEG-10k solution used as diffusion medium. These penetration percentages are presented as a function of the local biomass density ($S_{CH}^{biofilm}/S_{OH}$ ratio) in Figure 3.6.

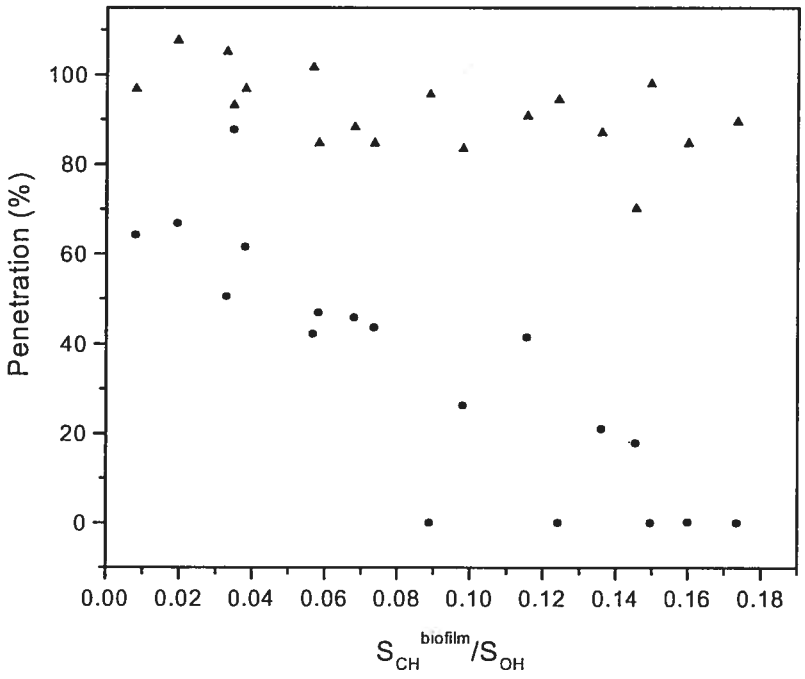

Figure 3.6 : Dependence of the penetration of PEG-10k (●), and of HOD (▲) in *S. mutans* biofilms on the biomass content.

Figure 3.6 presents the penetration of the HOD, and of PEG-10k inside the biofilm. The graph combines the measurements obtained from 3 independent experiments. In the case of HOD, the results show that water penetrates the biofilm in a homogeneous way: a complete penetration (100%) is observed, independently of the biomass concentration. There is only a small decrease in the penetration for water for high biomass concentrations. It corresponds to about 83 % for a $S_{CH}^{biofilm}/S_{OH}$ of 0.18. It is likely that there are a very large number of bacteria in these dense regions and HOD may not complete exchange, on the time scale of the measurement, with the intracellular water. In contrast, our results reveal that the penetration of PEG-10k in the biofilms is clearly limited. First, the penetration never reaches 100%: in the areas where there is a small biomass content, the penetration is about 70%. Second, the regions rich in organic matter display drastic reduction in PEG-10k content, reaching practically 0 in the densest regions. This result clearly establishes that large molecules have a limited access to biofilms and in fact, are excluded from the biomass clusters that likely correspond to bacteria microcolonies. PEGs are hydrophilic polymers that are known to interact minimally with biomaterials.[29] Indeed no bioaccumulation was found in any regions of the biofilms, indicating the absence of association of PEG with biomass components. The restricted penetration seems to be related to the size of the molecule. An impact of this behavior is that the effective dose of large antibacterials at the site of the microcolonies may be much less than expected. Along the same line, the use of fluorescent probes to label specific components of biofilms is associated to their good and uniform penetration in biofilms. Caution should be exerted with large probe molecules as their size may exclude them from some regions, preventing a proper and complete labeling. Related conclusions to those obtained from the spatial distribution of PEG in biofilms were inferred for other systems. It was shown, using confocal laser microscopy, that the penetration of isothiocyanate-conjugated dextrans in mixed-species biofilms was not homogeneous.[23] The percentage of the total area of the biofilms accessible to the dextrans was dependant on the molecular weight and the greatest penetration was

achieved with the smallest probes. Similarly, it was reported, using fluorescence correlation spectroscopy, that fluorescent latex beads with a radius of 55 nm could not diffuse inside the denser regions of *Stenotrophonas maltophilia* biofilms.[27] The authors concluded to a steric effect caused by the polysaccharide matrix. A study on polyspecies biofilms concluded to a heterogeneous spatial distribution of labeled dextran with a molecular weight of 10k, based on the analysis of confocal laser scanning micrographs.[26] Throughout the biofilms, regions corresponding to low levels of probe penetration were observed. The present findings are consistent with these previous reports and relate the inaccessible regions to high biomass concentrations. A methodology using Raman microspectroscopy has been proposed to determine the diffusion coefficient of solutes in biofilms and this approach has been successfully applied to the characterization of the diffusion of chlorhexidine digluconate in *Candida albicans* biofilms.[16] That study also examined the spatial variation of the chlorhexidine transport in biofilms. Because the considerable noise in the data, the authors could not conclude to spatial variations in the diffusion properties. The investigated biofilm surface was 10 x 60 μm^2, which is considerably smaller than that in the present study. In addition, chlorhexidine digluconate has a molecular weight of 899, which is significantly smaller than PEG-10k. Therefore, it is not unexpected that the chlorhexidine diffusion was more or less uniform, given the investigated length scale and the solute size. The Raman methodology determining the solute distribution in biofilms, at equilibrium, as described in the present manuscript, should provide useful and complementary information to this type of study. For example, in the case of heterogeneous diffusion, the findings could help to assess the relevant spatial scale prior to performing diffusion experiments that are more challenging from a sensitivity point of view.

3.5 Conclusion

To our knowledge, it is the first time that 2D chemical maps of a hydrated biofilm are obtained *in situ* by Raman microspectroscopy. The chemical mapping is successfully used to probe directly the water and the biomass distribution with a minimal sample treatment. The proposed approach is complementary to the microscopy techniques where specific components of the biofilms are stained.

The method constitutes also a novel approach to determine the penetration of solutes in biofilms. As a first result, we demonstrate here that PEG-10k molecules have a limited access to the biofilms and, moreover, its penetrability is heterogeneous and modulated by the biomass content. PEG-10k could be probed using the CH stretching region, despite the existing overlap with the contribution of the biofilm components at these wave numbers. It is likely that practically every solute can be investigated by this approach, as long as it displays a reasonable Raman scattering power. In some cases, isotopic labeling (deuteration for example) may be required to probe the solute in biofilms and this approach leads to an even broader utilization of the method.

3.6 Acknowledgements

The authors thank NSERC (Canada) and FRSQ (Québec) for their financial support. The Raman experiments were performed using the infrastructure of the Laboratoire de Caractérisation des Matériaux (LCM), Université de Montréal.

3.7 References

1. J. W. Costerton, Z. Lewandowski, D. de Beer, D. Caldwell, D. Korber and G. James, J. Bacteriol. **176**, 8, 2137 (1994)
2. J. W. Costerton, P. S. Stewart and E. P. Greenberg, Science **284**, 1318 (1999)
3. I. W. Sutherland, Microbiology **147**, 3 (2001)
4. J. Pratten, C. S. Andrews, D. Q. Craig and M. Wilson, FEMS Microbiol. Lett. **189**, 215 (2000)
5. J. R. Lawrence, T. R. Neu and G. D. W. Swerhone, J. Microbiol. Methods **32**, 253 (1998)
6. X. Zhang and P. L. Bishop, J. Environ. Eng. **127**, 9, 850 (2001)
7. P. S. Stewart, Biotechnol. Bioeng. **59**, 3, 261 (1998)
8. S. R. Wood, J. Kirkham, P. D. Marsh, R. C. Shore, B. Nattress and C. Robinson, J. Dent. Res. **79**, 1, 21 (2000)
9. D. E. Nivens, R. J. Palmer Jr. and D. C. White, J. Ind. Microbiol. **15**, 263 (1995)
10. S. B. Surman, J. T. Walker, D. T. Goddard, L. H. G. Morton, C. W. Keevil, W. Weaver, A. Skinner, K. Hanson, D. Caldwell and J. Kurtz, J. Microbiol. Methods **25**, 57 (1996)
11. J. Wimpenny, W. Manz and U. Szewzyk, FEMS Microbiol. Rev. **24**, 661 (2000)
12. R. J. Palmer Jr. and C. Sternberg, Curr. Opin. Biotech. **10**, 263 (1999)
13. G. Wolfaardt, J. Lawrence, R. Robarts, S. Caldwell and D. Caldwell, Appl. Environ. Microbiol. **60**, 434 (1994)
14. T. M. Auschill, N. B. Artweiler, L. Netuschil, M. Brecx, E. Reich and A. Sculean, Arch. Oral Biol. **46**, 471 (2001)
15. D. E. Caldwell, D. R. Korber and J. R. Lawrence, J. Microbiol. Methods **15**, 249 (1992)
16. P. A. Suci, G. G. Geesey and B. J. Tyler, J. Microbiol. Methods **46**, 193

(2001)

17. A. Brooun, S. Lui and K. Lewis, Antimicrob. Agents Chemother. **44**, 3, 640 (2000)
18. D. J. Evans, D. G. Allison, M. R. Brown and P. Gilbert , J. Antimicrob. Chemother. **27**, 177 (1991)
19. C. A. Gordon, N. A. Hodges and C. Marriott, J. Antimicrob. Chemother. **22**, 667 (1988)
20. J. N. Anderl, M. J. Franklin and P. S. Stewart, Antimicrob. Agents Chemother. **44**, 1818 (2000)
21. P. S. Stewart, F. Roe, J. Rayner, J. G. Elkins, Z. Lewandowski, U. A. Ochsner and D. J. Hassett, Appl. Environ. Microbiol. **66**, 836 (2000)
22. J. D. Bryers and F. Drummond, Biotechnol. Bioeng. **60**, 4, 462 (1998)
23. J. R. Lawrence, G. M. Wolfaardt and D. R. Korber, Appl. Environ. Microbiol. **60**, 4, 1166 (1994)
24. D. de Beer, P. Stoodley and Z. Lewandowski, Biotechnol. Bioeng. **53**, 151 (1997)
25. A. Tatevossian, Caries Res. **13**, 154 (1979)
26. T. Thurnheer, R. Gmür, S. Shapiro and B. Guggenheim, Appl. Environ. Microbiol. **69**, 3, 1702 (2003)
27. E. Guiot, P. Georges, A. Brun, M. P. Fontaine-Aupart, M. N. Bellon-Fontaine and R. Briandet, Photochem. Photobiol. **75**, 6, 570 (2002)
28. L. Marcotte, H. Thérien-Aubin, C. Sandt, J. Barbeau and M. Lafleur, *Solute Size Effects on the Diffusion in Biofilms of Streptococcus mutans*. accepted to Biofouling, August 2004
29. K. Ahmed, P. Gribbon and M. J. Jones, J. Liposome Res. **12**, 4, 285 (2002)
30. F. S. Parker. *Applications of Infrared, Raman, and Resonance Raman Spectroscopy in Biochemistry* (Plenum Press, New York, USA, 1983)
31. X. Yang, H. Beyenal, G. Harkin and Z. Lewandowski, J. Microbiol. Methods **39**, 109 (2000)
32. H. Beyenal and Z. Lewandowski, Biotechnology Progress **18**, 1, 55 (2002)

33. Z. Lewandowski, Water Res. **34**, 9, 2620 (2000)
34. J. R. Lawrence, D. R. Korber, B. D. Hoyle, J. W. Costerton and D. E. Caldwell, J. Bacteriol. **173**, 6558 (1991)
35. P. S. Stewart, J. Rayner, F. Roe and W. M. Rees, J. Appl. Microbiol. **91**, 525 (2001)

Chapitre 4

Influence of the Lipid Composition on the Membrane Affinity, and the Membrane-Perturbing Ability of Cetylpyridinium Chloride

Lucie Marcotte, Jean Barbeau, Katarina Edwards, Göran Karlsson, and Michel Lafleur, soumis à *Colloids and Surfaces A: Physicochemical and Engineering Aspect* (2004)

Keywords: Cetylpyridinium chloride, lipid membrane, ITC, affinity, permeability

Abbreviated title: Lipid composition effect on CPC affinity

4.1 Abstract

Cetylpyridinium chloride (CPC) is used for dental plaque control and has been shown to interact with *Streptococcus mutans* biofilms. Part of this effect may be related to interactions with bacterial plasmic membrane. We investigated the affinity of CPC for model bacteria membranes to examine the hypothesis that negatively charged membranes could favor the bactericide power of CPC. First, we determined the association constant (K) of CPC with model lipid membranes from isothermal titration calorimetry, and the influence of lipid composition on this affinity. Second, we tested the CPC influence on membrane permeability, by measuring the release of encapsulated fluorescent calcein in liposomes. We investigated 4 model membranes: one with only zwitterionic 1-palmitoyl-2-oleoyl-sn-glycerol-3-phosphocholine, two containing anionic phospholipids (1-palmitoyl-2-oleoyl-sn-glycerol-3-phosphoglycerol and cardiolipin), and one containing cholesterol. Our results revealed a limited influence of electrostatic interactions on K, indicating that the hydrophobic factor was predominant in the association of this surfactant with phospholipid membranes. CPC could induce release from the 3 model membranes composed only of phospholipids, with a kinetic of release more complex for negatively charged membrane. We suggest that the release process implies the passage of the detergent from the outer sheet of the bilayer to the inner one, and the process would be slowed down by the interaction of the CPC head group with anionic phospholipids. The cholesterol-containing membranes showed a smaller K and remain impermeable in the presence of CPC. The stiffness of the cholesterol-containing membrane may restrict the insertion of CPC in the membranes and limits its translocation across the membrane. The thermodynamic model of the partitioning of CPC micelle and lipid bilayer has also been demonstrated.

4.2 Introduction

Quaternary ammonium compounds (QACs) constitute a class of molecules that is currently used as bactericides.[1-5] It has been established that their mechanism of action involves a perturbation of the bacteria plasmic membrane, leading to the release of internal metabolites and ultimately to the death of bacteria.[2,4,6,7] Because of their amphipathic character, it is believed that the detergent molecules insert in the lipid membranes, self-associate and cause leaks or defects leading to the loss of cellular components.[4,8-10] Cetylpyridinium chloride (CPC) is a QAC which is commonly used in mouth washes (e.g. Cepacol® and Scope® [11,12]) to prevent the formation of dental plaque. It has been shown to be effective against *Streptococcus mutans,*[13,14] one of the main bacteria associated with dental plaque.[15,16] A recent study of the penetration of CPC in *Streptococcus mutans* biofilms has shown that CPC has a drastically reduced diffusion coefficient in these biofilms compared to that observed in water.[17] In addition, it was shown that the association of CPC with the biofilms was practically irreversible. This inhibition of mass transport in biofilms has been attributed to strong interactions between the cationic detergent and some biofilm components, including the bacterial cells themselves. The goal of the present work is to examine the interactions between CPC and model lipid membranes to assess whether interactions with bacterial cell membranes can account for the reduced diffusion.

The two main phospholipid constituents of *S. mutans* membranes are cardiolipin (card), and phosphoglycerol (PG), two anionic lipids.[18] The other membrane constituents are mainly neutral lipids such as diglyceride, fatty acid, and glycolipids.[18] In the present study, four model systems have been examined. First, 1-palmitoyl-2-oleoyl-sn-glycerol-3-phosphocholine (POPC) was used as a generic neutral membrane. POPC bilayers containing 1-palmitoyl-2-oleoyl-sn-glycerol-3-phosphoglycerol (POPG), or cardiolipin (card) were used to highlight the role of these negatively charged lipids in the interactions with CPC. Finally, the

POPC/cholesterol (chol) mixture was examined as cholesterol is a distinctive constituent of mammal plasmic membranes[19] and is thought to play a role in the restricted biocide power of antibacterials against our cells.[20] The affinity of CPC for these model membranes, and its ability to perturb their integrity has been characterized.

The affinity of a detergent for lipid bilayers can be described by its partitioning between the aqueous, and lipidic phases.[21-23] The partitioning is described by:

$$K_w = \frac{X_{Dm}}{X_{Dw}} \approx \frac{C_{Dm}}{C_L} \frac{C_w}{C_{Dw}} = C_w K \qquad \text{Eq. 4.1}$$

Where K_w is the partitioning constant, X_{Dm}, and X_{Dw} are the molar fractions of CPC in the lipid membranes, and in water respectively. C_{Dw} is the molar concentration of detergent free in water, C_{Dm}, the molar concentration of membrane-bound detergent, C_L, the molar concentration of lipid, C_w, the molar concentration of water (55 M). K is the partitioning constant expressed in M^{-1}. Isothermal titration calorimetry (ITC) is sufficiently sensitive to measure the heat involved in the transfer of detergent molecules from the aqueous phase to lipid membranes. From these data, it is possible to extract the thermodynamics parameters of the association of detergents with membranes.[21,23,24] During these titrations, a detergent solution in the cell is titrated with aliquots of a lipid suspension and the heat exchanges during this process are recorded. If one assumes that the area of each peak provides a measurement of the heat associated to the transfer of detergent molecules from the aqueous phase to the injected membranes, it is possible to calculate the molar enthalpy variation of the transfer (ΔH_{trans}), and K, using a method developed by Heerklotz, and Seelig,[23] and Hoyrup et al.[21] The experimental data can be fitted, considering K, and ΔH_{trans} as fitting parameters, by:

$$H_i = \Delta H_{trans} C_L^o C_D^o V^o \frac{Ki}{KC_L^o i + \frac{V^o}{V_{inj}} + i} \qquad \text{Eq. 4.2}$$

Where H_i is the total enthalpy after the i^{th} injection, C_L^o is the lipid concentration in the syringe, C_D^o, the initial CPC concentration in the calorimeter cell, V^o, the volume of the cell, and V_{inj}, the volume of a single injection of lipid suspension. The variation of molar Gibbs energy (ΔG_{trans}), and of molar entropy (ΔS_{trans}) associated to the transfer a CPC monomer from the aqueous environment to the lipid membranes were also calculated.

$$\Delta G_{trans} = -RT \ln KC_w \qquad \text{Eq. 4.3}$$

$$\Delta G_{trans} = \Delta H_{trans} - T\Delta S_{trans} \qquad \text{Eq. 4.4}$$

In parallel, we have examined the effect of CPC on the permeability of the model membranes, using a fluorescence approach based on the self-quenching of calcein.[25,26] Finally, the effects of CPC on the macrostructure of the lipid assemblies have been examined using electron cryo-microscopy. It has been shown that cationic detergents can lead to a major reorganization of the lipid self-assemblies.[27-29] For example, it was shown that increasing concentrations of cetyltrimethylammonium chloride added to lipid vesicles caused an increase of their volume, the formation of holes, a morphology transition toward lipid sheets and finally the formation of tubular mixed micelles.[27] We examined whether a similar behaviour is observed for the POPC/CPC system.

4.3 Materials and methods

Chemicals

CPC, MES (2-[N-Morpholino]ethanesulfonic acid), EDTA, cholesterol were bought from Sigma-Aldrich (Oakville, ON, Canada). POPC, POPG, and tetraoleoyl-cardiolipin (card), were purchased from Avanti Polar Lipids inc.(Birmingham, AL, USA). Calcein (2,4-bis-[N,N'-di(carboxymethyl) aminomethyl]fluorescein), and NaCl were obtained from Molecular Probes

(Eugene,OR, USA), and Anachemia (Rouses Point, USA), respectively. All aqueous solutions were prepared with ultra pure water (18 Mohms cm^{-1}).

Vesicles preparation

The lipid mixtures were prepared by mixing appropriate volume of stock solutions of individual lipid prepared in benzene:methanol (96/6, v/v). The lipid compositions were 8/2 (w/w) for both POPC/card, and POPC/POPG, and of 7/3 (mol/mol) for POPC/chol. Providing the weight proportions, in the case of negatively charged lipids, leads to a similar charge surface density for both POPG and cardiolipin. The organic solutions were frozen in liquid nitrogen, and freeze-dried for at least 16 h. The lipid powder was hydrated with a MES buffer. The mixture was submitted to 5 freeze-and-thaw cycles (from liquid nitrogen temperature to 40° C) and large unilamellar vesicles (LUV) were obtained by extrusion through two polycarbonate filters with pores with a diameter of 100 nm, using a commercial device from Lipex (Vancouver, BC, Canada), or Avestin (Ottawa, ON, Canada).

Critical micellar concentration determination

The critical micellar concentration (CMC) of CPC in the MES buffer (10 mM, containing NaCl 10 mM, and EDTA 5 mM with a pH of 6.5) was determined by ITC according to an established method.[23,30] The CPC concentration in the syringe was between 7.3 and 7.5 mM, and the injected volumes varied between 7 and 20 µL. For the determination of the membrane affinity constant, CPC monomers in the cell were titrated with LUVs. Typically, the injected volumes were between 5, and 8 µL, the lipid concentration was between 14, and 20 mM, and the CPC concentration in the cell was 20 or 40 µM. For the POPC/POPG system, we titrated a CPC suspension with a concentration of 300 µM, well above the CMC. For this specific experiment, a series of 10-µL injections of a POPC/POPG vesicular suspension (17 mM) were performed. Each experiment was performed in triplicates.

The measurements were performed using a VP-ITC calorimeter from Microcal inc. (Northampton, MA, USA). The volume of the cell was 1.4527 mL. The measurements were obtained at 25° C.

Release experiments

For the leakage experiment, the procedure previously described[25,26,31] was followed. Briefly, the initial calcein concentration in the vesicles was 80 mM. The internal buffer was MES (100 mM) containing NaCl (10 mM), and EDTA (5 mM), pH 6.5, whereas the isoosmotic external buffer was MES (100 mM), NaCl (120 mM), and EDTA (5 mM), pH 6.5. The lipid concentration in the cuvette was between 8 and 15 μM; the exact lipid concentration was determined using the Fiske-Subbarow assay.[32] An aliquot of a CPC solution was added to the cell containing the calcein-loaded LUVs, to obtain the desired incubation CPC/lipid molar ratio. The release profile was then followed as a function of time by determining the percentage of calcein release using:

$$\%\text{release} = [(I_a - I_b)/(I_T - I_b)]x100 \qquad \text{Eq. 4.5}$$

Where I_a corresponds to the fluorescence intensity at a given time, I_b is the background fluorescence intensity (i.e. prior to the CPC addition), and I_T is the fluorescence intensity associated to a complete release of calcein (induced by the addition of 0.05% (v/v) of Triton X-100, at the end of each experiment). The measurements were performed at room temperature, on a SPEX Fluorolog-2 spectrometer, with an excitation and an emission wavelength of 490, and 513 nm, respectively. The excitation and emission bandwidths were adjusted at 2.5 and 1.9 nm, respectively. The content of the cell was stirred with a magnetic bar. All the experiments were performed in triplicates. For the graphs representing the %release as a function of the CPC proportion, the data were grouped using the

clustering K-mean method, using MathPlus software. The error bars represent the standard deviation related to each cluster.

Cryo-transmission electron microscopy

Cryo-transmission electron microscopy (cryo-TEM) was used to examine the morphological changes of POPC LUVs in the presence of CPC. The lipid, and CPC concentrations were 2, and 15 mM, respectively. The buffer contained MES (10 mM), with NaCl (10 mM), and EDTA (5 mM), pH 6.5. Micrographs were recorded 10 minutes, 2 days and one week after the addition of CPC to preformed POPC vesicles. The cryo-TEM investigations were performed with a Zeiss EM 902A transmission electron microscope (Carl Zeiss NTS, Oberkochen, Germany). The instrument was operating at 80 kV and in zero loss bright-field mode. Digital images were recorded under low dose conditions with a BioVision Pro-SM Slow Scan CCD camera. (Proscan GmbH, Scheuring, Germany) and analySIS software. (Soft Imaging System, GmbH, Münster, Germany). In order to visualize as many details as possible, an underfocus of 1-2 µm was used to enhance the image contrast. The method for sample preparation and image recording consisted, in short, of the following (a more comprehensive description is available in 33). The samples were equilibrated at 25 °C and approximately 99 % relative humidity within a climate chamber. A small drop (~1µl) of sample was deposited on a copper grid covered with a perforated polymer film. Excess liquid was thereafter removed by means of blotting with a filter paper, leaving a thin film of the solution on the grid. Immediate after blotting the sample was vitrified in liquid ethane, held just above its freezing point. Samples were kept below -165° C and protected against atmospheric conditions during both transfer to the TEM and examination.

4.4 Results

A typical isothermal titration of CPC leading to the determination of its CMC is shown in Figure 4.1A.[ii] The first few peaks are more intense than the subsequent

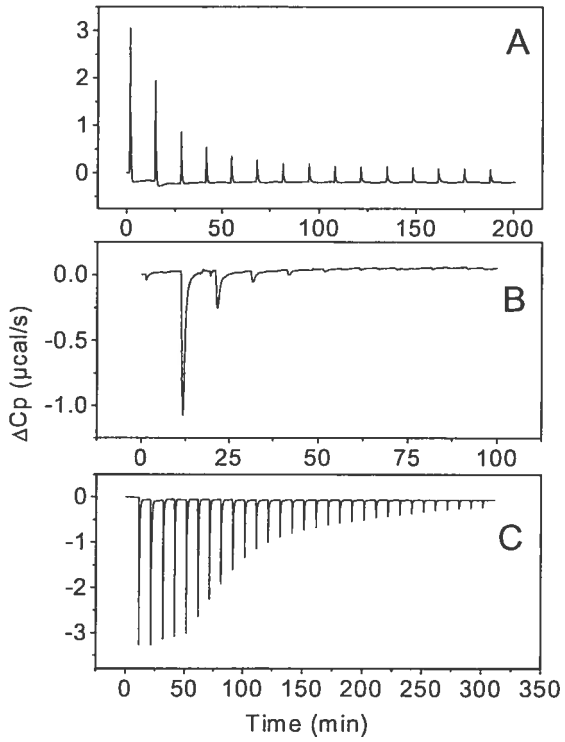

Figure 4.1 : A) Typical data of an ITC experiment to determine the CPC CMC. The peaks are associated to the injections of 10 μL of a CPC solution (7.3 mM in MES buffer) in the calorimeter cell filled with the buffer. B-C) Isothermal titrations of CPC with a POPC/POPG (8/2, w/w) suspension. The peaks represent injections of 8 μL of a lipid suspension (17 mM) to the cell filled with a CPC suspension of B) 40μM, or C) 300 μM.

[ii] Il est à noter que la courbe de tritration présentée ici pour déterminer la CMC du CPC dans le tampon diffère de celle présentée en introduction (p.23) où la CMC est déterminée dans l'eau.

ones as they involved the dilution of the micelles, their dissolution, and the dilution of the monomeric detergent. Their amplitude decreases progressively as the CPC concentration in the cell increases. Once the CPC concentration in the cell reaches the CMC, the peak intensities remain practically constant and are representative of the dilution enthalpy of the micelles. The CMC was determined by plotting the area of the peaks as a function of the CPC concentration in the cell. The first derivative of this curve was simulated using a Gaussian function and the CMC was estimated to correspond to the maximum of this function. We estimated the CMC of CPC in the MES buffer to 84 ± 8 μM (n=3). Using the relationship $\Delta G_{mic} \approx RT \ln(CMC/C_w)$,[34] the variation of molar Gibbs energy for the micellization of CPC (ΔG_{mic}) is estimated to -33.2 ± 0.2 kJ mol^{-1}. The molar enthalpy of micellization (ΔH_{mic}) was estimated to be -4.8 kJ mol^{-1} on the basis of the difference between the area of the peak associated to the first injection and those corresponding strictly to the micelle dilution (the last injections).

Figure 4.1B shows a typical titration of a CPC solution with POPC/POPG vesicles. The peaks indicate that the transfer of monomeric CPC molecules to the lipid bilayer is an exothermic process. The area of the peak decreases upon the titration and becomes very small, when most of the CPC molecules are membrane-associated. The data were analysed using Eq. 4.2. Typical data sets and simulations are reproduced in Figure 4.2. The least-square fitted parameters are presented in Table 4.1. Dynamic light scattering at the end of the titration with POPC showed no change in the vesicles morphology (data not show).

CPC micelles were titrated with POPC/POPG vesicles (Fig. 4.1C). The profile of the titration is considerably different than that of monomeric CPC. The area of the first three peaks, associated to an exothermic process, is relatively constant and much larger than those obtained upon the titration of CPC monomers. Subsequently the peak area decreases progressively to level off at a very small

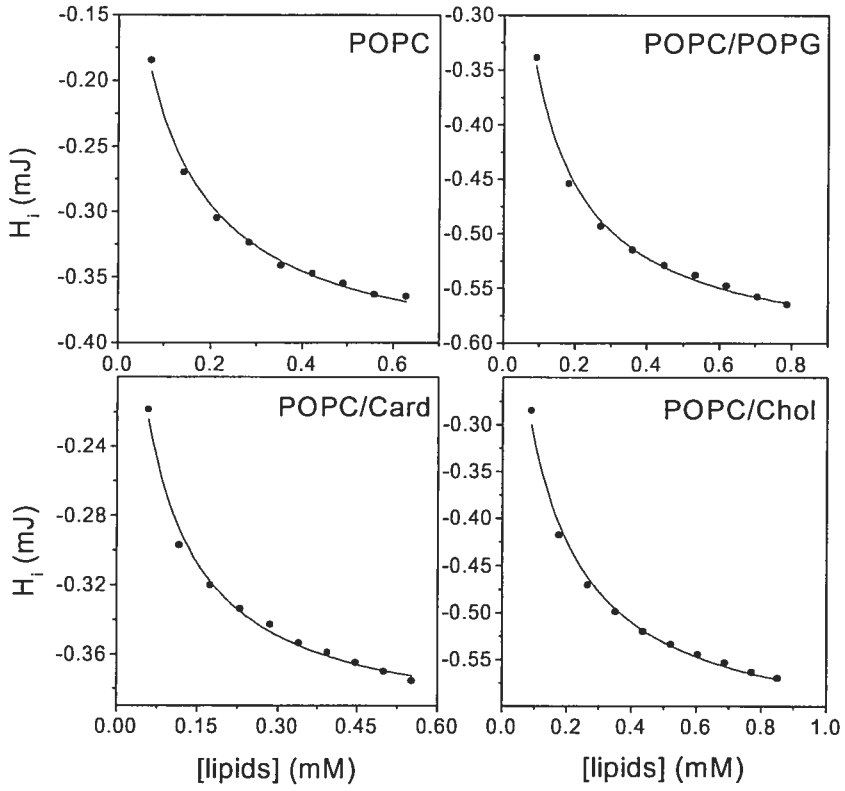

Figure 4.2 : Titration curves used to determine the thermodynamic constants of the association of CPC to lipid bilayers. The composition of the membrane is indicated in the figure. The points represent the enthalpy variations associated to the injections of lipid vesicles to the cell filled with a CPC solution. The full lines represent the fits obtained with Eq. 4.2.

Table 4.1 : Thermodynamic parameters associated to the transfer of CPC monomer from an aqueous environment to a lipid bilayer, as determined from ITC.

Systems	K (mM^{-1})	ΔG_{trans} (kJ mol^{-1})	ΔH_{trans} (kJ mol^{-1})	ΔS_{trans} (J $K^{-1}mol^{-1}$)
POPC	13.5 ± 0.4	-33.53 ± 0.07	-10.07 ± 0.10	78.6 ± 0.5
POPC : POPG	13.9 ± 0.3	-33.60 ± 0.04	-14.8 ± 0.4	63.1 ± 1.4
POPC : Cardiolipin	15.9 ± 0.3	-33.94 ± 0.05	-12.14 ± 0.12	73.0 ± 0.5
POPC : Cholesterol	7.05 ± 0.12	-31.92 ± 0.04	-8.70 ± 0.18	77.8 ± 0.7

value. This profile is complex due to the co-existence of micelles and monomers, and its description is provided in the discussion section.

Four typical calcein-release profiles induced by CPC are shown in Figure 4.3. They have been selected as they were caused by the same amount of CPC (a final concentration of 73 μM), and they illustrate the dependence of the release kinetics on the bilayer composition. In all 4 membrane compositions investigated, the addition of CPC causes a sudden release of the entrapped calcein over the first minute. For the two neutral systems (POPC, and POPC/chol), the leakage practically stops after this period. However, when the membranes contain negatively charged POPG or cardiolipin, the leakage continues with a complex dependence with time. The maximum leakage is observed after about 10, and 30 minutes for the POPG-, and the cardiolipin-containing membranes, respectively. To summarize, the release curves can be divided into two groups. First, the leakage from zwitterionic bilayers is mainly observed during the first minute after the addition of the detergent. Second, for membranes containing negatively charged lipids, the initial burst represents only a fraction of the release induced by CPC, and another phenomenon with a longer time scale is responsible for most of the probe release. The figure also indicates that, for a given incubation CPC/lipid molar ratio, the extent of calcein leakage is dependent on the lipid composition of the bilayers.

The release is dependent on the amount of added CPC. In Figure 4.4, we report the calcein leakage as a function of the incubation CPC/lipid molar ratio. The leakage was measured at the plateau except in the case of cardiolipin-containing vesicles where the reported values were obtained 700 s after the addition of the detergent. In the case of POPC, and POPC/POPG mixtures, CPC can completely release the probe from the vesicles if a sufficient amount of surfactant is added. In order to provide a quantitative description of the propensity of the lipid membrane to CPC-induced leakage, the incubation CPC/lipid molar ratio leading to 50% release (R_{50})

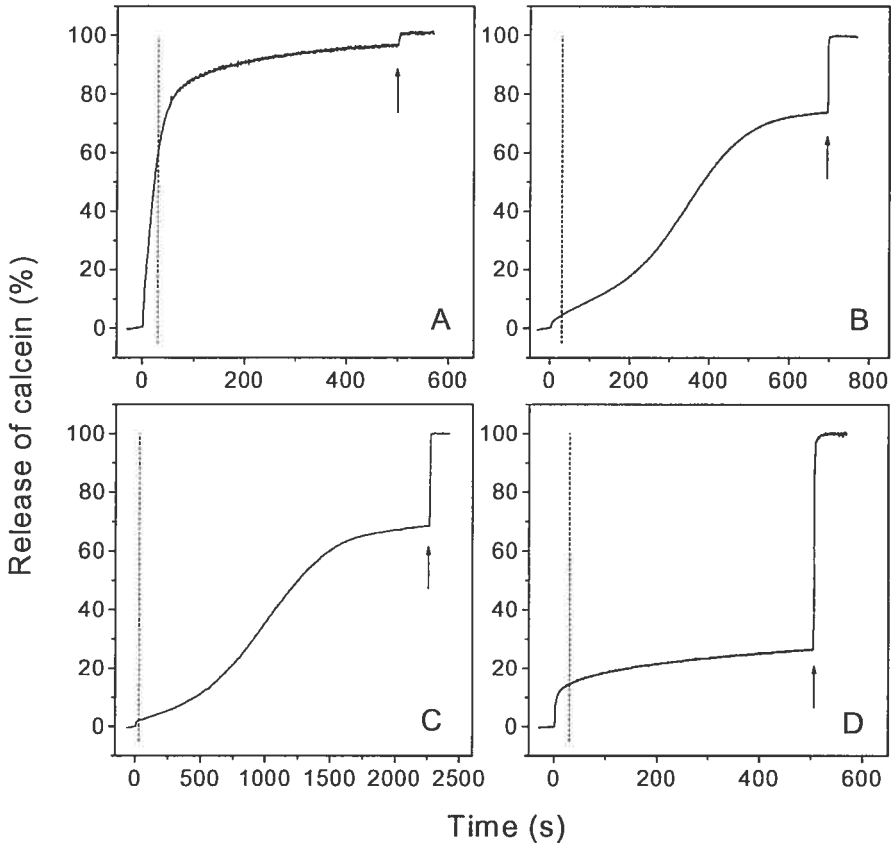

Figure 4.3 : Typical calcein-release curves resulting from the addition of CPC (73 μM), at time set as 0, to calcein-loaded vesicles (the lipid concentration was between 10, and 13 μM). The vertical lines indicate 30 s after the detergent addition. The arrows indicate the addition of Triton X-100 that was used to normalize the leakage curves. The lipid composition was A) POPC, B) POPC/POPG, C) POPC /card, and D) POPC/chol.

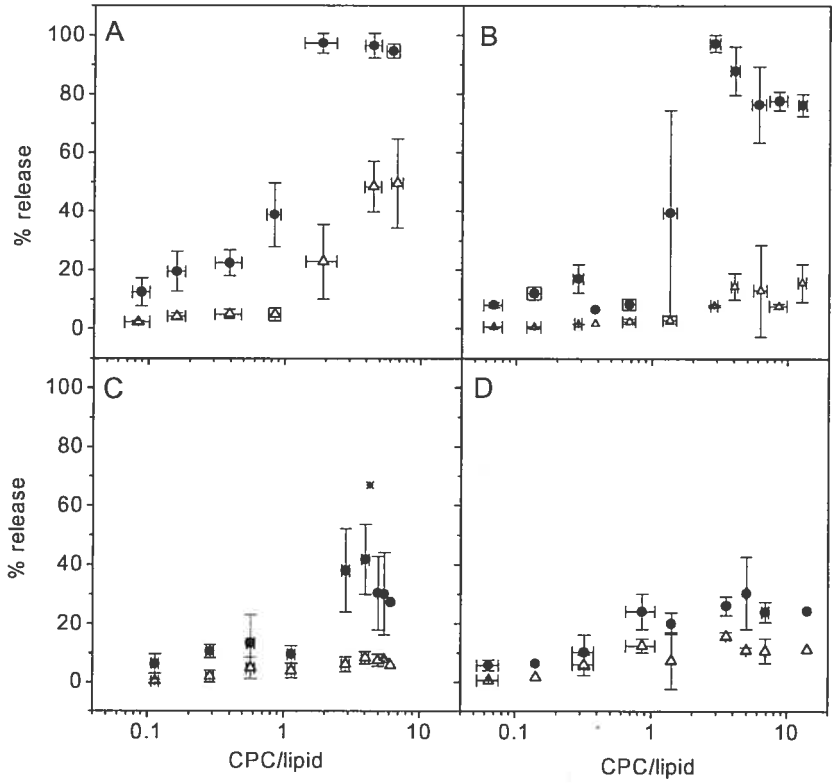

Figure 4.4 : Dependence of the calcein release on the CPC amount added to the lipid vesicles. The %release was measured (Δ) 30 s after the addition of CPC, and (•) at the plateau (or 700 s after the addition of CPC in the case of the POPC/card system). The %release at the plateau obtained when CPC was added to POPC/card vesicles in a CPC/lipid ratio of 4.3 is indicated by a *. The lipid composition was A) POPC, B) POPC/POPG, C) POPC/card, and D) POPC/chol.

was determined. For POPC, R_{50} was estimated to 0.9 whereas it is 1.7 for POPC/POPG bilayers. A complete calcein release from POPC/POPG vesicles was observed when the incubation CPC/lipid molar ratio was about 3. Unexpectedly, the addition of larger CPC amounts led to a decrease of the %release, down to 77 % when the incubation CPC/lipid molar ratio was 20. Further investigations are needed to understand this effect. In the case of cholesterol-containing membranes, the release was limited to about 20%, even for incubation CPC/lipid molar ratios as high as 20. This result clearly establishes the protective power of cholesterol relative to the CPC-induced leakage. In the case of cardiolipin-containing membranes, the release measured after 700 s was limited to about 40%. This is associated to the slow leakage observed for these membranes. Even when the leakage was measured at the plateau, the release from these membranes is more limited than that observed for POPC and POPC/POPG bilayers. The difference in the kinetics of release is also illustrated in Figure 4 by reporting the calcein releases observed 30 s after the addition of CPC. In the case of the zwitterionic membranes (POPC and POPC/chol systems), the variation of the release measured after 30 s as a function of the CPC/lipid ratio follows that measured at the plateau. This first burst always corresponds to about 60% of the complete release, independently of the CPC/lipid ratio. Conversely, in the case of negatively charged membranes, the release observed during the first 30 s is fairly independent on the CPC/lipid ratio and corresponds always to less than 20% of release, even for incubation CPC/lipid molar ratios as high as 20.

Cryo-TEM micrographs illustrating the effects of CPC on the morphology of lipid assemblies are presented in Figure 4.5. They were obtained from POPC vesicles to which CPC was added in an incubation CPC/lipid molar ratio of 1.5. Figure 4.5A and B display the micrographs of POPC LUVs prior to the addition of the detergent, and 10 minutes after the CPC addition, respectively. In both cases, the sample included mainly unilamellar vesicles and, on this time scale, CPC did not appear to have an effect on the morphology of the lipid assemblies. The main

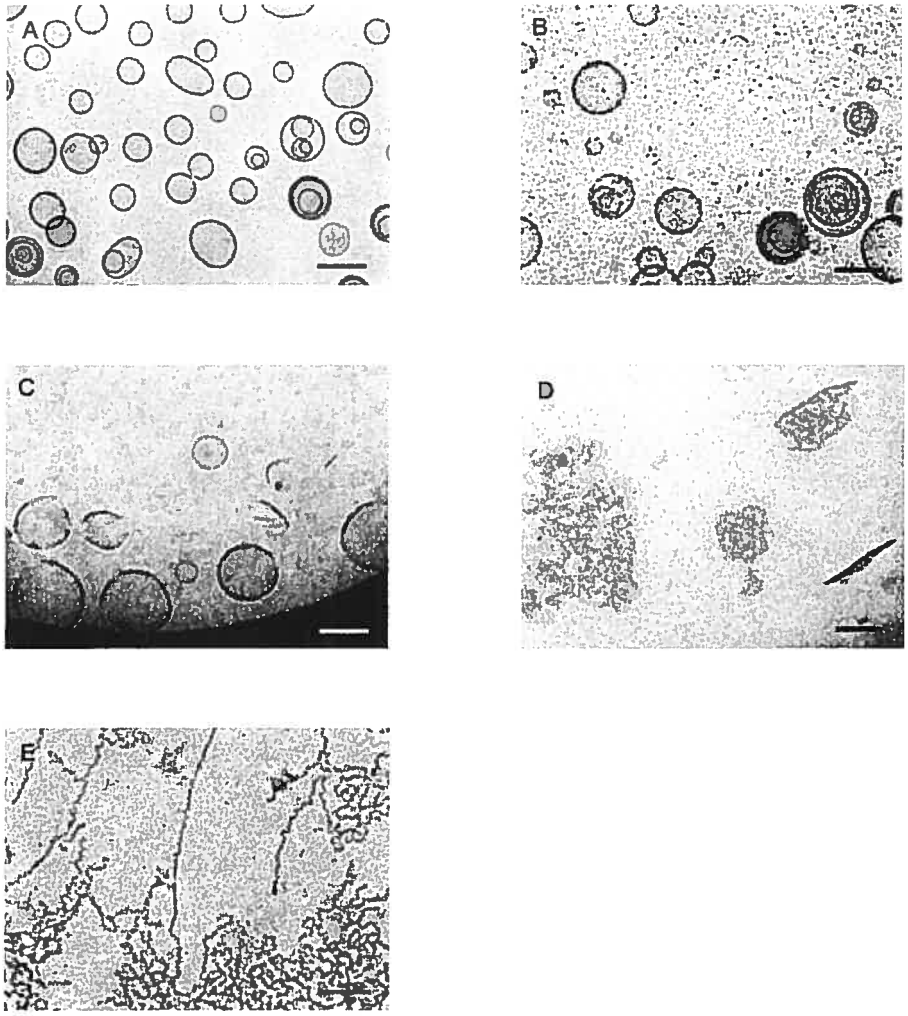

Figure 4.5 : Cryo-EM micrographs illustrating the effect of CPC (15 mM) on POPC vesicles (10 mM). A) Vesicles prior to the addition of the detergent; B) 10 minutes after the addition of CPC; C-E) 2 days after the addition of CPC. C) displays perforated vesicles, D) perforated bilayer sheets, and E) branched thread-like CPC/POPC mixed micelles.

difference between the two micrographs is that the more textured background of Figure 4.5B, due to the presence of CPC micelles. After a 48-h incubation (Figure 4.5 C, D, and E), CPC caused drastic changes in the morphology of the lipid assemblies. Perforated vesicles, lipid sheets, and long ribbons associated to lipid/CPC mixed micelles could be observed. Such structures have been previously observed for other phospholipid-cationic detergent systems.[27] After 2 weeks, only mixed micelles were observed. These results indicate that, in the presence of CPC, the morphology of the lipid assemblies is modified but these changes occur over a relatively long period.

4.5 Discussion

The partitioning equilibrium constants (K) of CPC for the investigated lipid systems (Table 4.1) indicate that the association of CPC monomers to lipid membranes is thermodynamically favourable. Also, about two thirds of ΔG_{trans} are associated to a gain in entropy related to the hydrophobic effect.[34] In fact, ΔG_{trans} are on the same order of magnitude as ΔG_{mic}, suggesting that bilayers and micelles both provide a similar environment, with polar, and apolar regions accommodating the amphipathic nature of CPC. The data relative to the affinity of CPC or QACs to membranes are rather sparse. Another study of the association of CPC with PC membranes also concluded that an entropy gain is the driving force for the CPC micelle formation and its insertion in bilayers.[35] Their affinity constant of CPC for POPC vesicles in pure water as determined by conductivity[35] is reported to be 1.89 x 10^2 M^{-1}. This value is two orders of magnitude weaker than the value that we determined; this is most likely a consequence of a salt effect. The insertion of CPC in PC bilayers leads to the formation of a positive membrane surface charge. As a consequence, this membrane surface potential should lead to a gradient of CPC concentration, from the surface toward the bulk solution.[36] This gradient is dependent on the ionic strength of the aqueous environment and should be

drastically more pronounced in pure water. A lower concentration near the interface would cause a decrease of the apparent partitioning constant.

Our permeability measurements indicate that CPC is effective to perturb lipid membrane permeability. To our knowledge, the perturbing power of CPC on lipid model membranes has never been assessed but it can be compared with studies characterizing other QACs. Similar leakage experiments were performed with hexadecyltrimethylammonium bromide (HTAB), and 3-(hexadecyldimethylammonio) propane-1-sulfonate (HDPS), two QACs bearing a saturated acyl chain 16-carbon atom long.[20] For POPC vesicles, the R_{50} were 10, and 36 for HTAB, and HDPS respectively. These values are higher than R_{50} obtained here for CPC ($R_{50} = 0.9$), suggesting a higher efficiency for the latter.

The values of K obtained for bilayers exclusively formed by phospholipids are similar, within 1%. Despite the fact that CPC is a positively charged detergent, it does not show a specific affinity for negatively charged membranes. This result is consistent with the absence of effect of the membrane charge (either positive or negative) on the critical alkyltrimethylammonium bromide concentration causing membrane solubilization.[37] The ΔH_{trans} values (Table 4.1) are slightly more negative for negatively charged membranes, suggesting a small electrostatic contribution. However the results suggest that these favorable interactions are counterbalanced by a reduced entropy increase. This enthalpy-entropy compensation inferred for the binding of CPC to lipid membrane would be similar to that observed for the binding of magainin to large and small unilamellar vesicles[38] and for the partitioning of phenothiazine drugs in phosphatidylcholine bilayers.[39] It is not excluded that the attractive electrostatic interactions between the detergent and the lipids limit the entropy within the bilayers. Along the same line, the ability of CPC to induce leaks in vesicles does not appear to be significantly influenced by the membrane surface charge density.

By opposition to the partitioning and the extent of leakage that are practically independent of the membrane surface charge, the kinetic of release presents different profiles for the neutral and the negatively charged membranes (Figure 4.3). This difference may be associated to the translocation of detergents across the membrane. Once incorporated in the bilayer, CPC molecules likely interact with the surface charges carried by the phospholipid head groups, as suggested for other QAC.[8,10] In the case of negatively charged POPG or cardiolipin, these interactions could be strong enough to lead to a slower translocation of the detergent. In the case of cardiolipin-containing membranes, the electrostatic interactions may be even stronger considering the two negative charges carried by a single molecule, and the very slow release that we observed. Moreover, cardiolipin restricts the motions of the lipid acyl chains in membrane.[40] As it will be discussed for cholesterol, the detergent translocation can be hindered by this increased order. Therefore the slow release observed for cardiolipin could be associated to a combined effect of attractive electrostatic interactions at the membrane surface, and of the ordering of the hydrophobic core. Despite the fact that the lipid composition of the membranes affects the release process, it does not seem that there is a simple relationship between the membrane affinity and the magnitude of the induced leakage.

In the case of cholesterol-containing membranes, both the membrane affinity and the induced leakage are decreased compared to the bilayers made exclusively of phospholipid. However, even taking into account the lower affinity constant, the leakage induced by CPC appears to be much lower than for POPC vesicles for the same bound CPC/lipid ratio. The presence of cholesterol in lipid bilayers lead to the formation of a fluid phase where the lipid acyl chains are highly ordered, referred to as the liquid ordered (l_o) phase.[41,42] The reduced CPC affinity could be associated with the tight lipid chain packing observed in the cholesterol-containing membranes; the compactness of the lipid chain packing can make the insertion of detergent acyl chain less favourable. Interestingly, the inhibition of the leakage by

cholesterol was also observed for HTAB, and HDPS.[20] It was proposed that some detergent molecules must reach the internal lipid layer in order to induce leakage and this translocation would be more difficult when the bilayer is in the l_o phase.[20] That hypothesis was reinforced by the fact that proton-ionizable analogs were not as sensitive to the presence of cholesterol in the bilayer.[20] It was proposed that the neutral amine formed by loss of a proton could translocate more easily than QACs, even across a cholesterol-containing bilayer. Similarly, an absence of influence of cholesterol-content membranes was also reported for neutral Triton X-100.[43,44] Therefore, it seems that the positive charge of QAC is essential for the effect observed in the presence of cholesterol.

The titration of the CPC micelles with lipid vesicles (Figure 4.1C) shows a more complex behaviour than that observed with the CPC monomers (Figure 4.1B). However, this behaviour could be reproduced using the thermodynamic parameters determined above. We propose that when lipid vesicles are added to the cell containing CPC monomers and micelles, the detergent monomers partition between the aqueous, and the lipid phases, and this is providing an equilibrium described by the partitioning constant determined above. At the beginning of the titration, the CPC monomer concentration remains at the CMC and therefore, the micelles act as a detergent reservoir to provide the CPC molecules that are incorporated in the lipid bilayers. The enthalpy variations measured in these conditions correspond to the number of moles of CPC transferred from the micelles to the bilayers times the sum of $-\Delta H_{mic}$, and ΔH_{trans}. Upon the titration, all the CPC molecules in the micellar form are transferred to the lipid phase, and the CPC monomer concentration becomes smaller than the CMC. The enthalpy variations measured in these conditions correspond to the number of moles of monomeric CPC transferred from the solution to the bilayers times ΔH_{trans}. Once most of the CPC is transferred to the bilayer, only small peaks corresponding to the dilution of the vesicles are observed. Another factor had to be taken into account. Because of the high CPC concentration at the beginning of the titration, the proportion of CPC in the bilayer

is large. As a consequence, a positive surface charge density is created, leading to a CPC concentration gradient, from the interface to the bulk of the solution. Such phenomenon has been included to rationalize the adsorption of charged species, such as SDS, on lipid membranes.[36,38,45] In these conditions, the monomer concentration in solution (C_{Dw} in Equation 4.1) in equilibrium with the CPC bound form can be considerably lower than that in the bulk. This difference can be estimated from the Gouy-Chapman theory. The surface charge density of the membrane is given by:[45]

$$\sigma = \left(\frac{e_o}{X_{lipids} A_l + X_{CPC} A_{CPC}} \right) \left(X_{POPG} Z_{POPG} + X_{CPC} Z_{CPC} \right) \quad \text{Eq. 4.6}$$

where e_o is the electron charge, X_{lipids}, X_{POPG} and X_{CPC} are the membrane molar fraction in lipids, POPG, and CPC, respectively. A_l is the area occupied by one lipid and it was assumed to be 68 $Å^2$ for both POPC, and POPG.[45] A_{CPC} is the interfacial area of CPC in membranes (32 $Å^2$)[46], Z_{POPG} and Z_{CPC} are the charge of POPG (-1), and of CPC (+1), respectively. From the surface charge density, the membrane surface potential (Ψ_0) can be estimated using:

$$\sigma^2 = 2000\, \varepsilon_o \varepsilon_R RT \sum_i C_{i,eq} \left(e^{-z_i F_o \Psi_o / RT} - 1 \right) \quad \text{Eq. 4.7}$$

where ε_o is the permittivity of vacuum, ε_R, the relative dielectric constant, R, the gas constant, T, the temperature, F_o, the Faraday constant, and $C_{i,eq}$, the concentration of the ion *i* bearing a charge of z_i. In our simulation, we took into account all the charged species and that half of the buffer molecules was dissociated. The relationship between the interfacial CPC monomer concentration (C_{Di}), and the CPC monomer concentration in the bulk phase (C_{Dw}^b), is given by [45]:

$$C_{Di} = C_{Dw}^b \exp\left[- \frac{Z_{CPC} F_0 \Psi_0}{RT} \right] \quad \text{Eq. 4.8}$$

For given CPC and lipid concentrations, the value of X_{CPC} for which Eq. 4.1, 4.6, 4.7, and 4.8 are consistent was found by an iterative method, taking into account the K value determined above (Table 4.1). This procedure was performed in two regimes. First, at the beginning of the titration, C_{Dw}^{b} was set to be the CMC. The fitted X_{CPC} provided the amount of bound CPC and, if the quantity of CPC in the cell was sufficient to bind this quantity and to leave enough CPC in solution to be above the CMC, this was considered the accepted solution. If the remaining CPC concentration in solution was below its CMC, C_{Dw}^{b} was allowed to vary. Once X_{CPC} was determined for every lipid concentration, the quantity of CPC micelles that were dissociated, and of CPC monomers transferred from the aqueous environment to the membranes were determined. From these values and the determined ΔH_{mic}, and ΔH_{trans}, the h_i and H_i associated to each injection was calculated. The simulation is completely independent of the experimental H_i and does not include any fitting parameters. It is strictly based on the values of K, ΔH_{mic}, and ΔH_{trans} determined in other experiments. The agreement of the simulation with the experimental data (Figure 4.6) illustrates, first, the reliability of these values and, second, that the behaviour of this complex systems can be described simply by an equilibrium between CPC monomers, CPC micelles, and bound CPC on the time scale of the titration.

Cryo-TEM micrographs show that CPC modifies drastically the morphology of the POPC self-assemblies, with a pattern similar to the behaviour observed for other cationic detergents.[27,47] These micrographs were obtained from samples with a large amount of CPC. The results show that no significant changes are observed 10 minutes after the addition of the detergent, indicating that the observed calcein release was not associated with the lysis or destruction of the vesicles, at the microscopic level. It seems that the leakage is associated with more local (molecular) defects. Similarly, the lipid self-assemblies remained vesicular during the ITC experiments, as confirm by dynamic light scattering (data not show). It is beyond the scope of this paper to describe the details of the kinetics of these

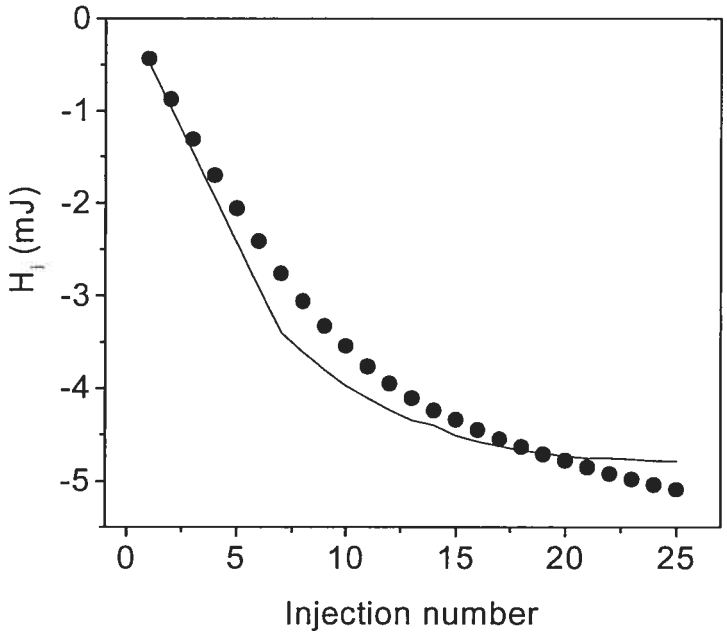

Figure 4.6 : Titration curve of CPC solution (300 µM) with a lipid suspension (17 mM), corresponding to the data in Figure 4.1C. The points represent the enthalpy variations associated to the injections of lipid vesicles to the cell filled with a CPC solution. The full line represents the fit obtained from the model presented in the discussion section.

morphological changes. However the micrographs recorded after a 48-h incubation show the co-existence of several morphologies, representative of structural intermediates. For the investigated lipid/CPC proportion, the final structure appeared to be tubular mixed micelles.

Despite the intuitive increase of affinity of CPC for negatively charged membranes, our results show that the presence of POPG or cardiolipin, two anionic lipids present in bacterial membranes, do not lead to higher binding constant or to increased leakage. The association of CPC with lipid membranes appears to be mainly caused by hydrophobic interactions and attractive electrostatic interactions do not play a significant role. The thermodynamic data suggest an enthalpy-entropy compensation. The binding constants measured for CPC are not very high; in fact they are in the same order of magnitude as those obtained for other detergents including SDS, a negatively charged amphiphile.[36] This absence of significant effects of electrostatic interactions between CPC and negatively charged membranes illustrates the limited knowledge of the molecular details of the antibacterial mechanism of QACs. Electrostatic effects involving QACs have been reported however. For example, a decrease of the bactericidal efficiency of QACs against *Salmonella typhimurium* and of its binding to these bacteria is observed when the conditions give to the cell membrane a reduced net negative charge.[6] A reduction of alkyltrimethylammonium binding to the bacterial membranes was also observed when the membrane charge was decreased.[6] Similarly, dendrimers decorated with quaternary ammonium groups were showed to interact with bacterial membranes and high concentrations of Ca^{2+} reduced the biocide power of these compounds.[48] Moreover, the bioaccumulation of CPC in bacterial biofilms[17] appears to be practically irreversible. These observations cannot be associated straightforward to electrostatic attractive interactions. Other "sites" associated with other biofilm components may explain this attraction. These potential sites include membrane lipids that were not examined in this study, and negatively charged exopolysaccharides present in some biofilms.

4.6 Conclusion

CPC associates with lipid membranes and alters their permeability. This association is influenced by the presence of cholesterol, most likely by the dense chain packing that prevents the detergent insertion. CPC-induced leakage is modulated by the lipid composition and these effects are suggested to be related to the translocation of the detergent across the bilayer. In the presence of cholesterol, CPC translocation would be very unfavourable because of the net positive charge of the quaternary ammonium, as previously suggested for other QACs.[20] The attractive electrostatic interactions between negatively charged phospholipid head groups and CPC may hinder the detergent translocation and be the origin of the slow calcein release observed in the presence of POPG or cardiolipin. These findings are of interest in the development of novel biocides based on QAC motifs that optimize their affinity for bacterial cell membrane and their ability to disrupt the membrane integrity.

4.7 Acknowledgements

The authors acknowledge the financial support from Natural Sciences and Engineering Research Council of Canada, the Fonds de recherche sur la nature et les technologies of Québec (M.L.), the Swedish Research Council, and the Swedish Foundation for Strategic Research (K.E.). M.L. is also grateful to the Royal Academy of Arts and Sciences of Uppsala for its financial support during his stay at Uppsala University. This work was performed as a research project of the Center for Self-Assembled Chemical Structures (CSACS).

4.8 References

1. C. Campanac, L. Pineau, A. Payard, G. Baziard-Mouysset and C. Roques, Antimicrob. Agents Chemother. **46**, 5, 1469 (2002)
2. B. Ahlström, M. Chelminska-Bertilsson, R. A. Thompson and L. Edebo, Antimicrob. Agents Chemother. **41**, 3, 544 (1997)
3. G. McDonnell and A. D. Russell, Clin. Microbiol. Rev. **12**, 1, 147 (1999)
4. A. D. Russell and I. Chopra. *Understanding Antibacterial Action and Resistance* (Ellis Horwood, Chichester, 1990)
5. A. D. Russell, Lancet Infect. Dis. **3**, 794 (2003)
6. B. Ahlström, R. A. Thompson and L. Edebo, APMIS **107**, 318 (1999)
7. B. Ahlström and L. Edebo, Microbiology **144**, 2497 (1998)
8. S. P. Denyer, Int. Biodeterior. Biodegrad. **36**, 227 (1995)
9. S. Przestalski, J. Sarapuk, H. Kleszczynska, J. Gabrielska, J. Hladyszowski, Z. Trela and J. Kuczera, Acta Biochim. Pol. **47**, 3, 627 (2000)
10. S. P. Denyer, Int. Biodeter. **26**, 89 (1990)
11. P. Sreenivasan and A. Gaffar, J. Clin. Periodontol. **29**, 11, 965 (2002)
12. A. S. Landa, H. C. van der Mei and H. J. Busscher, Adv. Dent. Res. **11**, 4, 528 (1997)
13. Y. Shimazaki, M. Mitoma, T. Oho, Y. Nakano, Y. Yamashita, K. Okano, Y. Nakano, M. Fukuyama, N. Fujihara, Y. Nada and T. Koga, Clin. Diagn. Lab. Immunol. **8**, 6, 1136 (2001)
14. J. Ali, R. Khar, A. Ahuja and R. Kalra, Int. J. Pharm. **283**, 1-2, 93 (2002)
15. H. N. Newman and M. Wilson. *Dental Plaque Revisited Oral Biofilms in Healt and Desease* (Bioline, London, 1999)
16. R. J. Nisengard and M. G. Newman. *Oral Microbiology and Immunology* (W. B. Saunders Company, Philadelphia, 1994)
17. L. Marcotte, H. Thérien-Aubin, C. Sandt, J. Barbeau and M. Lafleur, Biofouling ***in press***,(2004)

18. E. I. Szabo, B. H. Amdur and S. S. Socransky, Caries Res. **12**, 21 (1978)
19. M. Bloom, Phys. Can. **48**, 7 (1992)
20. S. Watanabe and S. L. Regen, J. Am. Chem. Soc. **116**, 5762 (1994)
21. P. Hoyrup, J. Davidsen and K. Jorgensen, J. Chem. Phys. B **105**, 2649 (2001)
22. M. R. Wenk and J. Seelig, J. Chem. Phys. B **101**, 5224 (1997)
23. H. Heerklotz and J. Seelig, Biochim. Biophys. Acta **1508**, 69 (2000)
24. B. Rozycka-Roszak, R. Zylka, T. Kral and A. Przyczyna, Z. Naturforsch. **56c**, 407 (2001)
25. R. El Jastimi, K. Edwards and M. Lafleur, Biophys. J. **77**, 842 (1999)
26. Allen, A. T. Liposome technology, CRC Press: Boca Raton, Fl, 1984; pp 177-182.
27. K. Edwards, J. Gustafsson, M. Almgren and G. Karlsson, J. Colloid Interface Sci. **161**, 299 (1993)
28. J. Gallova, F. Devinsky and P. Balgavy, Chem. Phys. Lipids **53**, 231 (1990)
29. T. Inoue, T. Yamahata and R. Shimozawa, J. Colloid Interface Sci. **149**, 2, 345 (1992)
30. P. R. Majhi and S. P. Moulik, Langmuir **14**, 3986 (1998)
31. T. Benachir and M. Lafleur, Biochim. Biophys. Acta **1235**, 452 (1995)
32. C. H. Fiske and Y. Subbarow, J. Biol. Chem. **66**, 375 (1925)
33. M. Almgrem, K. Edwards and G. Karlsson, Colloids Surf. A **174**, 3 (2000)
34. J. Israelachvili. *Intermolecular and Surface Forces, 2th Edition* (Academic Press inc., London, 1992)
35. H.-K. Stao and W. L. Tseng, J. Chem. Phys. **115**, 17, 8125 (2001)
36. A. Tan, A. Ziegler, B. Steinbauer and J. Seelig, Biophys. J. **83**, 1547 (2002)
37. A. de la Maza and J. L. Parra, J. Controlled Release **37**, 33 (1995)
38. T. Wieprecht, O. Apostolov and J. Seelig, Biophys. Chem. **85**, 2-3, 187 (2000)
39. S. Takegami, K. Kitamura, T. Kitade, A. Kitagawa and K. Kawamura, Chem. Pharm. Bull. **51**, 9, 1056 (2003)
40. C. A. Valcarcel, M. D. Serra, C. Potrich, I. Bernhart, M. Tejuca, D. Martinez, F. Pazos, M. E. Lanio and G. Menestrina, Biophys. J. **80**, 2761 (2001)

41. J. L. Thewalt and M. Bloom, Biophys. J. **63**, 1176 (1992)
42. F. M. Linseisen, J. L. Thewalt, M. Bloom and T. M. Bayerl, Chem. Phys. Lipids **65**, 141 (1993)
43. Y. Nagawa and S. L. Regen, J. Am. Chem. Soc. **113**, 7237 (1991)
44. R. El Jastimi and M. Lafleur, Biospectroscopy **5**, 133 (1999)
45. A. Percot, X. X. Zhu and M. Lafleur, Biopolymers **50**, 647 (1999)
46. Mingotaud, A.-F.; Mingotaud, C.; Patterson, L. K. *Handbook of Monolayer;* Academic Press inc.: Sandiego, 1993; Vol. 1.
47. M. Almgren, Biochim. Biophys. Acta **1508**, 146 (2000)
48. C. Z. Chen and S. L. Cooper, Biomaterials **23**, 3359 (2002)

Chapitre 5

Permeability and Thermodynamics Study of Quaternary Ammonium Surfactants - Phosphocholine Vesicle System.

Lucie Marcotte, Jean Barbeau and Michel Lafleur

Soumis à *Journal of Colloids and Interface Science* (2004)

Keywords: QAC, POPC, permeability, ITC, affinity

Abbreviated title: QACs effect on phosphocholine vesicle system.

5.1 Abstract

Quaternary ammonium compounds (QACs) are recognized as membrane active agents widely used as biocides. The main purpose of this work was to investigate the influence of the QAC head group and acyl chain length on their permeability-perturbing power and on their affinity for lipidic membranes. Permeability perturbations were assessed by measuring the release of calcein entrapped inside vesicles. The affinity of QACs for bilayers was investigated by isothermal titration calorimetry (ITC). QACs bearing C_{16} chain were found to be more efficient to decrease the membrane permeability than their C_{12} analogues. On the other hand, the chemical nature of the ammonium head group has practically no influence on the permeability perturbations caused by QACs bearing C_{16} chains. It was difficult to assess the partitioning of the QACs between the aqueous and lipid phases since the ITC signals could also be associated to parallel phenomena such as vesicle aggregation. For the systems for which reliable thermodynamic parameters could be obtained, the Gibbs energy of transfer were similar to that for the micellization. The entropy variation represented the main contribution to the Gibbs energy, indicating that the insertion of QACs inside lipidic bilayers is driven by hydrophobic interactions.

5.2 Introduction

Quaternary ammonium compounds (QACs) constitute a family of detergents that are used as biocides.[1-4] Despite their current use, the details of their mechanism of action are not well identified. Several observations indicate that QACs act at the bacteria membrane level [1,5] and lead to the leakage of internal metabolites (K^+ and PO_4^-), the loss of membrane enzymes, and the cell lysis.[1,2,4] These effects could be the result of various processes and it has been suggested [6,7] that they are the results of perturbations of the lipid bilayer caused by the insertion of QACs in membranes. The attractive interactions between QACs and the membrane phospholipids are believed to be of electrostatic nature.

Several QACs used as biocides have different polar head groups, and alkyl chain lengths. Three head groups commonly reported are: benzalkonium, alkylpyridinium and tetraalkylammonium.[1-4,8-10] The chemical nature of the polar head influences the bactericidal efficiencies. For example, Gram-negative bacteria, from the genera *Serratia*, *Enterobacter*, *Escherichia*, and *Pseudomonas*, have been shown to be more sensitive to alkylpyridinium compare to benzalkonium and alkyltrimethylammonium.[3] In addition, the head group influences some properties of these detergents, such as their critical micelle concentration (CMC), and their micelle shape.[10] However, there is a limited knowledge rationalizing the influence of the head group on these properties and the biocide power. The aliphatic chain length is another molecular feature of QACs that influences their efficiencies. Typically, QACs include a saturated, and linear chain whose length varies between 8 and 18 carbon atoms.[1] The acyl chain length was shown to have a prime influence on the biocidal activity and selectivity.[4,9,10] It was suggested that an increase in hydrophobicity was the origin of the enhanced biocide efficacy.

The effects of surfactants on model membranes have been studied by different techniques, including light scattering, NMR, infrared spectroscopy, and cryo-transmission electron microscopy.[11] Several studies characterized the solubilization steps of lipid bilayers as a function of the detergent concentration.[12-14] Surfactants were shown to cause morphological and phase changes in bilayers.[12,15,16] At low surfactant concentration, there is a partition between the aqueous phase and the bilayer. As the surfactant concentration increases, the lipid bilayers start to break into micellar aggregates. Eventually, at high surfactant concentrations, the complete dissolution of the bilayers into mixed micelles is obtained.[12,15] QACs have been reported to increase the fluidity of model bilayers[11,17] as well as real bacterial membranes.[18] However, a higher fluidization did not correlate with a higher bactericidal activity.[18]

In this work, we aimed at gaining some insights into the influence of molecular features of QACs on their biocidal activity. Two aspects of their membrane activity were characterized: their effect on membrane permeability, and their association with lipidic bilayers. We have examined the influence of the nature of the polar head, and the aliphatic chain length on these phenomena. In order to study the effect of QACs on the permeability of 1-palmitoyl-2-oleolyl-phosphocholine (POPC) membranes, we followed the QAC-induced release of a fluorescent probe (calcein) entrapped in POPC vesicles, using an established fluorescence assay.[19,20] Furthermore, we verified the morphology of the POPC-QACs systems using dynamic light scattering (DLS). The association of QACs to POPC membranes was characterized using isotherm titration microcalorimetry (ITC) technique[21,22] as it is versatile and does not required the labelling of the surfactant.

5.3 Materials and Methods

From the QACs known for their biocidal activity, we selected three different types of polar head group: two quaternary ammonia composed of an aromatic ring (benzyldimethylammonium, and pyridinium), and one including only methyl groups (trimethylammonium). From an acyl chain length point of view, we selected dodecyl (12-carbon atoms), and hexadecyl or cetyl (16-carbon atoms). Figure 5.1 presents the molecular formula for the six selected QACs. The study was made with model membranes composed of POPC, a zwitterionic phospholipid that forms stable bilayers.

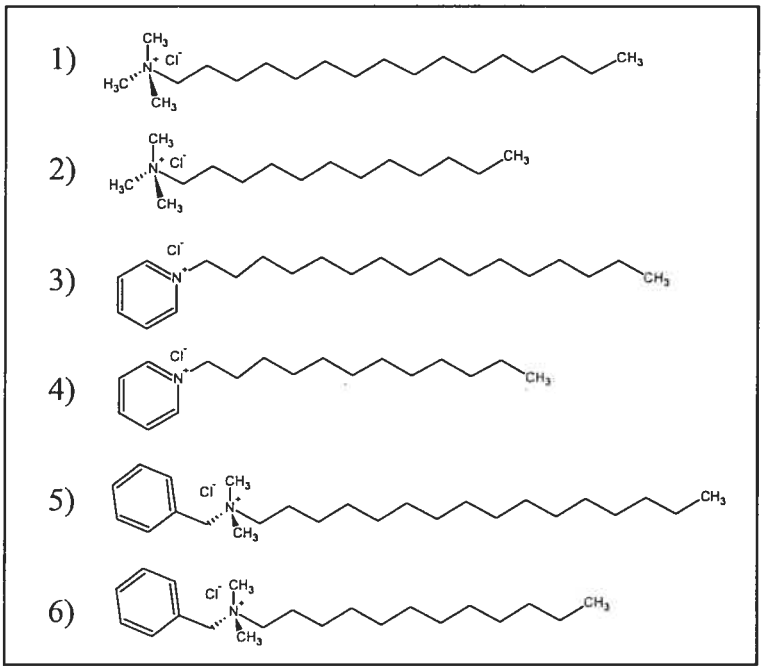

Figure 5.1 : Representation of the molecular structure of the investigated QACs. 1) cetyltrimethylammonium chloride; 2) dodecyltrimetylammonium chloride; 3) cetylpyridinium chloride; 4) dodecylpyridinium chloride; 5) benzyldimethylhexadecylammonium chloride; 6)benzyldimethyldodecylammonium chloride.

Cetylpyridinium chloride (CPC), 1-dodecylpyridinium chloride (DPC), and cetyltrimethylammonium chloride (CTAC), 25 (w/w) % solution in water, were purchased from Sigma-Aldrich (Oakville, ON, Canada). Benzyldimethyldodecylammonium chloride (BDDAC), benzyldimethylhexadecylammonium chloride (BDHAC) and dodecyltrimethylammonium chloride (DTAC) were obtained from Fluka (Oakville, ON, Canada). 2-[N-Morpholino]ethanesulfonic acid (MES), and ethylene-diaminetetraacetic acid (EDTA) were obtained from Sigma-Aldrich while NaCl, and calcein (2,4-bis-[N,N-di(caboxymethyl)aminomethyl]fluorescein) were purchased from Anachemia (Rouses Point, NY, USA) and Molecular Probes (Eugene, OR, USA) respectively. POPC was purchased from Avanti Polar Lipids inc. (Birmingham, Al, USA). All the suspensions were prepared with ultra-pure water (Ω = 18 Mhoms cm^{-1}).

Critical micellar concentration (CMC)

The critical micellar concentration (CMC) of each QAC was first determined by isothermal titration calorimetry (ITC).[21,23] The CMC were obtained in the MES buffer used for the other experiments (10 mM MES, 10 mM NaCl, 5 mM EDTA, pH = 6.5). The ITC experiments were performed using a microcalorimeter VP-ITC from Microcal inc. (Northampton, MA, USA). The sample cell volume was 1.4527 mL. All the measurements were performed at 25° C. The QAC concentration and the volume of an injection were optimized for each surfactant (CATC: 5-µL injections of a 200 µM solution; DTAC: 10-µL injections of a 154 mM solution; DPC: 5-µL injections of a 200 mM solution; CPC: 7 to 10-µL injections of 7.4 mM solution; BDHAC: 10-µL injections of a 264 µM solution; and BDDAC: 10-µL injections of a 50 mM solution). The number of injections was between 10 and 20. In order to define the CMC, the area of each peak was integrated and then normalized for the amount of injected detergent. These values were plotted as a function of the detergent concentration in the cell after each injection. The first

derivatives of these curves were simulated using a Gaussian function and the center of the peak was considered to be the CMC. We also estimated the enthalpy of micellization (ΔH_{mic}) from the titration experiments by calculating the difference between the mean molar enthalpy of the first 3 injections (i.e. performed at a detergent concentration in the cell below its CMC) minus the mean molar enthalpy of the last 3 injections (i.e. performed with a detergent concentration in the cell above the CMC).[23]

Permeability measurements

For the permeability experiments,[19,20,24] we used calcein (80 mM) in MES buffer (MES 100 mM, NaCl 10 mM, EDTA 5 mM, pH 6.5) entrapped into large unilamellar vesicles (LUVs) made of POPC. The LUVs were obtained by extrusion through two polycarbonate filters with pore size of 100 nm in diameter, using an extruder from Avestin (Ottawa, ON, Canada). During the exclusion chromatography step used to isolate the calcein-loaded vesicles from the free probe, the iso-osmotic elution buffer was MES buffer (100 mM) pH 6.5, with NaCl 120 mM and EDTA 5 mM. The more concentrated LUV fraction (about 1.5 mL) was diluted to obtain a suspension of about 10 μM in lipids. The exact lipids concentration was determined by the Fiske-Subbarow assay.[25] Typically, an aliquot of a detergent solution (between 0 to 73 μM) was added to 2 mL of the vesicle suspension. The release of calcein as a function of time was measured by the increase of calcein fluorescence intensity as the probe leaked out the vesicles and was diluted in the external buffer. The percentage of probe release (%L) was calculated according to:

$$\%L(t)=[(I(t)-I_b)/(I_T-I_b)]x100 \qquad \text{Eq. 5.1}$$

where I(t) is the fluorescence intensity at time=t, I_b the background fluorescence intensity prior to the detergent addition, and I_T is the fluorescence intensity corresponding to the complete release, induced by the addition of 0.10 (v/v) % of

Triton X-100. Each experiments were performed in triplicate. The release data were grouped using the K-means clustering method from the Math Plus software. The error bars represent the standard deviation for each cluster. The measurements were recorded on a fluorimeter SPEX Fluorolog-2 with an excitation wavelength set at 490 nm and an emission wavelength of 513 nm. The band widths were adjusted at 2.5 nm for the excitation and at 1.9 nm for the emission. The sample in the cell was stirred and the measurements were performed at room temperature.

The POPC vesicle samples for the DLS, and ITC experiments were prepared by hydrating powder lipid with MES buffer (10 mM) containing 10 mM NaCl, and 5 mM EDTA, pH = 6.5. The lipid concentration varied between 5 and 20 mM. The 100-nm vesicles were prepared by extrusion using a similar protocol as described above. The exact lipid concentrations were determined by the Fiske-Subbarow assay.[25]

DLS measurements were performed on a Malvern 4800 apparatus (Worcestershire, UK), with the Ar-laser line at 488 nm. The measurements were made at 90° for three periods of 180 s, at 25° C. The QAC and lipid concentrations corresponded to those obtained at the end of the ITC experiences. A 20-minute incubation prior to the measurements was performed.

Partition coefficient

In order to determine the partition coefficient of the QACs between POPC bilayers and water, LUVs were injected in the calorimeter cell containing a QAC. The QAC concentration in the cell was 6 mM for DTAC, 40 µM for CTAC, 4.4 mM for DPC, 20 µM for CPC, 1 mM for BDDAC, and 21 µM BDHAC. Between 8 and 10 injections of 5 or 10 µL of lipids suspension were made into the QAC solutions. The lipid concentration was 20 mM in the case of CPC, and BDDAC experiments, 15 mM for DPC and CTAC, 10 mM for DTAC, and 5 mM for BDHAC. These

conditions were optimized to provide a complete titration with a reasonable signal to noise ratio.

We used the model proposed by Heerklootz and Seeling[21] and Hoyrup et al[22] to determine the partition constant (K), and the molar enthalpy of transfer (ΔH_{trans}) from the ITC curves. The model is based on the partitioning of the detergent between the aqueous phase and the bilayer, which is considered as an organic pseudo-phase. This partitioning is characterized by a constant, K_w:[21,22]

$$K_w = \frac{X_{Dm}}{X_{Dw}} \approx \frac{C_{Dm} C_w}{C_L C_{Dw}} = C_w K \qquad \text{Eq. 5.2}$$

where K_w is the partition constant of a QAC between water and the membranes. X_{Dm} and X_{Dw} are the molar fractions of the detergent in the membranes, and in water, respectively. C_{Dw} is the molar concentration of free detergent in water, C_L, the molar concentration lipid concentration in the cell, C_w, the molar concentration of water (55 M), and C_{Dm}, the molar concentration of detergent associated to the membranes. The peak integration gives the enthalpy variation associated to each injection, h_i. The total enthalpy, H_i, corresponds to the total enthalpy variation obtained from the beginning of the titration up to the i^{th} injection ($H_i = \sum_i h_i$).

These values are corrected for the enthalpy variation associated to the dilution of the POPC vesicles. The dilution enthalpy of POPC vesicles was determined by injecting POPC suspension in the buffer (50 ± 5 J mol^{-1}, n=4). There was no significant signal for the dilution of the surfactants. The variation of H_i as a function of *i* is described by the equation :[21]

$$H_i = \Delta H_{trans} C_L^o C_D^o V^o \frac{Ki}{KC_L^o i + \frac{V^o}{V_{inj}} + i} \qquad \text{Eq. 5.3}$$

where C_L^o is the molar lipid concentration in the syringe, C_D^o is the molar detergent concentration in the cell, V^o is the volume of the cell, and V_{inj} is the volume of one injection. K and ΔH_{trans} were obtained from the simulation of the experimental data

with Eq. 5.3. This approach assumes that these two parameters are constant over the titration. The variation of Gibbs molar energy (ΔG_{trans}) and the molar entropy of transfer (ΔS_{trans}) were determined using:

$$\Delta G_{trans} = -RT \ln KC_w \qquad \text{Eq. 5.4}$$

$$\Delta G_{trans} = \Delta H_{trans} - T\Delta S_{trans} \qquad \text{Eq. 5.5}$$

where R is the perfect gas constant and T the temperature in Kelvin.

5.4 Results

The CMC values obtained for each detergent are reported in Table 5.1. The CMC obtained for BDDAC was 2.7 mM, a value similar to that previously measured in water (5.6 mM);[7] the difference is likely related to the use of buffer in our study. The CMC of QACs with an aliphatic tail of 12 carbon atoms were in the order of mM, whereas those with an aliphatic tail of 16 carbon atoms had a CMC in the order of μM. The nature of hydrophilic head also influences the CMC, an effect more pronounced in the case of the QACs with an acyl chain of 12 carbons. For an equivalent chain length, the CMC of the detergents decreases in the following order: trimethyl ammonium > pyridinium > benzyldimethyl ammonium.

Table 5.1: Critical micellar concentration of QACs and their Gibbs energy (ΔG_{mic}) of micellization.[iii]

Surfactant	CMC (mM)	ΔG_{mic} (kJ mol^{-1})	$\Delta(\Delta G_{mic})/ CH_2$ (kJ mol^{-1})	ΔH_{mic} kJ mol^{-1}	ΔS_{mic} (J K^{-1} mol^{-1})
DTAC	11.6 ± 1.9	-21.0 ± 0.4	-4.2 ± 0.5	4.0 ± 0.6	84 ± 14
CTAC	0.012 ± 0.005	-38.0 ± 1.0		-2.6 ± 0.1	119 ± 8
DPC	5.9 ± 0.1	-22.7 ± 0.4	-2.6 ± 0.3	3.5 ± 0.2	88 ± 6
CPC	0.084 ± 0.008	-33.2 ± 0.2		-4.8 ± 2.1	95 ± 42
BDDAC	2.7 ± 0.4	-24.6 ± 0.4	-4.0 ± 0.8	3.9 ± 0.2	95 ± 6
BDHAC	0.004 ± 0.002	-40.7 ± 1.2		4.6 ± 0.7	152 ± 28

The Gibbs energy of micellization (ΔG_{mic}) for the QACs with aliphatic chains containing 12 carbon atoms varies from -21.0 to -24.6 kJ mol^{-1}, whereas it varies from -33.2 to -40.7 kJ mol^{-1} for the QACs with aliphatic chain of 16 carbon atoms (Table 5.1). If two QACs with the same polar head are compared, a ΔG_{mic} variation ($\Delta(\Delta G_{mic})$) between -2.6 and -4.3 kJ mol^{-1} per CH_2 is obtained. The enthalpy of micellization (ΔH_{mic}) and the entropy of micellization (ΔS_{mic}) were also determined (Table 5.1). In all the cases, $T\Delta S_{mic}$ represents 85 % or more of the ΔG_{mic}, suggesting that the hydrophobic effect is the driving force for the self-assembly. Moreover, for a given head group detergent, the ΔS_{mic} is higher for the longer aliphatic chain. There is no correlation between the CMC and the ΔH_{mic} values. Surprisingly, for the same polar head group, the sign of the ΔH_{mic} value for pyridinium and trimethylammonium is different depending of the chain length.

The effect of QACs on the permeability of POPC membranes is reported in Figure 5.2. The percentage of release is expressed as a function of the incubation detergent/lipid molar ratio. For the DTAC and DPC, there is no release observed even when there are 10 detergent molecules for 1 lipid molecule. For the 4 other detergents, at detergent/lipid ratio under 1, a limited release is induced. When the

[iii] Le tampon utilisé pour effectuer les mesures ITC était composé de MES 10 mM, NaCl 10 mM et EDTA 5 mM avec un pH = 6.5.

incubation detergent/lipid molar ratio reaches 1, there is an abrupt increase in the leakage. The % release can reach 100% in these 4 cases when enough detergent is

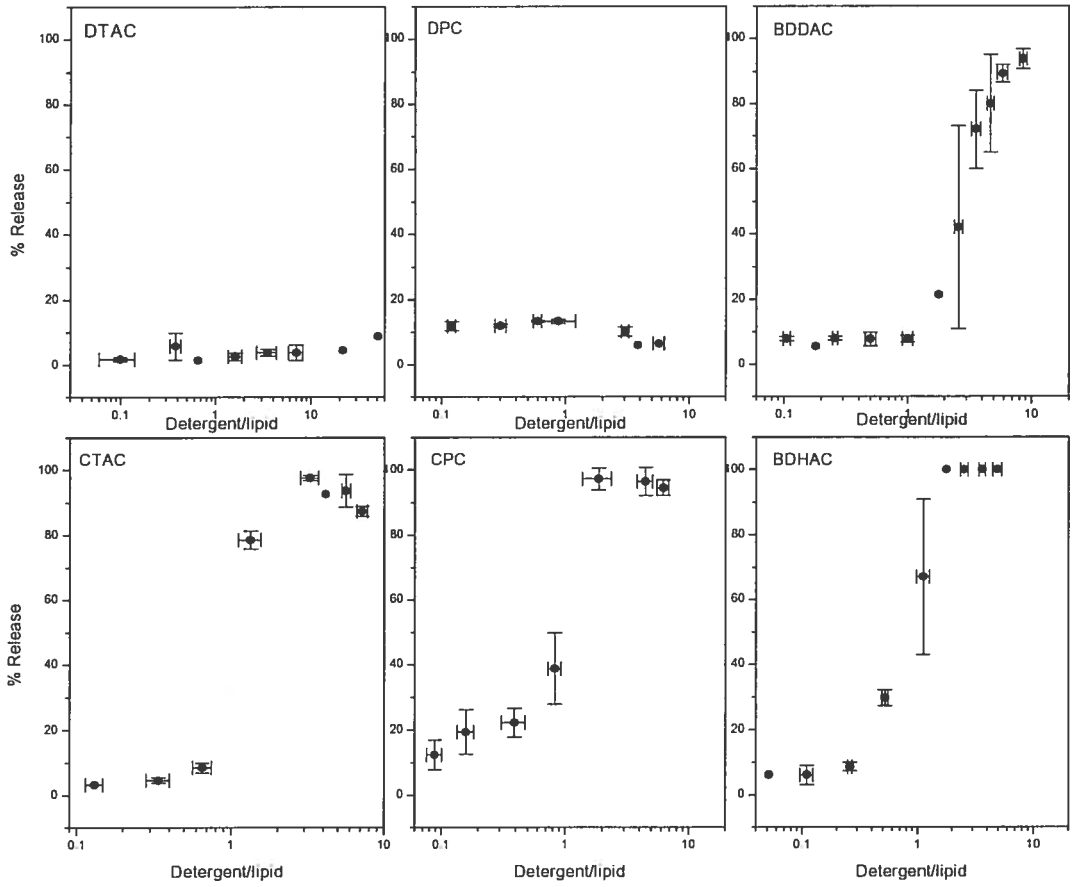

Figure 5.2 : Effect of QACs on the POPC membrane permeability, probed by the calcein release. The R_{50} values for CTAC, CPC and BDHAC are ≈ 1 whereas it is ≈ 2.8 for DBBAC. [lipid] ≈ 10μM

added. The detergent-induced release can be characterized by the R_{50}, corresponding to the incubation detergent/lipid molar ratio for which 50% of calcein release is observed. In the case of detergents with an aliphatic chain of 16 carbon atoms, the R_{50} values are around 1. For BDDAC, the R_{50} is estimated to be around 3.

The hydrodynamic radii of the POPC vesicles in the presence and the absence of QAC were measured by DLS, and the results are reported in Table 5.2. POPC LUVs in the absence of QAC had a mean diameter of 105.2 ± 0.8 nm. The addition of CPC or BDHAC did not affect significantly the diameter of the vesicles; they were of 98.9 ± 1.2 nm and 102.7 ± 1.5 nm respectively. On the other hand, the presence of DTAC and BDDAC caused an aggregation of the vesicles after an incubation for ~20 minutes, and the resulting particles had a mean diameter about 20 times larger than that of the LUVs prior to the addition of detergent. In the case of CTAC and DPC, the majority of the POPC LUVs remained relatively intact (85% for the CTAC and of 51% for the DPC). The remaining lipids however appeared to aggregate to form a second population with a larger hydrodynamic diameter. These measurements were stable over at least 5 hours. A lipid flocculation was observable by visual inspection for the samples containing a majority of large particles detected by QELS.

Table 5.2: Hydrodynamic radius variation of the POPC vesicles incubated in the presence of QACs.

Mixture	Percentage of small particles	Mean dimension (nm)	Percentage of large particles	Mean dimension (nm)
POPC	100	105.2 ± 0.8	-	-
DTAC/POPC	-	-	100	1913 ± 265
CTAC/POPC	85 ± 7	86 ± 6	15 ± 7	1345 ± 125
DPC/POPC	51 ± 11	60 ± 10	48 ± 11	1415 ± 142
CPC/POPC	100	98.9 ± 1.2	-	-
BDDAC/POPC	-	-	100	2045 ± 246
BDHAC /POPC	100	102.7 ± 1.5	-	-

In order to examine the affinity of the QACs for POPC membranes, calorimetric isothermal titration was performed. Typical results are presented in Figure 5.3. During these titrations, lipids vesicles were added to the cell containing a detergent solution. For DPC, CPC and CTAC, the titration profiles were similar and the observed peaks corresponded to an exothermic phenomenon. The peaks corresponding to the first injections were more intense because there was a large amount of detergent in the cell available to partition in the added lipid membranes. Then the peak areas decreased as the concentration of free detergent in the cell decreased, until practically no signals could be detected. In the case of DPC, CPC and CTAC, the titration appeared to be complete. The last peaks displayed an area corresponding to the dilution enthalpy of POPC vesicles. DTAC, and BDDAC presented different profiles compared to the previous ones. In the case of BDDAC, endothermic signals were recorded. Upon titration, the signal area progressively decreased. For DTAC, the first two injections led to an exothermic process, but endothermic peaks were observed for the subsequently injections of liposomes. As pointed out above, the dilution of QACs by the buffer and the dilution of the vesicles in the cell filled with buffer showed small exothermic peaks or no significant signal. Therefore the endothermic signals are associated to phenomena occurring upon mixing the detergent with lipid vesicles. For BDDAC and DTAC,

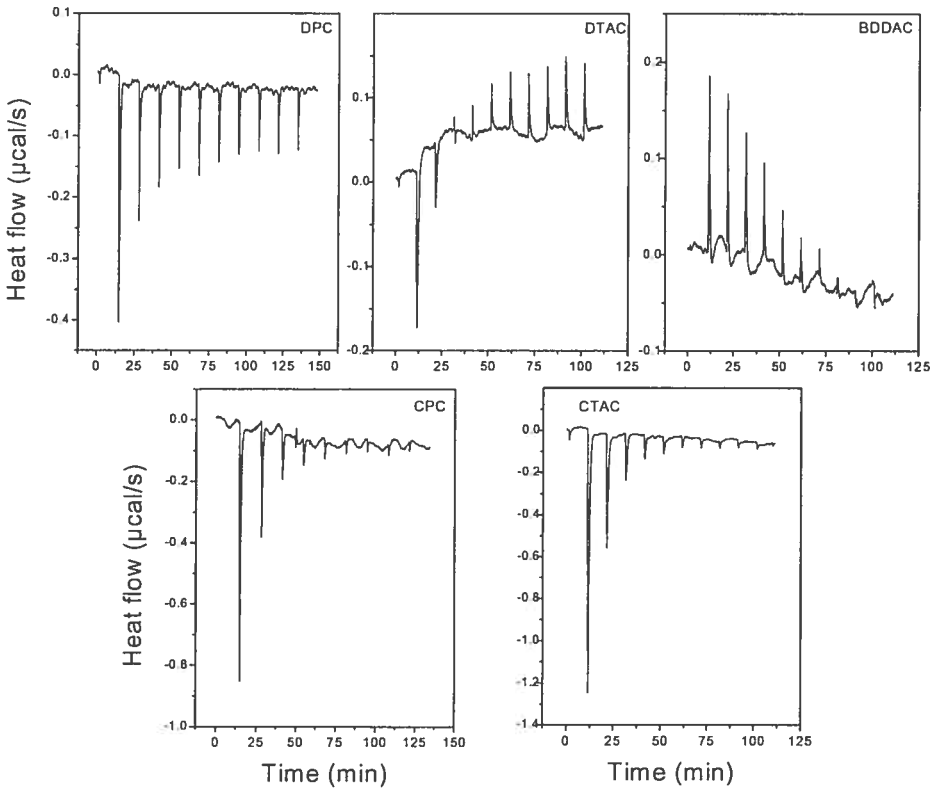

Figure 5.3 : Typical profiles obtained for the titration of a QAC solution with a POPC vesicle suspension. The detergent is indicated in the upper right corner of each panel.

lipid aggregation, as determined by the DLS measurements, was confirmed by the opalescent solution recuperated from the calorimeter cell at the end of titration. To obtain workable signals, the BDHAC concentration in the cell was about 5 times its CMC in order. This lead to a situation where the enthalpy of demicellization contributed in a significant and complicated manner during the titration. We therefore did not apply the simple partition model to the BDHAC. In the case of CTAC, despite the fact that the detergent concentration in the cell was initially greater than its CMC, it was found that the enthalpy contribution of the demicellization was negligible taking into account the small ΔH_{mic} (Table 5.1) compared to the energy recorded during the titration. Furthermore, all the points could be fitted with the simple partition model and, according to the extracted values, the free detergent concentration was lower than the CMC right after the first lipid injection.

The calorimetric isotherm titration can be interpreted in terms of the partitioning of the detergents between the aqueous phase, and the lipid bilayer (pseudo) phase.[21,22] Figure 5.4 shows two examples of the variation of H_i as a function of the number of injections, and the fit obtained from the simulation using Eq. 5.3. From this fit, K, and ΔH are extracted and reported in Table 5.3. Because of the complex profiles obtained for the titration with DTAC and BDDAC, we could not convincingly conclude that the detected heat flow was exclusively associated with the QAC transfer from aqueous media to lipidic membranes. Even though it was possible to fit the experimental data with the model, we do not report the calculated parameter because of this ambiguity.

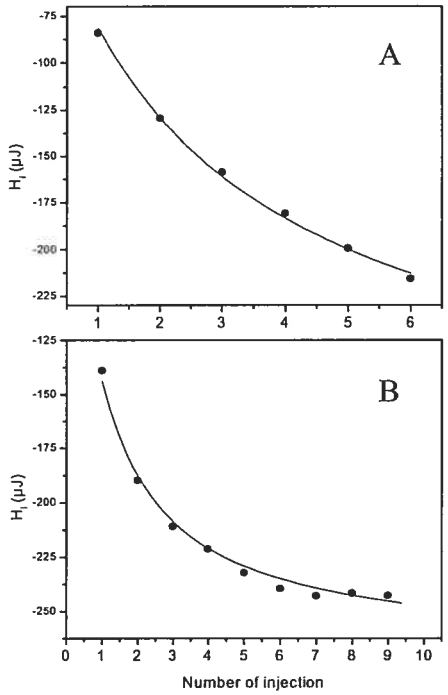

Figure 5.4 : Examples of the fitting of the experimental data with equation 5.2 used to determine the partition constant (K) and molar enthalpy (ΔH_{trans}) associated to the partitioning of QAC between the aqueous phase and POPC membranes. A) DPC B) CPC

Table 5.3: Thermodynamic constants associated to the partition of QAC between the aqueous phase and POPC vesicles.

Surfactant	K ((x 10^3) M^{-1})	ΔG_{trans} (kJ mol^{-1})	ΔH_{trans} (kJ mol^{-1})	ΔS_{trans} (J K^{-1} mol^{-1})
CTAC	9.5 ± 0.5	-32.64 ± 0.13	-11.6 ± 0.080	70.6 ± 0.8
DPC	2.90 ± 0.14	-29.703 ± 0.023	-0.060 ± 0.003	100 ± 5
CPC	14.9 ± 0.5	-33.76 ± 0.08	-8.6 ± 0.4	84 ± 4

5.5 Discussion

For the CMC measurements, we found that 16-carbon atom acyl chain had smaller CMC values then the 12-carbon atom ones, in agreement with previous studies.[10] The differences of ΔG_{mic} per CH_2 calculated here are consistent with the $\Delta(\Delta G_{mic})$ reported for the transfer of alkanes from an aqueous to a non-polar medium, corresponding to -1.7 to -2.8 kJ mol^{-1} per CH_2.[26] This similarity indicates the importance of the hydrophobic interactions in the free energy involved in the transfer of a detergent monomer into its micelle. The results also show that the presence of the benzyl group reduced the CMC values for the same acyl chain length, as previously reported[10]; this effect was proposed to be a consequence of the hydrophobicity of the benzyl group and/or a π-π stacking effect. The enthalpy of micellization is sensitive to the molecular details of the QACs but it is rather difficult to propose a rationale explaining these variations. To illustrate the sensitivity of ΔH_{mic} and the difficulty to pin point its origin, we can mention that changing the counter ion of benzyldimethyldodecylammonium from chloride to bromide leads to a variation of ΔH_{mic} from +2.4 to -4.9 kJ mol^{-1}.[7]

Our results show that the QACs with an acyl chain of 16-carbon atoms are more efficient to disturb the membrane permeability compare to that with a C12 chain. At this point, the origin of the specific efficiency of BDDAC is not understood. The influence of chain length has been reported for phenomena that happen at high QACs concentration. Solubilization of vesicles, a more drastic structural perturbation of lipid membranes, occurs at a lower concentration for QACs with 16-carbon atoms chain length compare to shorter ones.[17,27] The specific efficiency of the benzyldimethylammonium group observed in the case of the C_{12} QAC is not additive to the chain length influence since BDHAC did not display a smaller R_{50} compared to the two other with the same chain length. A R_{50} of 36 was reported for the perturbation of POPC membrane by CTABr, i.e. a QAC of the same structure of CTAC but with a bromide instead of a chloride.[28] This considerable

difference may be a consequence of the counter ion effect, as the nature of the counter ion was reported to change some surfactant properties.[7,10,29]

Unfortunately, the titration of 3 QACs led to untreatable data regarding the detergent transfer from water to membranes. In the case of BDHAC, the concentration providing a sufficient signal corresponded to the micellelar form of the surfactant and did not suit the goal of determining the thermodynamics of transfer of the monomeric detergent to membranes. For the DTAC and the BDDAC, DLS detected large particles (Table 5.2) likely corresponding to lipid aggregation that was a consequence of the surfactant insertion in the bilayers.[30] The isothermal titration curves for these two surfactants were not considered because the signals could not be attributed solely, in an unequivocal manner, to the detergent transfer. It is possible that the lipid reorganization contributes also to the recorded heat flow. The endothermic signals measured at the end of the titration with DTAC suggest that phenomena other than partition occurred in the cell.

The determined K values for DPC, CPC and CTAC were 2.90×10^3, 14.9×10^3 and 9.5×10^3 M^{-1} respectively (Table 5.3). Those values are 1000 times higher than those reported by Tsao and Tseng for similar systems, using conductimetry measurements.[31] This difference can be explained by the fact that those measurements were obtained in pure water instead of in a buffer. We did the test with CPC in pure water, the association constant that we obtained was of the same order of wath is reported by Stao and Steng (data not show). The insertion of cationic surfactants in PC bilayers leads to the formation of a positive membrane surface charge. As a consequence, this membrane surface potential should lead to a gradient of QAC concentration, from the surface toward the bulk solution, as inferred for other charged species.[32-34] This gradient, dependent on the ionic strength of the aqueous environment, is indeed more pronounced in pure water. A lower concentration of QAC in solution near the bilayer interface would lead to a

considerable decrease of the inserted surfactant proportion, and a reduced apparent affinity constant.

The ΔG_{trans} values are similar for CTAC and CPC, both bearing a 16-carbon chain. A decrease in ΔG_{trans} is observed going from DPC to CPC (Table 5.3); the $\Delta(\Delta G_{trans})$ corresponds to about 1 kJ/mol of CH_2. It is slightly smaller than the reported value for the transfer of an alkane from water to organic phase.[26] It suggests an important hydrophobic contribution in the partition process. Tsao and Tseng reported this trend for both cationic and anionic detergents and they concluded that the hydrophobic effect was the main contribution in the partition process.[31] Similar decreases of the partition coefficient as a function of the chain length are reported in several studies, and linear relationships between ΔG_{trans} (or ln(K)) and ln(CMC) have been reported.[21,22,35] For the detergents investigated in our study, this trend is observed but the limited number of data points (n=3) prevents us from assessing, in a reliable manner, a linear relationship.

The ΔH_{trans} reported in Table 5.3 are different to those observed for the micelle formation (ΔH_{mic}) (Table 5.1). Even though the transfer is principally driven by hydrophobic effect ($T\Delta S_{trans}$ accounting for about 70% of the ΔG_{trans}), it seems that other interactions favour the insertion of detergents inside a lipidic bilayer, as ΔH_{trans} is systematically more negative then ΔH_{mic} for the three investigated detergents. These favourable enthalpic contributions can origin from attractive interactions between the positively charged ammonium group of the QAC and the zwitterionic POPC head group. Larger enthalpy variations observed during the insertion of sodium dodecylsulfate, an anionic surfactant, inside POPC membranes has been reported and specific electrostatic interactions between the phospholipid and the detergent polar head groups were proposed.[34]

Surprisingly, ΔS_{trans} of DPC was higher than for CPC, despite its shorter chain. This behaviour is the opposite of that observed for the micellization process. In the

case of transfer, the order of the lipid acyl chains must be taken into account. An electronic spin resonance study has shown that a higher disorder was found in bilayers containing hexyltrimetylammonium than in those containing octadecyltrimethylammonium.[17] The presence of shorter chains in the lipid matrix can lead to an increase of the free volume allowing more gauche conformations along the chains and more disorder in the system. A similar rationale may be at the origin of the ΔS_{trans} values measured for DPC, and CPC.

5.6 Conclusion

This study provides new insights into the effects of the molecular details of QACs on their interactions with phosphocholine bilayers. Even though the putative site of action of these biocides is the lipid bilayer of bacterial membranes,[6,7] the extrapolation of the observations obtained from the model membranes to the microbiological studies is not straightforward. On one hand, the smaller R_{50} values obtained for QACs with 16-carbon aliphatic chain are consistent with the increased bactericide power of QACs with long aliphatic chain.[4,9,10] These effects could likely be associated to the enhanced affinity of these QACs for cytoplasmic membranes. On the other hand, the absence of release observed when DTAC is added to lipid model membranes, even at high detergent/lipid proportion, is in apparent contradiction with the bactericidal effect of DTAC on *Staphylococcus aureus*,[9] and of DTABr on *Candida albicans*.[4] Similarly, no specific differences could be observed in the calcein release induced by CPC, CTAC, or BDHAC from the model membranes, in contrast with the higher sensitivity of Gram-negative bacteria towards alkylpyridinium.[3] It has also been reported that the optimal concentration for bactericidal effect appears near the CMC of the QACs, a concentration where the highest quantity of free monomers is found.[10] The absence of correlation between the calcein release from model membranes reported here,

and the QACs' CMC also illustrates the apparent discrepancies between the results obtained on model lipid systems, and the action of QACs on bacteria. This gap indicates that viewing the QACs activity strictly as a detergent perturbation of the lipid portion of bacterial plasmic membranes is an oversimplified view and that the molecular details of their antibacterial mechanism are largely unknown. Efforts should be devoted to gain a better understanding of the mechanism of their biocide activity in order to improve the efficiency of QACs and related analogues.

5.7 Acknowledgements

The authors thank NSERC (Canada), FRSQ (Québec), and FQRNT (Québec) for their financial support. This work was performed as a research project of the Chemical Self-Assembled Chemical Structures (CSACS).

5.8 References

1. A. D. Russell and I. Chopra. *Understanding Antibacterial Action and Resistance* (Ellis Horwood, Chichester, 1990)
2. A. D. Russell, Lancet Infect. Dis. **3**, 794 (2003)
3. S. Rajagopal, N. Eis and K. W. Nickerson, Can. J. Microbiol. **49**, 12, 775 (2003)
4. B. Ahlström, M. Chelminska-Bertilsson, R. A. Thompson and L. Edebo, Antimicrob. Agents Chemother. **41**, 3, 544 (1997)
5. G. McDonnell and A. D. Russell, Clin. Microbiol. Rev. **12**, 1, 147 (1999)
6. S. P. Denyer, Int. Biodeterior. Biodegrad. **36**, 227 (1995)
7. B. Rozycka-Roszak, R. Zylka, T. Kral and A. Przyczyna, Z. Naturforsch. **56c**, 407 (2001)
8. M. J. Smith, T. H. Flowers, M. J. Cowling and H. J. Duncan, Water Res. **36**, 1423 (2002)

9. C. Campanac, L. Pineau, A. Payard, G. Baziard-Mouysset and C. Roques, Antimicrob. Agents Chemother. **46**, 5, 1469 (2002)

10. F. Kopecky, Pharmazie **51**, 3, 135 (1996)

11. F. M. Goni and A. Alonso, Biochim. Biophys. Acta **1508**, 51 (2000)

12. M. Almgren, Biochim. Biophys. Acta **1508**, 146 (2000)

13. T. Inoue, T. Yamahata and R. Shimozawa, J. Colloid Interface Sci. **149**, 2, 345 (1992)

14. M. N. Jones, Int. J. Pharm. **177**, 137-159,(1999)

15. R. Koynova and B. Tenchov, Curr. Opin. Colloid Surf. Sci. **6**, 277 (2001)

16. R. N. A. H. Lewis and R. N. McElhaney, Biophys. J. **79**, 1455 (2000)

17. J. Gallova, F. Devinsky and P. Balgavy, Chem. Phys. Lipids **53**, 231 (1990)

18. R. E. Glover, R. R. Smith, M. V. Jones, S. K. Jackson and C. C. Rowlands, FEMS Microbiol. Lett. **177**, 57 (1999)

19. T. Benachir and M. Lafleur, Biochim. Biophys. Acta **1235**, 452 (1995)

20. R. El Jastimi, K. Edwards and M. Lafleur, Biophys. J. **77**, 842 (1999)

21. H. Heerklotz and J. Seelig, Biochim. Biophys. Acta **1508**, 69 (2000)

22. P. Hoyrup, J. Davidsen and K. Jorgensen, J. Chem. Phys. B **105**, 2649 (2001)

23. P. R. Majhi and S. P. Moulik, Langmuir **14**, 3986 (1998)

24. T. Benachir, M. Monette, J. Grenier and M. Lafleur, Eur. Biophys. J. **25**, 201 (1997)

25. C. H. Fiske and Y. Subbarow, J. Biol. Chem. **66**, 375 (1925)

26. J. Israelachvili. *Intermolecular and Surface Forces, 2th Edition* (Academic Press inc., London, 1992)

27. A. de la Maza and J. L. Parra, J. Controlled Release **37**, 33 (1995)

28. S. Watanabe and S. L. Regen, J. Am. Chem. Soc. **116**, 5762 (1994)

29. B. Rozycka-Roszak, R. Zylka and J. Sarapuk, Z. Naturforsch. **56 c**, 154 (2001)

30. R. Saez, F. M. Goni and A. Alonso, FEBS Lett. **179**, 2, 311 (1985)

31. H.-K. Stao and W. L. Tseng, J. Chem. Phys. **115**, 17, 8125 (2001)

32. A. Percot, X. X. Zhu and M. Lafleur, Biopolymers **50**, 647 (1999)

33. R. Lehrmann and J. Seelig, Biochim. Biophys. Acta **1189**, 89 (1994)

34. A. Tan, A. Ziegler, B. Steinbauer and J. Seelig, Biophys. J. **83**, 1547 (2002)

35. J. Lasch, Biochim. Biophys. Acta **1241**, 269 (1995)

Chapitre 6

Conclusion

Les biofilms bactériens présentent une résistance aux antibiotiques, ainsi qu'aux bactéricides, comparativement à ces mêmes bactéries qui se développent sous forme planctonique.[1,2] Les travaux de cette thèse ont permis de mieux comprendre deux aspects importants qui pourraient jouer un rôle dans cette résistance des biofilms.

Premièrement, nous avons montré que les molécules inertes, même relativement petites (Rh de 4 Å), ne sont pas arrivées à pénétrer à 100 % les biofilms étudiés au cours de ces travaux. Effectivement, un volume considérable leur est exclu. La cartographie Raman a montré que ces régions d'exclusion correspondaient aux régions riches en biomasse, soit probablement les microcolonies. En conséquence, il est proposé que la concentration effective d'antibiotiques à la proximité des bactéries enfouies dans un biofilm soit considérablement moindre que la concentration attendue. Cette différence pourrait jouer un rôle dans la résistance au bactéricides qui est observée chez les biofilms. Nos travaux suggèrent donc que pour rendre un bactéricide efficace, il faut soit se tourner vers le développement de petites molécules capables d'atteindre les bactéries dans les régions denses de la biomasse, soit désorganiser la matrice entourant les bactéries, rendant leur accessibilité plus facile. Des efforts ont déjà été développer dans ce sens an ajoutant de l'EDTA à une solution anti-biofilm.[3]

Le biofilm utilisé dans notre étude demeure un modèle. Les biofilms qui sont trouvés dans la nature s'avèrent très souvent composés de plus d'une espèce et leur conformation dépend beaucoup des conditions de croissance.[4] Il est donc important d'examiner les propriétés de transport dans des biofilms de structures différentes et composés de d'autres espèces de micro-organismes de manière à

valider que les conclusions présentées dans ce travail peuvent être transférables à la réalité. De plus, il est rapporté que la densité de biomasse dépend de la vélocité de son environnement de croissance[5] et des nutriments auxquels les bactéries ont accès pour se multiplier.[6] Il serait donc important d'examiner l'effet de la densité de la matrice sur la diffusion moléculaire à l'intérieur des biofilms. Par exemple, des mesures de spectroscopie IR-ATR et Raman, tel que présenté dans cette thèse, pourraient être appliquées sur un même biofilm, mais cultivé dans différentes conditions (diverses températures, nutriments différents — milieu riche *vs* milieu pauvre, présence de turbulences, etc.) afin d'en vérifier l'effet sur la capacité de pénétration des bactéricides potentiels. Les possibilités sont immenses et pourraient mener à une meilleure compréhension des facteurs menant à la résistance des biofilms aux bactéricides, un domaine où beaucoup d'hypothèses s'opposent tel que mentionné précédemment (Chapitre 1).

De plus, l'utilisation de la spectroscopie IR-ATR se présente comme une technique complémentaire aux autres techniques qui sont rapportées dans la littérature pour les mesures de diffusion. La méthode FRAP, entre autres, donne une mesure d'auto-diffusion. C'est-à-dire, la diffusion d'un soluté en absence de gradient de concentration ce qui est différent de ce qui est trouvé par la spectroscopie IR-ATR. Les mesures de CLSM peuvent être faites de manière à obtenir un coefficient de diffusion en fonction d'un gradient de concentration. Par contre, les molécules utilisées sont souvent des dextrans combinés à la fluorescéine et dont les dimensions se situent au-delà de ce qui a été étudié dans le présent travail. La sélection des PEGs utilisés dans notre étude a d'ailleurs permis de couvrir un domaine de dimension pour lequel les valeurs dans la littérature étaient plutôt rares.

Par contre, bien que la taille influence grandement l'accessibilité du biofilm par le soluté, il semble que les molécules chargées présentent un potentiel de pénétration plus élevé. Effectivement, nous avons obtenu des pourcentages de pénétration deux fois plus élevés pour des macroassemblages chargés ayant des dimensions

similaires aux PEGs étudiés. Aussi, les coefficients de diffusion relatifs se sont montrés beaucoup plus petits que ceux des PEGs de dimensions similaires laissant croire que les macroassemblages chargés interagiraient de manière plus importante avec le biofilm. Par contre, il reste à voir si les molécules chargées pénètrent davantage dans le biofilm ou si elles s'accumulent aux pourtours des microcolonies préservant ainsi les bactéries qui se trouvent au cœur de celles-ci. D'ailleurs, nos mesures de diffusion sur le CPC par spectroscopie IR ont montré une association irréversible avec le biofilm et une diffusion beaucoup plus lente que pour tous les autres solutés étudiés. La cartographie Raman se présente alors comme un choix de premier ordre pour étudier les changements de morphologie après le passage de détergents chargés et de situer dans l'espace un soluté (comme le CPC) qui présente une forte affinité pour le biofilm. D'ailleurs, plusieurs autres bactéricides d'intérêt pourraient être étudiés sur variété de biofilms par la microscopie Raman. Cette dernière technique est complémentaire aux autres techniques de microscopie, par le fait qu'elle apporte une information spatiale sur la nature moléculaire des espèces qui se trouvent dans le biofilm.

Aussi, maintenant que l'effet de taille sur la diffusion a été démontré, il serait intéressant d'explorer davantage l'effet de charge. On pourrait imaginer de suivre, à l'aide de la spectroscopie IR par ATR, la diffusion de macromolécules de mêmes tailles, mais dont la charge globale varierait. Notre étude sur l'effet de la charge sur le coefficient de diffusion a été effectuée avec des macroassemblages. Cette démarche a pour faiblesse qu'il demeure un doute quant à l'intégrité des micelles lorsqu'elles sont mises en contact avec le biofilm. L'utilisation d'une macromolécule éliminerait ce doute.

Dans la deuxième partie de cette thèse, nos travaux ont montré, d'une manière générale, que l'association des QACs aux membranes modèles procède principalement par effet hydrophobe. Nous avons identifié que la longueur de la chaîne acyle est un élément déterminant dans cette association. De plus, l'insertion

du détergent dans une membrane contenant du cholestérol, pour laquelle l'ordre des chaînes est élevé, est plus limitée. Finalement, nous avons montré que la présence de charges négatives à l'interface membranaire n'affecte pas de manière significative l'association détergent-membrane Ces résultats sont similaires à ce qui est rapporté dans la littérature pour l'affinité de d'autres détergents pour des membranes lipidiques où, là aussi, ont conclu à un effet hydrophobe.[7]

Par contre, nos mesures de perméabilité ont montré des profils de relargage pour les membranes anioniques avec un processus de fuite en deux étapes. Le mécanisme de fuite pourrait dépendre du passage des détergents du feuillet externe vers le feuillet interne de la bicouche lipidique (le flip-flop). La présence de charges anioniques ayant pour effet de ralentir le transfert du détergent. La vérification de l'effet du flip-flop dans le mécanisme de relargage n'a pu être approfondie dans le cadre de cette thèse. Par contre, l'auteure croit que cet aspect devrait être exploré davantage puisqu'il détient peut-être un indice important sur le mode de fonctionnement du CPC. L'utilisation de la spectroscopie à résonance magnétique nucléaire pourrait répondre à cette question. Le ratio de eggPG entre la couche extérieure et la couche intérieure des LUVs ayant été déterminé via cette méthode par Hope et al.[8] Ou encore, l'élaboration d'une expérience en fluorescence où le QAC viendrait éteindre une sonde fluorescente encapsulée dans les vésicules pourrait faire la lumière sur cette hypothèse.

Les composés d'ammoniums quaternaires (QACs) sont réputés en tant que bactéricide pour agir sur la membrane bactérienne.[9] Nos résultats d'affinité et de perméabilité sont difficiles à corréler avec les pouvoirs bactéricides rapportés dans la littérature pour ces détergents. Bien que nos mesures de diffusion du CPC dans les biofilms par spectroscopie IR-ATR aient montré une association irréversible avec le biofilm, l'association du CPC pour les membranes composées de POPG et cardiolipines ne suggèrent pas que l'association irréversible ou l'accumulation du CPC proviennent de ces composés dans la membrane. L'effet des QACs ne semble

pas être un simple effet détergent de la membrane. S'il s'avérait que cela en était un, il se pourrait qu'il soit dû à une association spécifique à un autre type lipide de la membrane mais qui n'a pas été investigué dans nos travaux. L'association spécifique entre certaines protéines - reconnu pour leur effet bactéricide - avec les lipides chargés négativement est essentielle à leur intronisation dans la cellule.[10] Il faudrait donc étudier davantage les détails moléculaires des mécanismes d'action des QACs. Une meilleure compréhension de leur principe d'action nécessite probablement l'étude de leur association pour d'autres composantes membranaires (comme leur effet sur les chaînes latérales des protéines par exemple).

Aussi, l'efficacité des QACs vient peut-être de cette capacité d'association irréversible avec les biofilms. Il serait intéressant de mesurer l'énergie d'association des QACs pour d'autres composantes du biofilm (comme les constituants de la matrice extracellulaire). Ceci permettrait d'avoir une meilleure idée des sites potentiels de bioaccumulation des bactéricides dans le biofilm. Si les QACs s'associent préférentiellement avec la matrice d'exopolysaccharides, alors à des doses usuelles dans le cadre de traitement (soit beaucoup plus faible que celle utilisée dans l'étude de diffusion),[11] le bactéricide pourrait s'avérer inefficace. Aussi, si la cible et la composante active du QACs venaient qu'à être identifiée, le développement de nouveau bactéricide plus efficaces basé sur ces nouvelles données pourrait permettre une plus grande concentration du bactéricide dans le biofilm lorsque administré à faible dose.

6.1 Références

1. J. W. Costerton, P. S. Stewart and E. P. Greenberg, Science **284**, 1318 (1999)
2. P. Watnick and R. Kolter, J. Bacteriol. **182**, 10, 2675 (2000)
3. Barbeau, J.; Prévost, A.; Côté, L.; Charland R.; Faucher, E. USA 5,731,275.

4. L. V. Evans. *Biofilms: Recent Advances in Thier Study and Control.* (Harwood Academic Plublishers, Amsterdam, 2000)
5. H. Beyenal and Z. Lewandowski, Biotechnology Progress **18**, 1, 55 (2002)
6. J. Pratten, C. S. Andrews, D. Q. M. Craig and M. Wilson, FEMS Microbiol. Lett. **189**, 215 (2000)
7. P. Høyrup, J. Davidsen and K. Jørgensen, J. Chem. Phys. B **105**, 2649 (2001)
8. M. J. Hope, T. E. Redelmeier, K. F. Wong, W. Rodrigueza and P. R. Cullis, Biochemistry **28**, 10, 4181 (1989)
9. A. D. Russell, Lancet Infect. Dis. **3**, 794 (2003)
10. B. de Kruijff, FEBS Lett. **346**, 78 (1994)
11. A. S. Landa, H. C. van der Mei and H. J. Busscher, Adv. Dent. Res. **11**, 4, 528 (1997)

Annexe I

Au chapitre 4, nous avons fait le titrage calorimétrique isotherme du CPC par des vésicules composés de POPC:POPG (8:2) où le CPC était concentré à 300 µM (soit au delà de la CMC). Nous avons utilisé le modèle de Gouy-Chapman afin de reproduire les données expérimentales telles que montrées à la figure 4.6 du chapitre 4. Dans la présente annexe, nous présentons les détails du calcul ainsi que l'évolution des concentrations en cours de titrage telle qu'expliquée par le modèle.

Listes des équations et définitions des paramètres :

Éq. 1 $K=\frac{C_{DL}}{C_{DM}C_L}$

Éq. 2 $C_{DT}=C_{DL}+C_{DB}+C_{DR}$

Éq. 3 $C_{DM}=C_{DB}\exp(\frac{-zF\Psi}{RT})$

Éq. 4 $H_i=\frac{\Delta H}{n_i}\quad\frac{n_i}{V_T}=C_{DL}$

C_{DL} =concentration de détergent lié
C_{DM} =concentration de détergent libre à la membrane
C_{DB} =concentration de détergent dans le cœur de la solution
C_{DR} =concentration de détergent sous forme de micelle
C_{DT} =concentration de détergent totale
C_L =concentration de lipide
z =charge du détergent
F =constante de Faraday
Ψ =potentiel de la membrane lipidique (dépend de C_{DL})
R =constante des gaz parfaits
T =température (K)
H_i =enthalpie totale de transfert
n_i =nombre de mol de détergents liés
V_T =volume total

L'hypothèse de départ est que la constante d'équilibre K décrit l'équilibre entre le CPC dans la membrane et celui en solution sous forme monomère. Les micelles de détergents sont considérées comme des « réservoirs » de détergents.

Tant qu'il y a des micelles en solution, C_{DB} demeure constant et égal à la CMC, car les monomères qui se lient aux bicouches lipidiques sont remplacés en solution par les micelles qui se dissocient (cette situation correspond aux 7 premiers pics de la titration, soit avant le trait vertical noir sur la figure II.1). Il n'y a alors que C_{DL} et C_{DM} à déterminer à l'aide des équations 1 à 3. C_{DL} et C_{DM} sont trouvées par itération en posant d'abord C_{DM} dans l'éq.1 comme étant égale à la CMC. De l'éq. 1, un C_{DL} est trouvé et ceci permet de déterminer Ψ (Éq. 4.6 et 4.7). En reportant

Ψ dans l'éq. 3, comme C_{DB} est égale à la CMC, on trouve un nouveau C_{DM}. Puis, on refait cette démarche jusqu'à ce que le C_{DM} posé dans l'éq. 1 soit égal à celui trouvé dans l'éq. 3. La figure 1 montre que tant qu'il reste des micelles en solution C_{DM} reste constante. Ceci s'explique par le fait que l'équilibre est limité par la concentration en lipide (C_L) et non en détergent, car C_{DB} reste constante. La fraction molaire de détergent retrouvée dans les bicouches lipidiques suite au calcul itératif reste à 0.26 (soit légèrement plus d'une molécule de CPC par molécule de PG) et la densité de charge de la membrane reste constante soit a 0.03 C/m^2 (voir Figure II.1). La concentration en détergent trouvée à la membrane demeure donc inférieure à la concentration du cœur de la solution (et donc de la CMC) à cause de la répulsion électrostatique.

Lorsqu'il n'y a plus de détergents sous forme micellaire, l'équation 2° change et devient :

$$C_{DT} = C_{DL} + C_{DB}$$

Dès lors, C_{DL}, C_{DB} et C_{DM} sont inconnues. Seule K, C_L et C_{DT} sont déterminés. Pour résoudre ce problème, nous avons procédé encore une fois par itération. Nous avons supposé un C_{DM} dans l'équation 1. C_{DM} devait être posé de manière à ce que $C_{DL} < C_{DT}$. Les itérations identifiaient les valeurs de C_{DB} et C_{DM} qui rendaient les équations 1 et 3 cohérentes. À cette étape de la titration, ce n'est plus C_L qui est limitant dans l'équilibre mais C_{DM}. Comme il est montré à la figure II.1, C_{DL} continue d'augmenter à chaque injection, mais non plus de manière linéaire et tend vers un maximum qui correspond presque au transfert complet du détergent vers la forme associée. On voit aussi que la densité de charge de la membrane lipidique diminue en cours de titrage, passe par zéro et devient légèrement négative (figure II.1). À ce moment, la fraction molaire en détergent dans la membrane est de 0.11.

Une fois les C_{DL} trouvées pour chaque injection, il a été possible de déterminer le nombre de mole (n_i) de détergent qui s'était lié aux bicouches lipidiques, et de là, nous avons calculé le H_i théorique correspondant aux concentrations trouvés dans

la cellule après chaque des injections (équation 4). L'évolution de l'enthalpie totale est montrée à la figure I.1.

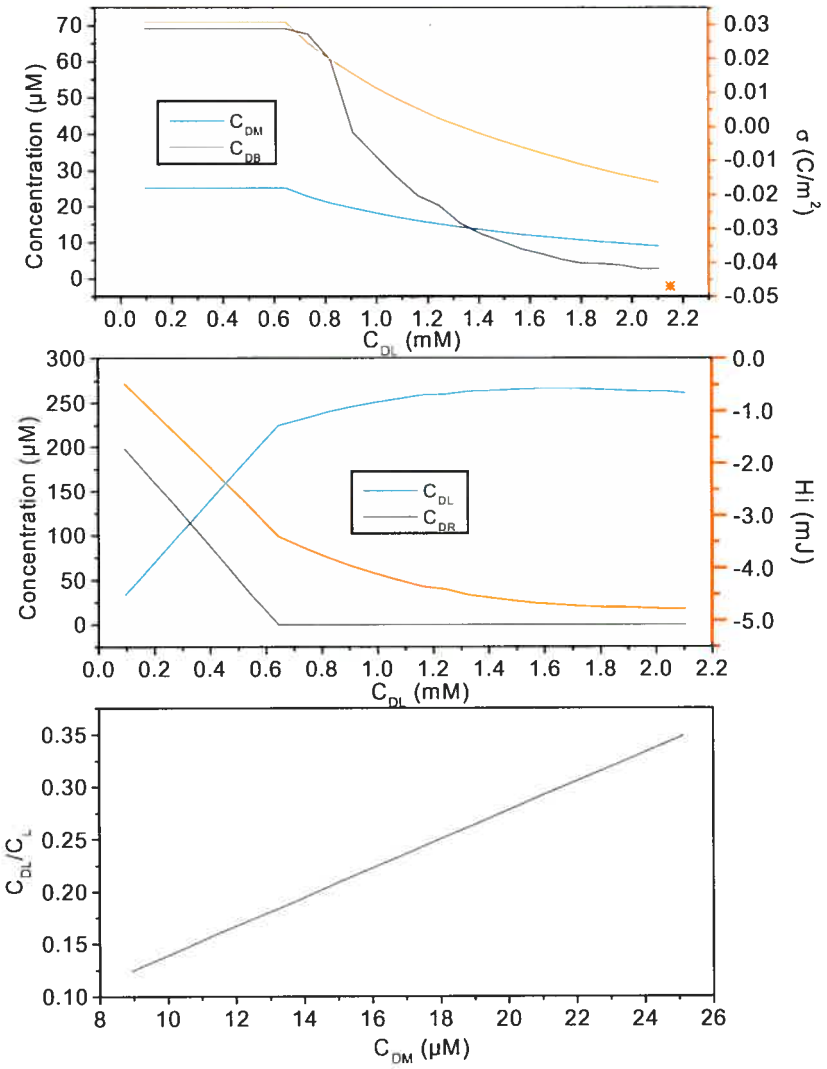

Figure I.1 : Évolution des concentrations en détergents et en lipides, de la densité de charge de la membrane et de l'enthalpie totale lors du titrage calorimétrique tel que prévu par le modèle. * montre la densité de charge de la membrane en abscence de détergent.